WATERTOWN ARSENAL LABORATORIES

Monograph Series

NUMBER 46

THE NATURE OF BUCKLING IN THIN SPHERICAL SHELLS

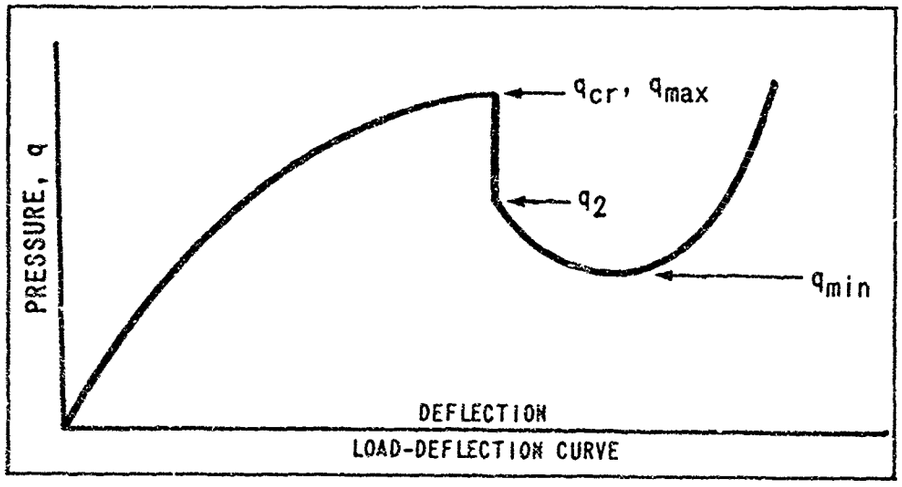

LOAD-DEFLECTION CURVE

By

LYNN SEAMAN

MAY 1962

ABSTRACT

THE NATURE OF BUCKLING IN THIN SPHERICAL SHELLS

by Lynn Seaman

The report deals with a number of questions concerning the buckling of thin elastic spherical shell segments under uniform external pressure. Both experimental and analytical studies were performed to determine the nature of the buckling phenomenon.

The experimental work was performed on plastic shells which buckled elastically so that tests could be repeated. The size and position of the buckle or dimple, effect of creep on buckling loads, importance of the precision of clamping conditions, and the reproducibility of buckling loads under unchanged conditions were determined. A general discussion was given of the shape of the load-deflection curve, the appearance of the buckle through the post-buckling range and the dependence of buckling pressures, unbuckling pressures and minimum pressures on the shape parameter λ . No correlation was possible between the observed imperfections and the buckling loads.

In the analysis, the nonlinear equation for total potential energy was derived for deep shell investigations. A formula for deflected shape, which was similar to that seen in the tests, was used to determine equilibrium positions for a number of shell configurations. Besides the usual shape parameter λ , a depth measure was also necessary since the shells were not shallow. The equilibrium positions were plotted into load-center deflection, load-average deflection, and energy-deflection curves. Computed buckling loads were much too high, probably due to neglecting the mode shapes which are small surface undulations which occur in the shell before buckling. The equation developed is adequate in the range near buckling but needs improvement for use in the large deflection range.

The experimental buckling loads were in a fairly narrow band midst those of other investigators. The repeatability of the tests added greatly to the value of the results. Analytical buckling loads were higher than previous results, and far above the test results.

ACKNOWLEDGEMENT

M.I.T Computation Center for machine time on the I.B.M. 7090 to complete the analysis.

Submitted in Partial Fulfillment of the Requirements for the Degree of Doctor of Sc! nce at the Massachusetts Institute of Technology.

TABLE OF CONTENTS

CHAPTER 1 INTRODUCTION

With the increased use of shell type structures in architecture, space exploration, and other projects, much interest has been evinced in the determination of the collapse or buckling loads of these structures. This report treats the buckling of thin elastic spherical shell segments under the action of uniform external pressure.

The object was to define the nature of the buckling phenomenon. This included the buckling load, shape of the load-deflection curve, the effect of imperfections and testing conditions, and the size and shape of the dimple which forms. Besides the buckling load (q_{cr}), other pressures of interest were the load to which the shell jumped at buckling (q_2), the load to which it jumped at unbuckling (q_{un}), and the minimum post buckling pressure (q_{min}). A further purpose was to find out if there was a difference between buckling loads obtained from tests with displacement control and those obtained from tests with pressure control.

In the analytical study the object was to derive equilibrium equations for the symmetrical deformations of deep shells and to use these equations for buckling. The attempt was to find a deflected shape andbuckling loads and to determine whether the equations were adequate. With a series of equilibrium positions, load-deflection curves could be constructed and compared with test results.

The relevant literature was reviewed in search of clues to the most successful approach to the problem. G. A. Thurston, B. Budiansky,

and others have investigated analytically the shape of the load-center deflection and/or load-average deflection curves and buckling loads. B. Budiansky and W. L. Chen have initiated the discovery of the importance of imperfections on buckling loads. A. Kaplan and Y. C. Fung have provided experimental knowledge about deflected shape as well as buckling loads. T. von Karman and H. S. Tsien have suggested energy criteria for buckling which contrast with a definition of buckling pressure as the first maximum point on the load-displacement curve.

The experiments were conducted on thin plastic shell segments with depth to span ratios from 1/500 to 1/11. For the shells λ, the shape parameter, ranged from 3.5 to 25. A function of both the thick ness to radius ratio and shell depth, this parameter has been found to govern all shallow shell buckling phenomena.

$$\lambda = \sqrt[4]{12(1-\nu^2)}\sqrt{\frac{a}{h}}\sin\alpha \qquad (1\text{-}1)$$

where a is the shell radius, h is thickness, and α is one half the opening angle of the shell.

Most of the tests were conducted by displacement control using water pressure above and below the shell. These tests provided a complete load-deflection curve from no load into the post-buckling range and back to zero load. A few tests were run with an approximation to pressure control. In all cases the shells behaved elastically and the tests could be repeated. Besides those topics mentioned above, the study included the effect of buckle position and creep on the buckling load and the variation of the pressures q_{cr}, q_2, q_{un}, and q_{min} with λ.

The results were used to check the possible validity of the energy criterion. In all this study the reproducibility of the tests was very helpful, permitting even an estimate of the importance of effects which have caused so much scatter in test results.

Analytically, equilibrium positions were determined by the principle of minimum potential energy. The energy equation was derived with the aid of an order of magnitude analysis and applied to finding buckling loads for a number of configurations like the shells tested.

The experimental work is presented in Chapter 4 and the analytical study in Chapter 5. The results from these two portions are brought together in the Summary, Chapter 6, and compared.

CHAPTER 2 NOTATION

a	shell radius
α	angle defining edge of shell, see Fig. 1
b	variable defining buckle extent
c	$\sqrt[4]{3(1-\nu^2)}\sqrt{\frac{a}{h}}$ ratio of extensional to bending stiffness
δ_0, δ_1	linear and nonlinear components of deflection used in an example
E	modulus of elasticity
E_1	modulus at one minute after loading
$E_{20}, E_{11}, E_{10}, E_{01}, E_{21}, E_{12}, E_{02}, E_{03}, E_{04}$	coefficients of energy terms defined by Eq. (5-28)
ε	strain
ε_{cr}	strain at buckling
$\varepsilon_{11}, \varepsilon_{22}, \varepsilon_{33}$	strain in ϕ, θ, Z directions or X, Y, Z directions
ε_{13}	shear strain between ϕ and Z directions or X and Z directions
$\varepsilon_{23}, \varepsilon_{12}$	shear strain between Y and Z, X and Y directions
$\bar{\varepsilon}_{11}, \bar{\varepsilon}_{22}$	strains in the middle surface in ϕ, θ directions
$e_{11}, e_{22}, e_{13}, e_{33}$	linear strains corresponding to $\varepsilon_{11}, \varepsilon_{22}, \varepsilon_{13}, \varepsilon_{33}$
g	creep coefficient
h	thickness of shell

H	central height of shell
$\varkappa_{11}, \varkappa_{22}$	nondimensional curvatures of the middle surface in the ϕ, θ directions (curvature times radius)
ϕ	position coordinate, see Fig. 1
$\mathcal{O}$	variation of tangential displacement through thickness
k_1, k_2	stiffness coefficients used in an example
$K(t,g)$	a function of creep and the time since commencement of loading
$K(T,g)$	a function of creep and duration of loading; it defines the effect of creep on the buckling load
λ	$\sqrt[4]{12(1-\nu^2)}\sqrt{\frac{a}{h}}\sin\alpha = \sqrt{2}\, c \sin\alpha$, shell shape parameter
L	dimensionless volume change, Eq. (5-26)
m	quantity assumed to be greater than 10 used to define orders of magnitude
M	a constraint
ν	Poisson's ratio, taken as 0.3 in the analysis
ω_2	rotation in ϕ-Z plane
P	q/q_T, nondimensional pressure
P_{cr}	critical or buckling pressure
P_2, P_{un}	nondimensional pressure to which shell jumps at buckling and at unbuckling, respectively
$(P_{cr})_N$	normalized pressure, see Eq. (4-4)
Π	total potential energy

$\bar{\Pi}$	dimensionless form of potential energy
q	pressure
q_T	linear buckling pressure
q_{min}, q_{max}	pressures of minimum and maximum points on the load-deflection curve
q_{cr}	buckling pressure
q_m	definition of buckling pressure given by K. O. Friedrichs
q_1	upper buckling pressure as defined by H. S. Tsien
q_2	pressure to which shell jumps at buckling
$(q_{cr})_N$	normalized buckling pressure, see Eq. (4-4)
Q	dimensionless pressure, see Eq. (5-26)
r	radius of shell segment in plan
S	shell surface
σ	stress
σ_{11}, σ_{22}, σ_{33}	stress in ϕ, θ, Z directions
σ_{cr}	critical stress
$(\sigma_{cr})_N$	normalized critical stress
t	time from beginning of loading
t_o	$e^{-\frac{1}{g}}$
τ	variable of integration used in Eq. (4-3)
T	time from beginning of loading to buckling
u_c	deflection tangential to middle surface
u	nondimensional deflection of middle surface tangential to the middle surface (deflection/radius)

U	strain energy
U_E, U_B	extensional and bending components of strain energy
$\bar{U}_1$, $\bar{U}_2$, $\bar{U}_3$, $\bar{U}_b$	dimensionless strain energy terms, see Eq. (5-26)
ϕ	position coordinate, see Fig. 1
v	displacement component in Y direction
V	volume
w_c	deflection normal to the middle surface
w	nondimensional deflection of the middle surface normal to the middle surface (deflection/radius), or displacement in the Z direction
w_o	nondimensional linear deflection
w_1	nondimensional depth of buckle at apex of shell (depth/radius)
W	work of the external forces
	variation of normal displacement through the shell thickness
X, Y, Z	rectangular coordinates
$\bar{X}$, $\bar{Y}$, $\bar{Z}$	surface loads in the coordinate directions
Z	position coordinate, see Fig. 1

CHAPTER 3 HISTORY OF THE PROBLEM

The first attempts to solve the buckling problem dealt with the linearized equations and assumed that buckling occurred when two adjacent equilibrium positions could be found for the same load. The solution of the case with axisymmetric deformations was given by R. Zoelly[1] in 1915. This derivation can be seen in Timoshenko: The Theory of Elastic Stability[2]. The critical pressure is given as

$$q_T = \frac{2E}{\sqrt{3(1-\nu^2)}}\left(\frac{h}{a}\right)^2 \qquad (3\text{-}1)$$

A. Van der Neut[3] later showed that unsymmetric buckling modes did not yield a lower critical value. Hence the linear buckling load for a complete spherical shell was established and served to define the important parameters in the problem. However, experimental buckling loads were generally $\frac{1}{2}$ to $\frac{1}{4}$ of this linear value so other criteria and methods of analyses were tried on the problem.

An important idea was the suggestion that the shell could jump from one position on the load-displacement curve to a position with lower or equal total potential energy if one were available. (A possible curve of pressure versus deflection is shown in Fig. 2.) T. von Karman and H. S. Tsien[4] announced the notion of an energy criterion by defining $q_{cr} = q_{min}$. For the critical load, K. O. Friedrichs[5] suggested q_m, the pressure at a point on the initial part of the curve which had the same energy level as a point on the post buckling curve.

T. von Karman and H. S. Tsien, K. M. Mushtari[6], and V. I. Feodosev[7] were investigators who used the energy or minimum load criterion that $q_{cr} = q_{min}$. Friedrichs used his criterion $q_{cr} = q_m$. All five used an energy method of analysis and all except Friedrichs analyzed a small segment of the dome as an isolated piece. Von Karman and Tsien, the initial investigators, assumed that $\epsilon_{22} = 0$, among other things, but found a q_{min} of .316 q_T, a good estimate of buckling pressures. This investigation also successfully predicted the size of the buckle. Friedrichs discarded many of the assumptions of von Karman and Tsien, refined the equations of equilibrium, and pointed out certain handy mathematical techniques which can be used on the problem. His equations indicated that q_{min} could be negative, thus showing the falsity of either his solution or the energy criterion. It is suggested here that his neglect of the boundary conditions caused occurrence of a negative load.

The first investigators were bothered by the edge conditions on the small segment they analyzed. Feodosev overcame this problem by specifying a deflected shape which could match the slope, shear, and moment induced in the rest of the shell. He found a negative value for q_{min}.

Mushtari, using different equations for deflected shape, and properly applying boundary conditions, found a small positive value for q_{min} (28% and 16% of q_T) in his two analyses. He also critically examined the analyses of von Karman and Tsien, Friedrichs, and Feodosev and pointed out errors in their calculations.

In a separate paper following Friedrich's publication, H. S. Tsien[8] augmented the theories of von Karman and Friedrichs by proposing that the shell should follow an energy deflection curve, rather than a load-deflection curve. He showed that a negative value of q_{cr} would be obtained from the von Karman criterion and that an additional restriction had to be made. Beside the condition that the total potential energy must be the same before and after the jump, he required that either the load must be the same (constant pressure case) or the volume enclosed under the shell must not change (constant volume case). In his analyses Tsien obtained different critical loads in the two cases, q_{cr} for the constant pressure case being about half that for constant volume. A number of tests performed under his direction verified his results for constant volume and one test gave some verification for his results for constant pressure.

The energy criteria have generally been applied only to deep shells or to shells with α at least 4^{o} or greater. The reason for this is that the analyses have been performed on the region of the shell where the dimple should form, neglecting the rest of the shell, and the total angle of the dimple is 7^{o} or 8^{o}

These criteria predict some possible load deflection path which is lower than the route over the maximum point of the curve. The peak of the curve and thus the buckling load may be reduced by imperfections or clamping conditions. Since the energy criteria can be used to find a minimum possible buckling load, the criteria should be useful in predicting the effect of imperfect conditions.

The energy criteria and the analyses based on them lead to a number of effects, some of which can be verified experimentally. The criteria require the presence of adequate external energy to produce a jump and thus it seems that buckling could occur at a range of pressures and not be very reproducible. Presumably the critical loads given in the analyses were minimum values at which buckling could occur and therefore test results should be equal to or above these theoretical values. The difference in buckling loads predicted for constant volume and constant pressure tests is probably the most significant effect and the most readily verified. It is significant because in practical situations of buckling under wind or snow loading, the failure is with nearly constant pressure conditions. Yet the tests of Kaplan and Fung[9], Homewood, Brine and Johnson[10], and most of the tests of Tsien were made with volume control. If it is a fact that buckling pressures with constant pressure tests are much lower than for constant volume conditions, this is important to know.

A number of investigators have attempted to solve the differential equations of equilibrium for the shell segment and have usually considered that the buckling load was the maximum point on the load-deflection curve. Cylindrical coordinates have been employed and the analysis has been restricted to fairly shallow shells (rise to span less than 1/8). The technique used has been to expand the dependent variables in terms of a power series of the center deflection to thickness ratio. Then the coefficients of the series are required to satisfy the governing differential equations. A. Kaplan and Y. C. Fung[9], R. R. Archer[11],

and H. J. Weinitschke[12a] have used variations on this method and found it gives results near test values only for very shallow shells. It can be pointed out from the analytical results of Weinitschke and Archer that, with enough terms in the series, an accurate value for critical load can be found. (That is, accurate theoretically, but not necessarily near experimental results) Therefore, it is apparent that the deflected shape is a series in which an extremely large number of terms is important.

The energy or variational approach has been used with the deflection expanded in a power series. With this method the investigators have found results only up to $\lambda = 7$. G. P. R. von Willich[13] derived the necessary equations and found results using only one parameter. W. L. Chen[14] used the same technique and two parameters. A. B. Caseman[15] extended the investigation to three parameters.

Chen also investigated the effect due to various types of symmetric imperfections such as grooves at midheight in the shell. His results show that the effect of an imperfection may be either positive or negative depending on the magnitude of the imprefection and the depth of the shell. Hence a correlation between imperfections and buckling loads is rather complex.

In dealing with shallow shells, many investigators have replaced the spherical segment by a paraboloid with the same height and plan dimensions. The approximation has the effect of introducing a symmetric imperfection with a magnitude of about $.002(h^2/a)\lambda^4$ at midheight on the shell. It can be seen from the formula that the error increases rapidly with λ.

H. B. Keller and E. L. Reiss[16b] have used a finite difference approach fairly successfully in the shallow shell range to define q_{cr}. They also found q_2 and q_m, the intermediate value suggested by Friedrichs.

Four recent attempts have been eminently successful in determining buckling loads for a large range of λ. These are of particular importance since they essentially agree on critical loads. Weinitschke[12b] augmented his earlier power series approach by expanding the series from both the center and edge and matching the terms at an interior point. This decreased the convergence problem a great deal because both series were shorter than a single series expanded about the apex, and the accuracy was correspondingly higher. G. A. Thurston[17] used a numerical integration technique to find solutions at various points up to $\lambda = 9$. B. Budiansky[18] transformed the governing differential equations into two simultaneous integral equations and found good results up to $\lambda = 13$. With the energy method Caseman found results up to $\lambda = 7$. Since these four methods are essentially different from each other, yet their results agree very well, it is reasonable to conclude that the buckling loads for the perfect shell under symmetric deformation have been determined in the shallow range. The buckling loads found in these analyses are plotted in Fig. 11.

It may be mentioned that all the deflected shapes used in the preceding analyses have been based purely on mathematical considerations, not on the appearance of the shell surface during loading.

Budiansky also considered the possibility of central imperfections and found a significant decrease in load for large imperfections. The central imperfection is deceptive since it implies a change in radius as well as an axisymmetric groove at midheight. If the central height is assumed to determine radius, then the imperfections of Chen and Budiansky are found to be quite similar. In fact, b, the imperfection magnitude of Chen is $3/16(\varepsilon H)$, where εH is the error in central height in Budiansky's notation. The effect of simply an error in height (and therefore in radius) can be found from the linear buckling load, rewritten as follows

$$q_T = \frac{Eh^2}{2\sqrt{3(1-\nu^2)}\, r^4} H^2$$

where r is the radius of the shell in plan and H is the central height of the shell segment. A small change, ΔH, in H gives a corresponding change in q_T of

$$\Delta q_T = \frac{Eh^2}{2\sqrt{3(1-\nu^2)}\, r^4} 2H\Delta H$$

Therefore

$$\frac{\Delta q_T}{q_T} = \frac{2\Delta H}{H} = \frac{2(\varepsilon H)}{H} = 2\varepsilon \qquad (3\text{-}2)$$

and ε is the nondimensional error in central height according to Budiansky. He obtained reductions of 10% to 30% in buckling load for $\varepsilon = 0.05$. A decrease of 10% caused merely by the change in radius could be found from Eq. (3-2). In addition, q_{cr} is a function of λ as well as of the variables in q_T and λ in turn is a function of

$\sqrt{H}$. Therefore a change in H should shift the curve of q_{cr} versus λ (see Fig. 11) down by $\frac{2\Delta H}{H} q_{cr}$ and to the right by $\frac{1}{2}\frac{\Delta H}{H}\lambda$. This predictable effect seems to be verified by the plots of buckling load given by Budiansky (and not reproduced herein).

Budiansky and Weinitschke have suggested that probably the consideration of unsymmetrical deformations will help to provide critical pressures closer to experimental values. Weinitschke stated in reference 12b that the circumferential stresses which he obtained were sometimes as high as twice the meridional stresses, thus suggesting the possibility of nonaxisymmetric buckling. A simple linear analysis by Rabotnov[19] showed that buckling should occur when either of the two stresses reached a critical value.

Extensive sets of tests have been performed by Kaplan and Fung; Tsien; Homewood, Brine, and Johnson; and K. Kloppel and O. Jungbluth[20]. The buckling loads obtained by these investigators are shown in Fig. 12. Kaplan and Fung performed an essential service by carefully testing a number of magnesium shells with λ values between 4 and 10. They not only found buckling loads, but also measured initial imperfections and deflected shapes as the shell approached buckling. The measurements were plotted to show that during loading (before buckling) the shell could form either a central dip, or a symmetric furrow about the shell between center and edge, or both dip and furrow, or some unsymmetric shape. Furthermore, the particular form depended on the value of λ, the more complex shapes occurring with the larger λ.

These different deflection patterns have usually been referred to as modes of deflection and appear quite similar to vibration modes. Reiss, Greenberg, and Keller[16a] Weinitschke, and Budiansky have also mentioned the changes of mode shapes. As λ is varied the mode seems to change at about $\lambda = 3.2, 5.3, 8.8, 16, 25, \ldots$ (These are equal logarithmic steps). The first value of λ is about the minimum at which buckling occurs. Between 3.2 and 5.3 a central dip forms during loading. Between 5.3 and 8.8 the maximum deflection may occur in a symmetric furrow about the shell. Beyond this point there is confusion as to whether the mode is symmetric or unsymmetric, and the changeover points are not well defined.

The tests of Tsien were for shells in a deeper range, from $\lambda = 15$ to 25 and the buckling loads were equal to or slightly above those of Kaplan and Fung.

Kloppel and Jungbluth tested a large number of ribbed domes to find the effect of stiffeners on buckling strength. Their shells were made by welding a series of meridional and circumferential ribs to a thin shell dome so that the structure became a composite of thin shell and frame types. There is no theoretically predicted buckling load for such a structure so it was assumed to be a uniform shell with some effective thickness.

An expression which can be used for this effective thickness is

$$Eh^2 = \sqrt{12\, S_E S_B} \qquad (3\text{-}3)$$

where S_E is an average extensional stiffness (Eh for a uniform shell) and S_B is the average bending stiffness ($\frac{1}{12}Eh^3$).

Kloppel and Jungbluth tried many combinations of rib sizes and distributions yet their buckling loads were rather close together as seen in Figure 12. Their procedure for finding an effective thickness (which is similar to Eq. 3-3) was somewhat validated by this lack of dispersion. Tests were performed under air pressure so that when failure occurred it was sudden and complete. Many of the specimens exhibited local failure before the snap-through tock place. It may be postulated that local failure occurred in all cases, but it was only observed in those where buckling did not occur immediately thereafter.

The buckling loads of Kloppel and Jungbluth are considerably lower than those of Tsien in the same range and this fact may be explained partially by the occurrence of local buckling and partially by the assumed equivalence of frame and uniform shells. Since many dome structures are actually composite, the work of these two investigators has a great deal of practical significance.

Quite recently R. H. Homewood, A. C. Brine, and A. E. Johnson[10] made a series of tests with λ from 6 to 20, thus connecting the experimental ranges of Kaplan and Fung and Tsien. Their results agreed well with Kaplan and Fung but were considerably below the buckling loads of Tsien. Two of their shells unbuckled when the pressure was removed showing that the material had not been stressed beyond the elastic range. These two were subsequently re-buckled and the second

buckling loads were nearly equal to the critical loads obtained the first time. Hence some reproducibility of buckling loads could be deduced from these tests.

The combined test results show a fairly large scatter, particularly between buckling loads of different investigators. The dispersion between test results of separate experimenters may be attributed to differences in shell material, test apparatus and procedures, clamping conditions, and the range of λ used.

The analyses and tests performed thus far have been adequate to solve a few problems of buckling and to raise a myriad of questions. From the tests it can be predicted that q_{cr} is between 15% and 80% of the linear buckling pressure. The shell surface does not remain uniform during loading but forms waves and the number of waves is partially predictable. A curve of buckling pressure versus λ has been found analytically for symmetric deformations of shallow shells, but this pressure does not correspond well with test results. The convergence of iteration, perturbation, and finite difference techniques often is not adequate near the buckling point. This suggests that the correct deflection shape is a power series with a large number of important terms. Imperfections have been considered both analytically and experimentally and so far the only indication is that the effect of imperfections is rather complex.

The scatter in test results and the disagreement between theoretical and experimental buckling loads prompted the author to consider a number of questions. The investigations of this report were designed to provide some answers for these problems. Some of the pertinent questions were the following:

1. Are imperfections important? What is the effect of size, shape and position of imperfections on buckling?

2. Are clamping conditions important?

3. Are buckling deformations symmetric?

4. Are buckling loads reproducible?

5. Is an energy criterion valid so that the critical loads depend on the ambient energy level?

6. What is the position of the dimple which forms at buckling and does the position affect the critical load?

7. Does the type of loading -- constant volume or constant pressure -- affect the buckling pressure?

8. Is buckling precipitated by yielding or local failure in cases where q_{cr} is below the analytically predicted pressure?

CHAPTER 4 EXPERIMENTAL STUDY

A Introduction

The purpose of this experimental project was to investigate the nature of buckling of thin, clamped, spherical shells under uniform pressure. Under this general topic the following specific items were considered:

a. Shape of the load-displacement curve from no load to post-buckling and the rebound or unbuckling curve.

b. Size, shape, and position of the buckle which formed.

c. Reproducibility of buckling loads.

d. Eifect of shell imperfections or clamping conditions on the load-displacement curve and the buckling load.

e. Effect of creep on the buckling load.

Most of the tests were performed with control of the volume enclosed under the shell and were therefore so-called constant volume tests. This name comes from the fact that the enclosed volume does not change during buckling. Such a restriction can be accomplished by having an incompressible fluid filling the space under the shell. This type of test was chosen so that a load-displacement curve could be determined since both pressure and a measure of deflection were known at any time. The change in enclosed volume is proportional to the change in average deflection of the shell under an increment of pressure. The constant volume test was also chosen so that the buckling process could be partially controlled and forced to occur

gradually. In addition it seemed desirable to have either constant pressure or constant volume conditions so that the results could be applied to the discussion of the energy criterion of Tsien. (In a constant pressure test, the pressure remains constant during buckling.)

In a practical situation the conditions often approximate those of a constant pressure test. Consider a hemispherical structure under a wind loading. If buckling occurs and a dimple forms, the internal air may be compressed and produce some small resistance to volume change. Thus the buckling action, although mainly a constant pressure situation, is really somewhere between constant pressure and constant volume. Therefore it was necessary to make some constant pressure tests. The latter tests were made with the same conditions as the constant volume tests so that a relation between buckling loads in the two cases might be found. With such a relation, buckling loads in practical situations could be predicted from the results of constant volume tests.

In the usual structure pressure is not uniformly distributed over the shell but may have a variety of patterns. However, the rate of change of pressure over a shell surface is usually small and buckling would probably occur under a region of maximum pressure. If only the small segment which forms a buckle is considered, there is nearly a uniform pressure applied. Therefore, it is reasonable to test using a uniform pressure. Also the uniform case is easier to reproduce and easier to compare with other test results. A uniform pressure was therefore used in these tests.

A plastic was chosen as the shell material rather than aluminum or other light metals which have usually been used. There were a number of reasons for preferring a plastic material. A plastic was relatively inexpensive and easy to form by vacuum drawing; it had reasonably small thickness variation; and there was no strain-hardening nor residual stresses developed during the forming operation. It was desired to test entirely in the elastic range of the material so that each shell could be buckled many times and not cause material failure or yielding. The large ratio of yield stress to modulus of elasticity for the plastic allowed the large deformations of buckling to occur while the strains remained elastic. An added benefit was that the pressures used for testing the plastic shells were 1/20 to 1/60 of that for comparable metallic shells. With the lower pressures, the equipment was simpler, less expensive, and more convenient to use. One difficulty with the plastic material was its creep characteristic. The nature of this creep was investigated so that test results could be reported in a uniform and meaningful manner and extended to apply to non-creeping materials. The particular plastic chosen was a polyvinyl chloride which was available in thicknesses from 0.010" to 0.080".

As mentioned in Chapter 3, the form of deflection seems to change at certain values of λ. To study the effect of the mode changes on critical loads, it was decided to test a number of shells with λ values at 3.2, 5.3, 8.8, 16, and 25, that is, at the supposed changeover points. As a check, shells with $\lambda = 7.0$, 12 and 20 were also used. To study reproducibility of loads and variations of loads between shells, a large

number of shells were formed for $\lambda = 7.0$ and 12. In Fig. 13 it is apparent that the tests are grouped about certain values of λ. That the results are in groups instead of a single line shows that the desired λ's were only achieved approximately. Procedures described below were used to find the dimensions of the shells after forming and these dimensions were used in computing the λ for each shell. After choosing λ's, it was necessary to select values of thickness and radius which would give the desired λ's. This choice was limited by specifying that the buckling pressure must be greater than 0.05psi. and that the sum of bending and extensional stress at the edge must be less than 500 psi at $q = \frac{1}{2} q_T$. From Fig. 3 it is apparent that these restrictions left only a narrow region for acceptable combinations of $\underline{h}$ and $\underline{a}$. The possibility was considered that λ was not the only necessary shape parameter. Consequently, where possible alternate combinations of $\underline{h}$ and $\underline{a}$ were made for a single λ. The small circles in Fig. 3 show the combinations which were chosen. For each set several shells were formed and tested. In the experiments a total of 39 shells were used.

Due to the presence of creep the test procedures are quite important and are described in detail. The test results are discussed with a view to answering some of the questions which have been raised by earlier tests and analyses and which are mentioned in Chapter 3.

B Preparatory Considerations

- Shell Forming -

The shell segments were formed from polyvinyl chloride (P.V.C.) sheets by a process known as vacuum drawing. In this method a single mold, the female, was required. The plastic sheet was heated, drawn into the mold, and allowed to cool in the new shape.

Since the shells were to have five different radii -- 15", 25", 35", 45", and 80" -- as shown in Fig. 3, five molds were needed. These molds were made from aluminum plate with a thickness at least ½" greater than the height of the shell to be formed. In Fig. 4A there is a sketch of one such mold. Aluminum is relatively easy to machine but has better surface and is stronger than many of the other possible mold materials such as wood or graphite. A cavity with one of the desired radii was machined in the plate and a 1/16" diameter hole was drilled in the center of the cavity for access to the vacuum.

The rest of the forming equipment can be seen in Fig. 4A also. The wooden clamping rings held the sheet in place during forming. The large cylinder was needed to provide a vacuum chamber and to hold the sheet slightly above the mold so that the mold was insulated while the sheet was being heated. The cylinder was located in a large oven and a line to a vacuum pump was connected to control pressure in the cylinder.

The forming process began with the cutting from a polyvinyl chloride sheet of a circular piece with the diameter of the wooden

clamping rings. The piece was rinsed in hot running water to remove grease, dust, and other foreign particles. Wiping the sheet clean was not feasible due to electrostatic effects. yet cleaning was necessary or bumps would appear during forming. The piece was clamped into the wooden rings with negator clamps and placed in the oven atop the cylinder as shown in the lower sketch of Fig. 4A. With the sheet to be formed in place, the oven was heated to 150° - 170°C. The sheet seemed to be properly heated when the steam from the rinsing water had disappeared from it. Then the vacuum of one atmosphere was applied and the sheet immediately dropped to fit the mold. The heat was turned off and the oven opened to speed the cooling. About one minute was allowed for annealing and then cold water was poured in to fill the cavity in the center and the gutter which formed just outside the mold (see the second sketch in Fig. 4A). The newly formed shell was allowed to cool under full vacuum for 5 to 15 minutes. The longer period of cooling was required for the sheets 0.080" thick while the thinnest sheets needed only a very short time. After the cooling process the vacuum was turned off and the shell was lifted out of the mold. Then shell and rings were dashed together into a vat of cool water so that the shell could cool uniformly, and the rings were removed. At this time the mold was also taken out of the oven so that it would be cool for the next forming.

The finished shell was then examined to find any visible imperfections caused by the presence of steam, etc. If the fault was in the forming, the cycle could be restarted by rinsing, reclamping and heating as before.

On heating, the shell became planar again and was ready for redrawing. If the shell passed inspection, the excess edge material was trimmed off so that only 3/4" of flat rim remained and the specimen was ready for testing (see Fig. 4A).

The vacuum drawing process described above gradually evolved during the production of the shells for this research. Hence some of the imperfections in the first shells produced were eliminated in later production. The rim slope (see Fig. 7) was caused by too short a cooling time under vacuum and/or not enough heat. Watermarks (shallow bumps) were caused by trapped steam. Either of these imperfections could have been corrected by reheating and redrawing.

- Shell Shape Determination -

After forming the shells it was necessary to find the thickness and radius to which the shell actually conformed. Thicknesses were read to the nearest ten thousandth of an inch with an Ames Dial gage at five positions in the shell - one at the apex of the shell, and the other four at points halfway between the apex and the edge. An average of the five readings was taken as the shell thickness. The thickness variation was about 1% except for the very thin shells where variations were 10% to 12%.

The radius of the spherical shell can be found if the rise in the center is known. The rise was measured to the nearest thousandth of an

inch. Radius was then computed from the formula

$$a = \frac{r^2}{2H} + \frac{H}{2} \qquad (4\text{-}1)$$

where H is the central rise of the shell, and r = 5.25", the radius of the supported circular edge as seen in plan. Unfortunately some of the rims of the shells were not flat but had a slope either upward or downward as shown in Fig. 7. The radius determinations for these shells were made while the shells were clamped into the testing cylinders in order to obtain the "a· tested" radius if possible.

- Creep Effect on Buckling -

The creep behavior of the plastic material used in the experiments is similar to that found in most plastics. The total creep strain at low stress levels was fairly small, around 5% (at room temperature). The creep rate was very high so that creeping was essentially complete in twenty minutes. The creep became nonlinear for stresses over a few thousand psi, that is, the creep rate became a function of stress level as well as of time. The creep rate varied somewhat with temperature and humidity. At moderate stresses the creep could be termed elastic since the strain was completely recovered after some time. In fact, the unloading curve matched the loading curve.

For the polyvinylchloride material used in the experiments the following formula was found to describe the stress-strain relation

adequately:

$$\varepsilon = \frac{\sigma}{E_1}[1 + g \ln(t + t_o)] \qquad (4\text{-}2)$$

In order that $\varepsilon = 0$ at $t = 0$, t_o was defined by

$$1 + g \ln t_o = 0 \qquad \text{or} \qquad t_o = e^{-\frac{1}{g}}$$

This makes t_o extremely small so that it can be neglected for most purposes but it makes the evaluations of the integrals more reasonable. g is a creep coefficient and E_1 is the modulus at one minute after loading.

In order to find the effect of creep on the critical load, certain assumptions were made. As some investigators have suggested, buckling occurs when a critical strain is reached at some point in the structure and does not depend directly on the stress level. In the following derivation the strain was assumed to be a linear function of displacement. This condition is reasonably correct to the point of buckling, after which nonlinearities become important.

The applied load may not be constant but vary with time τ. In this case Eq. (4-2) is still applicable but the stress and strain must be replaced by the infinitesimal quantities $d\varepsilon$ and $d\sigma$. A general treatment of creep strain relations is available in reference 27. As shown there, in a short time interval from τ to $\tau + d\tau$ the stress is changed by $\frac{d\sigma}{d\tau} d\tau$. At some later time t, the load $\frac{d\sigma}{d\tau} d\tau$ has been on for a time $t - \tau$. The increment of strain caused by this load can be seen from Eq. (4-2) to be

$$d\varepsilon = \frac{1}{E_1}\frac{d\sigma}{d\tau}d\tau\left[1 + g\ln(t - \tau + t_o)\right] \qquad (4\text{-}3)$$

In this equation τ can assume any value from 0 to t. The total strain at the critical point in the shell at any time t can be found by integrating the preceding equation with respect to τ from $\tau = 0$ to $\tau = t$.

$$\varepsilon(t) = \frac{1}{E_1}\int_0^t \frac{d\sigma}{d\tau}\left[1 + g\ln(t - \tau + t_o)\right]d\tau$$

If the load is applied at a constant rate, then $\sigma = \sigma_{cr}\frac{\tau}{T}$ where T is the time at buckling.

$$\varepsilon(t) = \frac{\sigma_{cr}}{E_1}\frac{t}{T}\left[1 - g + g\ln(t + t_o)\right] = \frac{\sigma_{cr}}{E_1}\frac{1}{K(t,g)}$$

When t = T, the time at buckling, $\varepsilon(t) = \varepsilon_{cr}$, and the critical stress is

$$\sigma_{cr} = E_1\varepsilon_{cr}K(T,g)$$

where $$K(T,g) = \frac{1}{1 - g + g\ln(T + t_o)}$$

A normalized stress can be defined as

$$(\sigma_{cr})_N = \frac{\sigma_{cr}}{K(T,g)} = E_1\varepsilon_{cr}$$

The normalized stress is a function only of E_1 and ε_{cr}, neither of which is a function of the duration of loading T, or the creep coefficient g; therefore, $(\sigma_{cr})_N$ is not a function of T or g. If stress is

proportional to laod, then normalized buckling pressures can be similarly defined.

$$(q_{cr})_N = \frac{q_{cr}}{K(T,g)}$$
$$(P_{cr})_N = \frac{P_{cr}}{K(T,g)} \qquad (4\text{-}4)$$

P_{cr} is a nondimensional form of buckling pressure defined as the critical pressure, q_{cr}, divided by the linear buckling load, q_T.

In equation (4-4), q_{cr} is the actual pressure measured dur ng the test and $(q_{cr})_N$ can be interpreted as the pressure for a hypothetical test with a duration of 2.728 minutes; that is, for $K(T,g) \doteq 1.000 + \frac{}{2.728} \doteq 1.000$ (since t_0 can be neglected). If the theory is correct, the normalized pressure, like the normalized stress, is not a function of either T or g. Hence, this value of pressure can be compared to the buckling loads for noncreeping materials for which g is zero.

Since creep adds a certain amount of nonlinearity, it is of interest to find the effect of creep on the shape of the load-deflection curve up to the point of buckling. An estimate of this effect was obtained using the constants mentioned previously and a T of twenty minutes. Then points on the stress-strain curve were obtained for various values of t from the equation

$$\varepsilon(t) = \frac{\sigma_{cr}}{E_1}\frac{t}{T}\left[1 - g + g \ln (t + t_0)\right] \qquad (4\text{-}5)$$

A linear extrapolation of the initial portion of the curve was made to obtain a stress at the abscissa of critical strain. This value from the linear extrapolation was then compared with the critical stress obtained from

the equation. The difference in this case was only 0.3%. Therefore it is fairly safe to say that creep did not account for nonlinearities found in the load-deflection curves.

- Modulus Determination -

In order to relate these test results to other materials, some procedure had to be found for evaluating the modulus of elasticity. Simple tensile tests were run on samples of each sheet using SR-4 strain gages and a dead weight. Beam tests were also run in an attempt to determine the compressive modulus in case it differed from the tensile. Both sets of tests were conducted on 6" by $1\frac{1}{2}$" specimens. In the beam tests the specimens were supported as simple beams with a load at the midpoints and the end rotations were measured by the motion of a wire fixed to the beam near the end. Although the beam deflections were extremely large, the relation between load and end rotation was essentially linear. In Appendix B it is shown that the end rotation equals

$$\gamma_L + \frac{\gamma_L^3}{6} + \cdots$$

where γ_L is the end rotation in the linear theory. Hence for a rotation of 6° or 0.1 radians, which was about the maximum used, the nonlinear correction was less than 0.2%. Because of the presence of creep, the modulus changed with time. It was decided to use E_1, the modulus at one minute after loading. E_1 is defined by the creep equation

$$\varepsilon = \frac{\sigma}{E_1}\left[1 + g \ln (t + t_0)\right] \qquad (4\text{-}2)$$

Since t_o is negligible, t = 1 minute gives $\varepsilon = \frac{\sigma}{E_t}$ and there is no creep correction required for the determination of the modulus. The beam tests gave the most uniform results for modulus, the average value being 498,000 psi. A summary of these determinations is in Appendix B.

The tensile tests were not so reliable due to the presence of the strain gages. On such small specimens the stiffness of the gage produced an important effect on the strains and hence on the modulus of elasticity. However the electric strain gages could be read with more precision than the beam rotations. Therefore the gages were valuable in determining creep which is a small variation on the total strain. Hence the creep equation (4-2) and creep coefficient, g, are based on the tensile tests mainly. Results from these creep and modulus tests are also given in Appendix B.

C Testing

- Test Apparatus -

The main tests were constant volume tests which required the presence of an incompressible fluid in a chamber below the shell (shell convex up). Water was selected as the most convenient fluid for this purpose. But with water below and air above the net pressure on the shell would be hydrostatic and vary over the shell surface. Therefore there had to be a water chamber above the shell also. Tests were run by applying a displacement and measuring the pressure taken by the shell. Hence the required apparatus was a set of water tight chambers between which the shell could be clamped, a device for withdrawing water from the lower chamber, and a system for measuring pressures above and below the shell.

The completed equipment can be seen in Fig. 4. The lower chamber consisted of a heavy pipe section bolted to a base plate. These two pieces were rather heavy so that they would not alter the enclosed volume much as the pressures changed. The upper chamber was made of plexiglas and allowed observation of the shell, the buckles, and bubbles which were trapped in the chambers. Holes for inlets and outlets were made at three places around the lower chamber. These were necessary in order to allow the water to come in and the air bubbles to be forced out. It was found convenient to use water from a large jug which maintained a nearly constant water temperature so that the volume would not change due to temperature fluctuations.

The tubing which connected the reservoirs, chambers, and manometers was of transparent plastic which allowed observation of bubbles in the line. When bubbles were present, the manometer readings were very unsteady since each motion of the bubbles seemed to upset the equilibrium of the gages, too.

The manometers were capillary tubes with an inside diameter of 1.8 mm. These were used so that when the pressure changed, the change in the amount of liquid in the tube would not greatly alter the total volume under the shell. The tubes for registering upper and lower pressure had equal diameters so that the capillary rise ($\frac{1}{2}$" to 1") would be the same and no correction was required. The capillary rise was quite a bit larger in pure water than in impure and so small amounts of liquid soap were added in both tubes to make certain the water was impure. The soap reduced wall friction between glass and water and so also produced freer and more accurate motion of the water.

The faucet for allowing withdrawal of water from the lower chamber was at first a high vacuum glass valve. Later the valve was replaced by a short rubber tube with a small clamp on it. With the clamp there was good control of the rate at which water drops came out so that a desired speed of volume change could be maintained.

The rubber gaskets used in clamping the shell may have caused some inaccuracies. The narrow rim all around each shell was supposed to be clamped against all motion. However, the thick gaskets in the

clamping rings probably allowed some outward displacement and rotation of the edges. Rough calculations show that the amount of displacement would be quite small compared to the total shortening of a meridian and is therefore not too important as a cause for snapping through. The edge rotation would not approach that for the simply supported case, yet the theoretical buckling load for the latter case is at least 3/4ths of that for the fixed condition according to the calculations of Weinitschke[12b].

- Test Procedure -

There were two basically different types of tests used. The constant volume test was the most important and it was of the controlled displacement type. It proceeded much like an ordinary tensile test. A certain strain or displacement was applied to the shell and the pressure which was required to make the shell stay in that position was read. The other type, the constant pressure test, was carried out by increasing the load until buckling occurred and hence the control was on the load, not on the displacement.

Preparation for the constant volume tests was commenced by placing the shell between the clamping rings of the test cylinders and bolting them together, as shown in Fig. 4. Then the chambers were filled with water, beginning with the lower chamber. The tube to the top chamber was connected to the small elevated reservoir and the tube to the lower chamber was connected to the taller capillary tube as shown in Fig. 4.

Equal heights were obtained in the upper and lower chamber manometers by letting water either in or out of the lower chamber through the faucet. To force water in, the reversing standpipe shown in Fig. 4 was attached to the valve and filled with water. With equal pressure above and below the shell, the shell was sustaining a net load of zero.

Testing began by opening the faucet and allowing a number of drops of water to come out from the lower chamber. The shell had to move downward in order to keep in contact with the water and thus the displacement was applied to the shell. Of course, a certain pressure was required to hold the shell in the deflected shape and this pressure was given by the difference between pressures in the upper and lower chambers. Hence the load on the shell could be found from the readings of the two manometers. So the normal procedure was to open the tap, let out a number of drops, close the tap, read manometers, and then repeat. The information recorded in each cycle was the number of drops and both manometer readings. At buckling the height in the lower chamber manometer increased suddenly and readings were taken both before and after the jump. Then the usual procedure was continued on to some point in the post-buckling range. For deep shells the q_2, the pressure to which the shell jumped at buckling, and q_{min}, the pressure at the minimum point of the load-deflection curve (see Fig. 2), coincided and so the test was often halted just after buckling. For shallower shells, the curve looked more like the one in Figure 2 and the test was continued until q_{min} had been passed. See Figure 10 for some typical load-displacement curves.

After the test the total amount of water taken out during the test was determined by weighing. This information was used to associate a volume change with each pressure reading by apportioning the total change according to the total drops up to each point. For plotting load versus volume change curves, it was necessary only to plot the pressure versus the cumulative number of drops. The drops were found to be somewhat nonuniform in size but not enough to make the initial portion of the load-deflection curve appear nonlinear. Therefore, the number of drops was probably an adequately reliable measure of volume change.

In order to unbuckle the shell the reversing column was attached to the faucet. Then the normal testing procedure was to open the tap, allow a certain amount of water to run into the lower chamber, close the tap, and read the heights of manometers and reversing column. The difference between the current reversing column reading and the previous one gave the volume change because the column was calibrated. The procedure was repeated until some point on the initial portion of the load-deflection curve was reached.

With the presence of creep, time became a factor in the test. The steps of the constant volume test enumerated below were adopted to standardize the effect of time.

a. The pressures in the water manometers and the time were recorded.

b. The tap was opened to allow a number of drops (say 10) to escape from the lower chamber and the number was recorded.

c. Again the pressures in the gages were read and noted. At some specified time (say 30 seconds) after the last time the tap was opened, step b was repeated. By using an equal time interval during each cycle, the loading rate was made to be constant stepwise.

d. At buckling the tap was immediately turned off and the time, pressure readings, and number of drops in the last cycle were recorded. The remainder of the experiment proceeded without being timed.

e. Steps b and c were repeated until the desired point on the post-buckling curve had been reached.

The loading process was then reversed by attaching the reversing column to the tap and filling it with water. In the rebound test a procedure similar to that above was followed.

a. The pressures in the water manometers and the height of the reversing column were read and recorded.

b. The tap was opened to allow a number of centimeters of water from the column to enter the lower chamber.

c. Steps a and b were repeated until the shell had unbuckled and the pressure was reducing along the initial portion of the load-deflection curve. See Fig. 10 for some typical rebound curves.

The preceding tests give a complete curve of load versus displacement measured in terms ofthe change in volume under the shell. After the nature of this curve was known for a shell or a group of similar shells, the only things that were required of further tests were certain significant pressures on the curve such as q_{cr}, q_2, q_{un}, and q_{min}. The following modified procedure gave these important pressures and was used for a majority of the tests.

a. The time was noted and the tap was opened.

b. A uniform drop rate was maintained. This was done visually for short buckling times, but for long tests, the rate was kept even by passing an equal number of drops each minute.

c. While keeping a uniform drop rate the pressure in the lower chamber manometer was observed continuously.

d. When buckling occurred, the faucet was shut off, and the time and the reading of the lower manometer prior to buckling were recorded. The pressure in the upper chamber manometer was read and recorded. At one minute after buckling the height of the lower manometer was read again. This latter reading was taken to find the so called lower buckling pressure, q_2, Just after buckling the height in the lower manometer was changing rather rapidly due to creep so the specification of a one minute wait was necessary to make the readings uniform.

e. The faucet was turned on again and the height of the lower manometer was observed. If the height increased and then decreased (pressure on the shell decreased and then increased) then a reading was taken at the maximum to give q_{min}. Otherwise it was assumed that $q_2 = q_{min}$.

f. The reversing column was used as before to force water back into the lower chamber. The tap was turned on and the lower chamber manometer was observed.

g. The warning for the onset of unbuckling was a gradually accelerated decrease in gage height. Near the time of unbuckling the tap was turned off and the shell was allowed to unbuckle without outside influence.

h. At one minute after unbuckling, the two gage readings were taken and recorded. The creep in gage height was generally not large in this case but still noticeable.

After the pressures in the two chambers were equalized following the test, a period of 20 minutes was allowed to elapse before the next test was commenced. This wait time seemed necessary so that the shell would have essentially no memory (due to creep) of the previous test.

In order to check the reproducibility of buckling loads, a series of tests was run without removing the shell from the testing cylinders. Then the shell was taken out and replaced in the test chambers and tested again. This procedure also served to demonstrate the effect of precision in clamping the shell in position.

After a series of constant volume tests had been run on some of the shells, the water was emptied out and a "constant pressure" test was run. Actually the volume of air was not great enough to allow for full collapse of the shell under the same pressure, but the test approximated constant pressure conditions to some degree. This degree may be estimated from the fact that a lower buckling load was obtained and that the buckle was about the same size as that for constant volume tests. The main distinction then was that the pressure was applied,

not the displacement. In these tests a U tube manometer and pressure inlet were both attached to the upper chamber. The lower chamber was open to the atmosphere. Pressure was built up gradually and the manometer was watched continuously. When buckling occurred, the maximum manometer height and duration of the test were recorded.

D Experimental Results

- General Discussion -

The data from both constant volume and constant pressure tests are given in Table 1 of Appendix A. The tests reported were made in accordance with the procedures just described. Individual tests are not reported, only series of tests which were made under the same conditions. For instance "a" is the designation for a series of constant volume tests and "a(air)" is a series of constant pressure tests run under the same clamping conditions as the constant volume tests. The values of P_{cr} in each series were normalized according to Eq. (4-4) and then averaged. This procedure removed the effect of different lengths of time in testing. Under series "a" were reported the averaged values of $(P_{cr})_n$, P_2, P_{un} and the position of the buckle which formed. Notice that during any series the buckle occurred in the same position. The one exception to this is the second series of tests on number 35.

The buckle and imperfection positions were given as:

- c center of shell
- n near center
- m midway between center and edge
- e adjacent to edge

For each shell the values of q_T, λ, a/h, and α are listed. This is followed by a brief description of observed imperfections. First was the slope of the rim of the shell. If the edge strip curled up (with

the shell convex up) after forming a positive slope was indicated. Next was the estimate of the height of bumps and their location on the shell.

From any series of tests run under the same conditions, it was found that the value of q_{cr} was nearly the same in all tests. When the buckling pressures were normalized according to Eq. (4-4) to account for creep, then the variations were less than 1% within any one series. With such small variations it was possible to conclude that buckling pressures were reproducible and dependent on conditions which were actually unvaried during a series of tests. Between series of tests there was much more spread in the buckling loads, but the variations were still of the order of 5 or 10%, which is quite reasonable. The greatest variations occurred between different shells with supposedly the same shape. In a number of cases the critical load for one shell was 50% of that for another with the identical gross dimensions. A number of test series were made with large variations in test durations in order to check on the creep correction, Eq. (4-4). One such series is plotted in Fig. 6 and from the correlation shown there between theory and experiment, it is apparent that the correction is of about the right magnitude.

The buckling pressures from the air pressure tests averaged about 3% higher than those from constant volume tests. This comparison is made between results from experiments all made without changing clamping conditions. That the conditions were quite constant between

the two types of tests is shown by the fact that the buckle formed in the same position in both cases. No explanation has been found for the increase in load under constant pressure conditions.

The value of λ for the shells were chosen at the points where the modes of deflected shape were expected to change, and at intermediate points. The buckle position does not seem to depend noticeably on whether or not λ is at a changeover point or not (Fig. 9a). Neither is there any particular difference in buckling pressures between shells in the two groups.

The nature of q_2, the pressure to which the shell jumped at buckling, and q_{un}, the pressure found at unbuckling, contrasted markedly with that of q_{cr}. (q_2 and q_{un} are from constant volume tests only.) The spread between q_2 and q_{un} was not very great as shown in Fig. 13. In fact it was reasonable to draw in the trend lines shown. In view of this uniformity of averaged results, it was surprising to find that q_2 and q_{un} were actually not very reproducible under the same conditions. For instance, in a single test series in which there was little variation in q_{cr}, the spread in values of q_2 might be 10% or even 30%. The variations between values of q_2 in different series was not greater than the variation within the series. Apparently all the conditions which affect the value of q_2 and q_{un} were not under control. No corrections were made for creep and that may have been a partial cause of the variations.

For the deep shells there was a long, level portion in the post-buckling curve and q_2 and q_{min} both fell on this part, so that $q_2 = q_{min}$. In the shallower shells q_2 was sometimes quite different from q_{min}. The upper sketch in Fig. 10 is for such a shallow shell.

Not all of the important pressures -- q_{cr}, q_2, q_{un}, and q_{min} -- depended solely on λ, although this shape parameter was dominant in most cases. From the plot of P_{cr} versus λ in Fig. 13a it can be seen that $P_{cr} = q_{cr}/qT$ was essentially independent of λ and there was enough spread in the data to obscure any minor trends. There is just a slight tendency for P_{cr} to decrease with increasing λ. q_2 and q_{un} seemed to be related more closely to λ, as evidenced by the trends seen in Fig. 13. In fact, q_2 and q_{un} were replotted versus α and versus a/h, but much better correlation was found in the plots with λ as abscissa. Since many analysts have predicted a negative value for q_{min} (which equals q_2 for large λ), it might be expected that q_2 would at least tend to zero as λ increases. Extrapolation is risky with such scattered results but the trend seems to indicate that the curve of q_2 would become asymptotic to zero but not reach a negative value.

The value of q_{min} (from constant volume tests) seemed to be related to shell height instead of to λ. This relationship was indicated by the differences in behavior between shells 8 and 14. These two have about the same value of λ, but the load-displacement curves associated with them are quite different. In Fig. 10 it is seen that after buckling, the pressure continued to decrease as the deflection increased. Thus q_{min} was much less than q_2. But with shell 14, the

curve started up again immediately after buckling so that $q_2 = q_{min}$. Probably q_{min} should be plotted with α as the abscissa for good correlation. Notwithstanding what has just been said, it appeared from Fig. 9b that $P_{cr} - P_{min}$ is probably a function of λ. The same plot was attempted with $P_{cr} - P_2$ and the scatter was worse in the low portion which determines the relationship. However, the conclusion that $P_{cr} - P_{min}$ is a functionof λ may have been due to a fortuitous scatter in values of P_{cr}.

- Buckling Process -

The entire load-displacement curve varies a great deal depending on the value of the parameter λ and on the shell depth. For the very shallow shells (small λ) the curve became extremely nonlinear before buckling and was essentially horizontal at the time of buckling. A curve for a fairly shallow shell is shown in the upper sketch of Fig. 10. Buckling then occurred by a gradual decrease in the pressure maintained by the shell. The pressure after buckling was only a few percent below the maximum or buckling pressure of the shell. For the case of large λ the situation was entirely different. Here the load-displacement curve was essentially linear up to the point of buckling. Buckling was extremely sudden, and without warning. The post-buckling pressure was about 1/4 to 1/6 of the maximum. A curve for a deep shell is also shown in Fig 10.

In all cases buckling was accompanied by the formation of one buckle or dimple (see Fig. 5). The buckle under water pressure was smooth, not jagged as in the constant pressure tests of Kloppel and Jungbluth[20]. The total central angle of the buckle is about 7° for all λ. Actually the size of the buckle is a peculiarity of the constant volume test and not of the buckling process or of the shell. When further volume was withdrawn after the occurrence of buckling, the size of the buckle increased. When the buckle was at maximum size, it extended over the entire shell. When still more volume was taken out after the buckle reached maximum size, the pressure taken by the shell began to increase. If volume was then forced back into the shell, the buckle decreased until its central angle was about 2° or 3° before snapping back through.

The buckle could occur at any location in the shell. However, if the shell was not removed from the cylinders between tests (no change in test conditions), then the buckle occurred again in the same position (except in test series 35b). But, under changed boundary conditions, as when the shell was unclamped and replaced in the test apparatus, it was not possible to predict the new location of the buckle.

For identification purposes, four buckle positions were chosen: near the edge, midway between the center and edge, near the center, and center. By correlating buckle positions with buckling loads for the shells, it was found that edge buckles were usually associated

with low loads, center buckles with high loads, and the other two have intermediate buckling loads. This correlation seems reasonable from the following viewpoint. In any given shell there will be some imperfections and some moments induced at the boundary by the clamping rings. If the effect of the imperfection dominates, the same load should be obtained in all tests, and the buckle should be formed in the vicinity of the imperfection. However, if the edge moments are dominant, the buckle will be formed near the edge and a lower load must be found, Since the imperfections will not be changed from test to test, the effect of any other influence must be either none or such as to decrease the buckling load. However, in this reasoning a very simple relation between imperfection and buckling load was assumed.

Unbuckling was accomplished by forcing water back under the shell. For the deeper shells an unbuckling action occurred much like the buckling. At some point there was a sudden increase in the pressure maintained by the shell. This occurred as the buckle snapped back through. Then the shell was back on the initial portion of the load-displacement curve and further volume change caused a decrease in the pressure in a linear manner. Just prior to unbuckling, it was observed that the dimple was vibrating at three or four cycles per second. No such motion was noticed at any other time during the loading or unloading process.

Various investigators have determined the minimum value of λ at which buckling occurs. Below this value the load deflection curve is a single-valued function of pressure. Kaplan and Fung found

λ = 2.1 theoretically, but λ= 5.0 experimentally as the minimum for buckling. In his analysis Weinitschke[12a] determined λ= 3.2 as the limiting value. In the tests of this report, one shell with λ = 3.3 exhibited an inflection point but no decrease in load with increase in deflection. Another shell with λ = 3.4 showed a slight decrease in pressure in some tests and none in others. These tests are therefore some verification for the theoretical value of Weinitschke.

- Effects of Imperfections -

One type of imperfection encountered in the shells was a slope of the rim as depicted in Fig. 7. The sign convention adopted was also shown in this figure. Some change in buckling loads might be expected due to this slope. When the shells were clamped into the test chambers, the rims were forced flat, thus inducing moments along the shell edge and, for large slopes, the shell height was even altered. Fig. 7 was plotted using the simple assumption that a positive slope would tend to increase the buckling load and a negative slope would have the opposite effect. However no trends at all are indicated in the figure.

Budiansky made an observation concerning the interaction of mode shapes and boundary conditions which may be used here. During loading a trough forms about the shell edge as a transition from the clamped boundary to the uniform deflection which occurs over the center of the shell. The mode shapes are also a series of troughs and crests, and the number and position of these waves depend on the

value of λ. For some values of λ a trough should appear at the edge, for others, a crest. Budiansky showed that when the mode shape produced a trough at the boundary, reinforcement occurred with the clamping trough and low loads were obtained at between $\lambda = 3.5$ and 5.5 and between 8 and 12. For λ between 5.5 and 8, cancellation occurred and buckling pressure was higher. As λ increases the oscillation in the P_{cr} versus λ curve dies out because the conditions at the apex and edge of the shell have less mutual influence. Fig. 7 was replotted using these ideas. For shells with λ between 3.5 and 5.5, 8 and 12, and between 16 and 25 the same sign convention was used for the rim slope. For the other shells the signs of the slopes were reversed. The figure which was thus produced looked no different from Fig. 7. That no trends appeared in either figure should not be taken as a sign that there was no effect from the slope of the rim. Rather it was an indication that the influence of slope on buckling pressure is small and obscured by other things.

Interest in the effect of clamping a sloping rim is not actually restricted to this set of tests. In a practical structure, edge restraint is provided generally by other deformable bodies which will tend to curl the shell edge up or down in a manner similar to the above effect

Various surface imperfections were found on the shells. Among these blemishes were central bumps which were caused by an irregularity in one of the molds and miscellaneous shallow bumps caused

by the presence of steam under the shell during forming. In a few shells there were very small sharp bumps caused by dust flecks present during forming. A further imperfection was caused if the hot sheet did not hit the mold uniformly when the vacuum was applied so that air pockets remained. Such an imperfection was a symmetric groove at midheight around shell 16. Shell 25 (and to a lesser extent, 24) had a large flat section at the apex. This seems to have reduced the load considerably and even flattened the load-deflection curve so that buckling occurred gradually, not suddenly.

Fig. 8 was a plot of imperfection magnitude versus the buckling pressure. No trend was evident but again this was based on a very simple idea about the effect of imperfections. It was not felt that a more valuable plot could be made using the knowledge which is presently at hand. The analysis of Chen has shown that buckling pressures may be either increased or decreased by imperfections depending on the value of λ and on the position, size, and direction of the imperfection. This is reasonable if one considers the fact that shell structures are usually built with ridges, grooves, and flat spots for added rigidity and strength. Yet in other cases grooves and flat spots would considerably increase the danger of buckling. For a refined treatment of imperfection effects it would be necessary to know the effect of a variety of sizes, shapes, and positions of blemishes. Also it would be necessary to know the mode shapes, both symmetric and unsymmetric. Finally, it is postulated that the position of the imperfection with respect to troughs in the deflected shape would have an effect on buckling pressures. Such

complex relationships make some sort of minimum load criterion very welcome although somewhat improbable.

Testing offered a further possibility for imperfect conditions. The latter can change from test to test while rim slope and surface imperfections will not. Hence variations in buckling pressures for a single shell are probably due to changes in test conditions. One source of error is the accuracy of clamping the shell into the test chambers. If the shell were placed slightly off center, the shell would not be held correctly and symmetrically, but in some unsymmetrical manner. This would tend to induce unsymmetric buckling and consequently lower loads. The variation in buckling pressure which may be attributed to this cause is about 7% as can be computed from the data of Table 1. During the air pressure tests, the nature of the effect of clamping conditions was studied for one shell. It was found that the buckle could be made to form in any part of the shell by shifting the shell around slightly in the test chambers. Early in the testing program this importance of clamping conditions was recognized so that great care was exercised in this regard. In the preliminary tests when no special precautions were taken, the reduction due to incorrect edge conditions was as much as 50%.

- Comparison with Other Work -

The buckling loads of this report seemed to fall in a sort of middle range between those of Tsien and Kloppel and Jungbluth, but are quite near the results of Kaplan and Fung, and Homewood, Brine, and Johnson. This was some verification that the results from the plastic material were valid.

In the History it was pointed out that if the energy criterion of Tsien were correct, buckling loads would depend on the ambient energy level and not be very reproducible from test to test. However, as was mentioned, the values of P_{cr} are very repeatable under unchanged conditions. The criterion was also used to predict that buckling loads under constant pressure would be about half those under constant volume testing conditions. Kaplan and Fung made both types of tests and found no indication of a difference; however, their experiments were in shallow shells beyond the range of Tsien's criterion. The tests of this report are evidence that the constant pressure buckling load may actually be above the constant volume load. Such a circumstance is not explainable either by the energy criterion or by the usual maximum-point-on-the-curve criterion.

The main importance of this experimental work was in the repeated testing and in the study of effects which could be investigated by this type of testing. Since the other investigators used metal shells which usually yielded on buckling, only one critical load was obtainable and many questions were raised as to why the shell buckled at that

pressure. Some of the possible causes have been studied in this report by using shells which buckled elastically and could be re-buckled any number of times. Thus the importance of clamping conditions has been pointed out and the time-dependence of buckling loads in material which creeps was considered. It was possible to conclude that the buckling was due to a geometric instability and not to material yield or to some local failure. Since the shells were buckled many times it was discovered that the dimple could appear in many positions in the shell and that the buckling loads and buckle positions were related. Finally, an unbuckling curve was determined which may shed further light on the buckling process.

CHAPTER 5 ANALYTICAL STUDY

A Introduction

The main purpose of an analysis in a report on buckling is the determination of buckling loads. However, with the large disparity between analytical results of previous investigators and test results, there was not much hope for finding better results for P_{cr} from this analysis. Rather, the computations were made to study the nature of the load-displacement curves. The loading curves were plotted both as load versus center displacement and load versus volume change. In addition, it was desired to know the variation of energy along these curves in order to assist in a consideration of Tsien's energy criterion.

The technique of calculation was the energy or variational method. Since this approach provides a series of equilibrium positions, the necessary curves could be plotted from the coordinates (pressure and deflection) of these positions. The required equation of total potential energy was first derived from the familiar principle of virtual work. Nonlinear strain-displacement relations were taken from Love[22] for use in the energy equation. Finally the energy equation was simplified to contain only terms important for large axisymmetric deflections of deep spherical shells with a buckle at the apex. Most previous derivations either were restricted to shallow shells, used different strain-displacement relations, or were linear and not applicable to the large deflection problem.

In order to continue the analysis, some estimate had to be made of an equation for deflected shape. The usual procedure at this point in the problem has been to propose a series of functions which seemed to fit the equations mathematically. The estimate used in this investigation was taken from observation of the actual buckling tests. The deflected shape was assumed to be a sum of terms: one for the uniform deflection as predicted by small deflection theory, one for the apparent shape of the buckle, and several others to satisfy boundary conditions. The formula represents quite well the appearance of the deflected shape, particularly in the post-buckling range.

The first maximum of the load-deflection curve was assumed to be the buckling load. This maximum point was found graphically by plotting a number of equilibrium positions near the maximum.

The calculations were carried out partially on the IBM 7090 computer because of the complexity of terms in the energy equation. Equilibrium positions were found for unrestricted deflection and for deflection where the buckle increased in depth but the average deflection over the shell remained constant.

B Derivation of Equations

In this section the well-known principle of virtual work was used to derive the principle of minimum total potential energy. In the application of the latter, a functional known as the total potential energy was calculated for use in determining equilibrium equations. In deriving the equation for the functional, various "order of importance" studies were made on the terms in the equation so that negligible terms could be discarded.

The principle of virtual work may be stated as follows (see K. Washizu, ref. 21): If infinitesimal virtual displacements of a body, u, v, w, which are compatible with the prescribed boundary conditions are imposed, then at an equilibrium position, the principle of virtual work gives

$$\iiint_{Volume} (\sigma_{11}\delta\varepsilon_{11} + \sigma_{22}\delta\varepsilon_{22} + \sigma_{33}\delta\varepsilon_{33} + \sigma_{23}\delta\varepsilon_{23} + \sigma_{13}\delta\varepsilon_{13} + \sigma_{12}\delta\varepsilon_{12})\,dV$$

$$- \iint_{Surface} (\bar{X}\delta u + \bar{Y}\delta v + \bar{Z}\delta w)\,dS = 0 \qquad (5\text{-}1)$$

The quantities $\bar{X}$, $\bar{Y}$, $\bar{Z}$ are forces on the surface acting in the coordinate directions, and u, v, and w, are displacements in the same directions. The strains, $\varepsilon_{11}, \varepsilon_{22}, \varepsilon_{33}, \varepsilon_{23}, \varepsilon_{13}$, and ε_{12} are derived from the displacements. Also the stresses are specified as functions of the strains by stress-strain relations, such as

$$\sigma_{11} = \frac{E}{1+\nu}\left[\varepsilon_{11} + \frac{\nu}{1-2\nu}(\varepsilon_{11} + \varepsilon_{22} + \varepsilon_{33})\right]$$

$$\sigma_{12} = \frac{E}{2(1+\nu)}\varepsilon_{12}$$

From the principle of virtual work Washizu has derived the principle of minimum potential energy which may be stated as follows: Of all the admissible u, v, and w which satisfy the prescribed geometric boundary conditions, the actual displacements are given by the extremum condition of a functional Π defined as

$$\Pi = \iiint_{Volume} (\sigma_{11}\varepsilon_{11} + \sigma_{22}\varepsilon_{22} + \sigma_{33}\varepsilon_{33} + \sigma_{23}\varepsilon_{23} + \sigma_{13}\varepsilon_{13} + \sigma_{12}\varepsilon_{12})\, dV - \iint_{Surface} (\bar{X}u + \bar{Y}v + \bar{Z}w)\, dS \tag{5-2}$$

If the first variation of Π, the total potential energy, is taken with respect to the displacements and strains, Eq. (5-1) is obtained. The same minimization procedure is valid for any number of independent displacement parameters and is not restricted to three orthogonal components.

In the usual application of the energy method, the total potential energy is evaluated and then varied with respect to the displacement parameters. The first variation provides the minimum condition

$$\delta\Pi = \frac{\partial \Pi}{\partial u}\delta u + \frac{\partial \Pi}{\partial v}\delta v + \frac{\partial \Pi}{\partial w}\delta w + \cdots = 0$$

Since the displacements δu, δv, δw, . . . are independent and may be specified arbitrarily, each partial derivative must be zero to ensure that $\delta\Pi = 0$. Therefore the minimization and equilibrium conditions are

$$\frac{\partial \Pi}{\partial u} = 0, \quad \frac{\partial \Pi}{\partial v} = 0, \quad \frac{\partial \Pi}{\partial w} = 0, \quad \cdots \tag{5-3}$$

If the displacement components are not independent, a slightly modified procedure can be followed. For a two-variable problem the usual equilibrium condition is

$$\delta\Pi = \frac{\partial \Pi}{\partial u}\delta u + \frac{\partial \Pi}{\partial v}\delta v = 0 \qquad (5\text{-}4)$$

but if u and v are not independent, there is a constraint condition in the form M(u,v) = 0. Therefore it is also true that

$$\delta M = \frac{\partial M}{\partial u}\delta u + \frac{\partial M}{\partial v}\delta v = 0$$

$$\text{or} \quad \delta u = -\left(\frac{\partial M}{\partial v}\Big/\frac{\partial M}{\partial u}\right)\delta v$$

Replace this expression into (5-4) and obtain

$$\delta\Pi = -\frac{\frac{\partial M}{\partial v}}{\frac{\partial M}{\partial u}}\frac{\partial \Pi}{\partial u}\delta v + \frac{\partial \Pi}{\partial v}\delta v = 0$$

Since δv can now be varied arbitrarily, the equilibrium condition is found to be

$$-\frac{\partial M}{\partial v}\frac{\partial \Pi}{\partial u} + \frac{\partial M}{\partial u}\frac{\partial \Pi}{\partial v} = 0$$

For convenience the total potential energy is often separated into two parts, thus

$$\Pi = U - W, \qquad (5\text{-}5)$$

where U is the strain energy and W is the work of the external forces.

The present problem may be considered as a linearly elastic case of plane stress, that is, the stress σ_{33} is taken as zero. Also Kirchhoff s assumption that a line in the shell which is normal to the middle surface before deformation remains normal after deformation,

will be taken. This merely requires that the shear strain will be neglected in finding deflections. Further it is assumed that it is reasonable to neglect terms which appear to be small according to some consistently applied criterion. In this problem the strain energy takes the simple form

$$U = \frac{1}{2}\iiint_{Volume}(\sigma_{11}\varepsilon_{11} + \sigma_{22}\varepsilon_{22})\,dV \tag{5-6}$$

and the stress-strain relations are

$$\begin{aligned}\sigma_{11} &= \frac{E}{1-\nu^2}(\varepsilon_{11} + \nu\varepsilon_{22}) \\ &= \frac{E}{1-\nu^2}\left(\bar{\varepsilon}_{11} + \frac{z}{a}\varkappa_{11} + \nu\bar{\varepsilon}_{22} + \nu\frac{z}{a}\varkappa_{22}\right) \\ \sigma_{22} &= \frac{E}{1-\nu^2}\left(\bar{\varepsilon}_{22} + \frac{z}{a}\varkappa_{22} + \nu\bar{\varepsilon}_{11} + \nu\frac{z}{a}\varkappa_{11}\right)\end{aligned} \tag{5-7}$$

The quantities $\varkappa_{11}$, $\varkappa_{22}$ are dimensionless curvatures of the middle surface in the ϕ and θ directions and $\bar{\varepsilon}_{11}$, $\bar{\varepsilon}_{22}$ are strains of the middle surface in those two directions.

Substitution of the relations (5-7) into Eq. (5-6) and integration in the direction of θ gives

$$\begin{aligned}U = {} & \frac{Eh\pi a^2}{1-\nu^2}\int\left[(\bar{\varepsilon}_{11} + \bar{\varepsilon}_{22})^2 - 2(1-\nu)\bar{\varepsilon}_{11}\bar{\varepsilon}_{22}\right]\sin\phi\,d\phi \\ & + \frac{Eh^3\pi}{12(1-\nu^2)}\int\left[(\varkappa_{11} + \varkappa_{22})^2 - 2(1-\nu)\varkappa_{11}\varkappa_{22}\right]\sin\phi\,d\phi\end{aligned} \tag{5-8}$$

The required strains and curvatures are taken from the nonlinear strain-displacement equations of A. E. H. Love[22]. The following procedure is outlined in Novozhilov[23a]. The relations are specialized

here for the case of symmetrical deformation of spherical shells.

The strains are

$$\begin{aligned}
\varepsilon_{11} &= e_{11} + \tfrac{1}{2}\left[e_{11}^2 + \left(\tfrac{1}{2}e_{13} - \omega_2\right)^2\right] \\
\varepsilon_{22} &= e_{22} + \tfrac{1}{2}e_{22}^2 \\
\varepsilon_{33} &= e_{33} + \tfrac{1}{2}\left[e_{33}^2 + \left(\tfrac{1}{2}e_{13} + \omega_2\right)^2\right] \\
\varepsilon_{13} &= e_{13} + e_{11}\left(\tfrac{1}{2}e_{13} + \omega_2\right) - e_{33}\left(\tfrac{1}{2}e_{13} - \omega_2\right)
\end{aligned} \tag{5-9}$$

where

$$\begin{aligned}
e_{11} &= \frac{1}{a+z}\left(\frac{du_c}{d\phi} + w_c\right) \\
e_{22} &= \frac{1}{a+z}\left(u_c \cot\phi + w_c\right) \\
e_{13} &= \frac{1}{a+z}\left(\frac{dw_c}{d\phi} - u_c\right) + \frac{du_c}{dz} \\
e_{33} &= \frac{dw_c}{dz} \\
2\omega_2 &= \frac{du_c}{dz} - \frac{1}{a+z}\left(\frac{dw_c}{d\phi} - u_c\right)
\end{aligned} \tag{5-9}$$

Here u_c and w_c are displacements tangential and normal to the middle surface and z is the distance outward from the middle surface.

In order to proceed further it is necessary to find a criterion to determine the relative importance of displacement terms so that small terms may be discarded. Edge loads and point loads on shells both produce sudden changes in geometry and high moments just as the buckle does. From the analysis of point loadings by Reissner[24] and edge loadings by Novozhilov[23b] the relative importance of the deflection terms can established. In these analyses, u_c, the tangential deflecti component, is small with respect to w_c, the normal component.

In other words, w_c is of the order of u_c times m, where m is a number which is larger than, say, 10. Also differentiation by ϕ or multiplication by $\cot\phi$ raise the order by one step, that is, increase the magnitude by one power of m. Therefore $u_c\cot\phi$ and u_c' are of the order of $(u_c)(m)$, w_c' and u_c'' are of the orderof $(u_c)(m^2)$, and w_c'' and $w_c'\cot\phi$ are of the order of $(u_c)(m^3)$. These orders of magnitude apply specifically near the apex where $\cot\phi$ is much greater than one and are not as applicable at the edge of a deep shell. In this analysis it is assumed that the highest order nonlinear terms in the strain-displacement relations are comparable to the highest order linear terms and that all other linear and nonlinear terms are negligible.

From Kirchhoff's assumption it follows that ε_{13} must vanish and the plane stress assumption requires that $\sigma_{33} = 0$. Therefore

$$\varepsilon_{13} = \frac{\partial u_c}{\partial z}\left[1 + \frac{1}{a+z}\left(\frac{\partial u_c}{\partial \phi} + w_c\right)\right] + \frac{1}{a+z}\left(\frac{\partial w_c}{\partial \phi} - u_c\right)\left(\frac{\partial w_c}{\partial z} + 1\right) = 0 \qquad (5\text{-}11)$$

$$\varepsilon_{33} = \frac{\partial w_c}{\partial z} + \frac{1}{2}\left[\left(\frac{\partial u_c}{\partial z}\right)^2 + \left(\frac{\partial w_c}{\partial z}\right)^2\right] = -\frac{\nu}{1-\nu}(\varepsilon_{11} + \varepsilon_{22}) \qquad (5\text{-}12)$$

Let
$$u_c = \bar{u} + z\theta$$
$$w_c = \bar{w} + z\chi \qquad (5\text{-}13)$$

where $\bar{u}$ and $\bar{w}$ are displacements of the middle surface and θ and χ are linear variations of displacement through the thickness. Substitute these values into the equations for ε_{13} and ε_{33} and

the results are

$$1 - \frac{2\nu}{1-\nu}(\varepsilon_{11} + \varepsilon_{22}) = (1+\chi)^2 + \theta^2$$

$$\frac{1+\chi}{a+\bar{z}}\left(\frac{d\bar{w}}{d\phi} - \bar{u}\right) + \left(1 + \frac{d\bar{u}}{d\phi} + \bar{w}\right)\theta = 0$$

Let $e_1 = u' + w$

$$e_2 = u\cot\phi + w \qquad (5\text{-}14)$$

$$e_3 = w' - u$$

where u and w are dimensionless terms for the displacements of the middle surface, that is, $u = \frac{\bar{u}}{a}$, $w = \frac{\bar{w}}{a}$. The primes refer to differentiation with respect to ϕ. Then

$$\theta = -\frac{e_3}{1+e_1}(1+\chi) \cong -e_3$$

and $$\chi = -\frac{1}{1-\nu}(e_1 + e_2) - \frac{1}{2}e_3^2 \qquad (5\text{-}15)$$

Now return to ε_{11} and ε_{22}. Use the substitution (5-13) and let

$\varepsilon_{11} = \bar{\varepsilon}_{11} + \frac{z}{a}\varkappa_{11}$ and $\varepsilon_{22} = \bar{\varepsilon}_{22} + \frac{z}{a}\varkappa_{22}$. Then

$$\bar{\varepsilon}_{11} = e_1 + \frac{1}{2}(e_1^2 + e_3^2) \cong e_1 + \frac{1}{2}w'^2$$

$$\bar{\varepsilon}_{22} = e_2 + \frac{1}{2}e_2^2 \cong e_2$$

$$\varkappa_{11} = -w'' + \frac{1}{2}w'^2 + uw' + \nu w w'' \cong -w'' \qquad (5\text{-}16)$$

$$\varkappa_{22} = -w'\cot\phi + u'w'\cot\phi - uw'\cot^2\phi + \nu w w'\cot\phi - \frac{1}{2}w'^2$$

$$\cong -w'\cot\phi$$

The results above have been found by keeping only the highest order linear and nonlinear terms as determined by the order of magnitude analysis.

The solution of the problem is greatly facilitated by solving for u in terms of w so that only w remains as an independent variable. The necessary condition is found by minimizing the total energy with respect to u. Since u appears only in the extensional energy,

$$\delta\Pi = \delta U = \delta\int(\bar{\varepsilon}_{11}^2 + \bar{\varepsilon}_{22}^2 + 2\nu\bar{\varepsilon}_{11}\bar{\varepsilon}_{22})\sin\phi\, d\phi$$

$$= -2\int[(e_1 + \nu e_2 + \tfrac{1}{2}e_3^2)\sin\phi]'\delta u\, d\phi$$

$$+2\int(e_2 + \nu e_1 + \tfrac{\nu}{2}e_3^2)\cos\phi\,\delta u\, d\phi = 0$$

or $$(\sigma_{11}\sin\phi)' - \sigma_{22}\cos\phi = 0 \qquad (5\text{-}17)$$

which is an equilibrium condition for a homogeneous case. This may also be transformed to

$$u'' + u'\cot\phi - u\csc^2\phi + (1-\nu)u = -(1+\nu)w' - w'w'' - \frac{(1-\nu)}{2}w'^2\cot\phi$$

The fourth term is of smaller order than the others in the equation and may be omitted. The rest can be arranged for integration as follows:

$$\left[\frac{1}{\sin\phi}(u\sin\phi)'\right]' = -(1+\nu)w' - \tfrac{1}{2}(w'^2)' - \frac{(1-\nu)}{2}w'^2\cot\phi \qquad (5\text{-}18)$$

Integration once gives

$$\frac{1}{\sin\phi}(u\sin\phi)' = u' + u\cot\phi =$$

$$= -(1+\nu)w - \frac{1}{2}w'^2 - \frac{1-\nu}{2}\int w'^2\cot\phi\,d\phi + A \qquad (5\text{-}19)$$

Here it is well to notice that there is a simple expression for the sum of the extensional strain

$$\bar{E}_{11} + \bar{E}_{22} = e_1 + e_2 + \frac{1}{2}w'^2$$

$$= u' + u\cot\phi + 2w + \frac{1}{2}w'^2 \qquad (5\text{-}20)$$

$$= (1-\nu)w - \frac{1-\nu}{2}\int w'^2\cot\phi\,d\phi + A$$

Notice that if w is a uniform expansion this equation is incorrect since $\bar{E}_{11} + \bar{E}_{22} = 2w$ for $w = \text{constant}$.

Another integration of (5-18) gives

$$u = -\frac{1+\nu}{\sin\phi}\int w\sin\phi\,d\phi - \frac{1}{2\sin\phi}\int w'^2\sin\phi\,d\phi \qquad (5\text{-}21)$$

$$-\frac{1-\nu}{2\sin\phi}\int\sin\phi\int w'^2\cot\phi\,d\phi\,d\phi + \frac{A(1-\cos\phi)}{\sin\phi} + \frac{B}{\sin\phi}$$

Imposition of the boundary conditions u = 0 at $\phi = 0, \alpha$ serves to specify A and B.

Since the sum of extensional strain, $\varepsilon_{11} + \varepsilon_{22}$, (see 5-20) is easy to calculate but the product, $\varepsilon_{11}\varepsilon_{22}$, is not, the strain energy formula will be modified, using Eq. (5-7). The extensional energy is

$$U_E = \frac{Eh\pi a^2}{1-\nu^2}\int(\bar{\varepsilon}_{11}^2 + \bar{\varepsilon}_{22}^2 + 2\nu\bar{\varepsilon}_{11}\bar{\varepsilon}_{22})\sin\phi\, d\phi$$

$$= \frac{Eh\pi a^2}{1-\nu^2}\int(\bar{\varepsilon}_{11} + \bar{\varepsilon}_{22})^2\sin\phi\, d\phi$$

$$- \frac{2(1+\nu)h\pi a^2}{E}\int\sigma_{11}\sigma_{22}\sin\phi\, d\phi$$

The last integral can be integrated partially using equation (5-17).

$$\frac{-2(1+\nu)h\pi a^2}{E}\int\sigma_{11}\sigma_{22}\sin\phi\, d\phi =$$

$$= \frac{-2(1+\nu)h\pi a^2}{E}\int\sigma_{11}\sin\phi(\sigma_{11}\sin\phi)'\sec\phi\, d\phi =$$

$$= \frac{-(1+\nu)h\pi a^2}{E}(\sigma_{11}\sin\phi)^2\sec\phi\Big]_0^{\alpha} + \frac{(1+\nu)h\pi a^2}{E}\int\sigma_{11}^2\frac{\sin^3\phi}{\cos^2\phi}\, d\phi$$

The first term is zero at the lower limit and only u' is nonzero at the upper limit. Therefore the integral of the strain product becomes:

$$\frac{-Eh\pi a^2\sin\alpha\tan\alpha\, u'^2}{(1-\nu)(1-\nu^2)}\Big|_{\alpha}$$

$$\frac{+Eh\pi a^2}{(1-\nu)(1-\nu^2)}\int(\varepsilon_{11} + \nu\varepsilon_{22})^2\frac{\sin^3\phi}{\cos^2\phi}\, d\phi$$

The integral is of the order of $1/m^2$ times the evaluated term and can therefore be integrated approximately or neglected.

The formula for bending energy can also be transformed by partial integration to a simpler form.

$$U_b = \frac{Eh^3\pi}{12(1-\nu^2)}\int\left[(\alpha_{11}+\alpha_{22})^2 - 2(1-\nu)\alpha_{11}\alpha_{22}\right]\sin\phi\, d\phi$$

$$= \frac{Eh^3\pi}{12(1-\nu^2)}\int(w''+w'\cot\phi)^2\sin\phi\, d\phi - \frac{Eh^3\pi}{6(1+\nu)}\int w''w'\cos\phi\, d\phi$$

The second term in U_b is integrable since

$$\int w''w'\cos\phi\, d\phi = \frac{1}{2}\int d(w'^2)\cos\phi\, d\phi$$

$$= \frac{1}{2}w'^2\cos\phi\Big]_0^{\alpha} + \frac{1}{2}\int w'^2\sin\phi\, d\phi$$

The evaluated term is identically zero and the integral is of the order of $1/m^2$ with respect to the first term in U_b. The nonlinear terms in the bending energy are found to be second order with respect to the comparable extensional energy terms and are therefore omitted.

The work done can be considered as a scalar product of force and distance, thus

$$W = q\iint(u\cos X + w\cos Z)\, a\, dS \qquad (5\text{-}22)$$

where cos X and cos Z are cosines of the angles between the surface normal and the ϕ and Z coordinate directions. Here

$$\cos X = \theta$$

$$\cos Z = 1 + \chi \qquad (5\text{-}23)$$

Therefore

$$W = 2\pi a^3 q \int \left[w\left(1 - \frac{\nu e_1}{1-\nu} - \frac{\nu e_2}{1-\nu} - \frac{1}{2}e_3^2\right) - u e_3 \right] \sin\phi \, d\phi$$

or approximately

$$W = 2\pi a^3 q \int w \sin\phi \, d\phi \tag{5-24}$$

The energy equation can now be written in the form:

$$\bar{\Pi} = \bar{U}_1 + \bar{U}_2 + \bar{U}_3 + \bar{U}_4 - QL \tag{5-25}$$

where the dimensionless quantities are

$$\bar{\Pi} = \frac{\Pi(1-\nu^2)}{Eh\pi a^2}$$

$$\bar{U}_1 = \frac{1+\nu}{1-\nu}\int_0^\alpha (\bar{\varepsilon}_{11} + \bar{\varepsilon}_{22})^2 \sin\phi \, d\phi$$

$$\bar{U}_2 = -\frac{1}{1-\nu} \sin\alpha \tan\alpha \, u'\Big|_\alpha^2$$

$$\bar{U}_3 = \frac{1}{1-\nu}\int_0^\alpha (\varepsilon_{11} + \nu\varepsilon_{22})^2 \frac{\sin^3\phi}{\cos^2\phi} \, d\phi \tag{5-26}$$

$$\bar{U}_4 = \frac{h^2}{12a^2}\int_0^\alpha (w'' + w'\cot\phi)^2 \sin\phi \, d\phi$$

$$Q = 2(1-\nu^2)\frac{8q}{Eh}$$

$$L = \int_0^\alpha w \sin\phi \, d\phi$$

C Deflected Shape

The deflected shape to be introduced into the equation for the energy functional is probably the main difference between this analysis and previous work. In the past the deflection was taken in a series with as many as 200 unknown coefficients. With fewer terms the shape was too restrcted and poor results were obtained. Also the number of terms increased rapidly as λ increased. For a deep shell (large λ) a power series might prove hopeless.

In this analysis a deflected shape was chosen which seemed to fit the appearance of the shell surface during loading. Up to buckling the deflection seemed to be uniform over most of the shell (this was observed under air pressure where loading could be applied rapidly so that deflection was visible). At buckling a dimple formed which was a shallow, bowl-like, circular depression. The edges seemed to be fairly well defined due to the reflection of light from the region of sharp curvature at the rim of the depression. Therefore it was possible to speak of a diameter or size of the buckle. This sharpness of curvature indicates the presence of large and rapid variations in shape, shear, slope and moment in limited areas of the surface. Such regions of high derivatives are difficult to depict analytically and require a long series of terms to make an adequate fit. In the shell the buckle appeared as almost a separate region in an otherwise unchanged spherical surface. No wonder many of the first investigators analyzed the buckle region as a separate entity.

The buckles seen in the tests were symmetrical only for the shallow shells with one exception. However the differences in buckle position apparently caused fairly minor changes in P_{cr}. Therefore if buckling loads for axisymmetric buckles were determined, the load associated with unsymmetric buckles should be just 5% or 10% lower. The axisymmetric case only is considered here because it is simpler mathematically and should depict adequately the nature of the loading curve.

Instead of trying to depict the whole shape of the shell surface as one term or one series of terms, the shape was divided naturally into its two components: the uniform deflection and the buckle depression. No mode shapes were considered since none were seen on the shells. These small undulations in the surface were probably just too small to be detected visually without special equipment. Omitting modal deformations from the assumed deflected shape probably led to a somewhat higher buckling load.

The equation for deflection which was chosen was as follows:

$$\begin{aligned} w = w_0 &- w_0\left[\sin c(\alpha-\phi) + \cos c(\alpha-\phi)\right]e^{-c(\alpha-\phi)} \\ &- w_1(\sin b\phi + \cos b\phi)e^{-b\phi} \\ &+ w_1(\sin b\alpha + \cos b\alpha)e^{-b\alpha} \\ &+ 2bw_1 \sin b\alpha\, e^{-b\alpha}\frac{(\cos\phi - \cos\alpha)}{\sin\alpha} \end{aligned} \qquad (5\text{-}27)$$

Each term here had a specific purpose. The first term, w_0, is a uniform expansion and $w_0\left[\sin c(\alpha-\phi) + \cos c(\alpha-\phi)\right]e^{-c(\alpha-\phi)}$ provides for the

clamped edge condition. Both of these deflection terms are known from small deflection or linear theory. The third term, $w_1(\sin b\phi + \cos b\phi)e^{-b\phi}$, describes the shape of the dimple which appears at buckling. For convenience these first three terms were plotted in Fig. 4B in various ways. Notice that the third term has no slope at $\phi = 0$, and that it goes to zero at $b\phi = 2.35$ radians. For larger values of $b\phi$, the contribution of this term becomes very small. $1/b$ is a measure of buckle extent since the diameter of the dimple is about $4.7a/b$.

The succeeding two terms were needed to satisfy boundary conditions for w and w'. With the clamped edge it was necessary that

$$w = w' = 0 \quad \text{at } \phi = \alpha \text{, the edge}$$

$$w' = 0 \quad \text{at } \phi = 0, \text{ the apex}$$

and w had to be finite at $\phi = 0$. These boundary conditions are not satisfied exactly but approximately, since the edge correction has both a deflection and slope at the apex. The deflection in the center of the buckle is

$$w_o - w_o(\sin c\alpha + \cos c\alpha)e^{-c\alpha} - w_1 + w_1(\sin b\alpha + \cos b\alpha)e^{-b\alpha}$$

$$+ bw_1 \sin b\alpha\, e^{-b\alpha} \sin\alpha$$

but for most purposes it was adequate to assume that the buckle depth at the apex was

$$- w_o + w_1$$

(the terms were written with different signs, but in actuality both are inward deflections and therefore add since w_o is always negative.)

In general both c and b will be large, that is, between 10 and 100. This means that the number of important terms in the series expansion for w would be extremely large and this seems to be the case for deeper shells. The factor b is the basis for all order of magnitude analyses and exactly fits the scheme earlier specified. Near $\phi = 0$, it is assumed that $b\phi$ is of the order of unity. This deflection equation is reasonable for shells of a certain depth only, where the edge and buckle terms do not significantly overlap and is not necessarily applicable to very shallow shells. For the deeper shells it is possible to let $e^{-c\alpha}$ equal zero in the evaluations of theintegrals. $e^{-b\alpha}$ cannot be neglected since it increases on differentiation with respect to b.

The energy equation can be written in the following general form:

$$\begin{aligned}\bar{\Pi} = {} & E_{20} w_0^2 + E_{11} w_0 w_1 + E_{21} w_0^2 w_1 \\ & + E_{12} w_0 w_1^2 + E_{02} w_1^2 + E_{03} w_1^3 \\ & + E_{04} w_1^4 - E_{10} Q w_0 - E_{01} Q w_1 \end{aligned} \tag{5-28}$$

The E's contain exponential and trigonometric functions of b and c. Equilibrium equations are now found by calculating

$$\frac{\partial \bar{\Pi}}{\partial w_0} = 0, \quad \frac{\partial \bar{\Pi}}{\partial w_1} = 0, \quad \frac{\partial \bar{\Pi}}{\partial b} = 0, \quad \frac{\partial \bar{\Pi}}{\partial c} = 0$$

The problem is simplified by using

$$w_0 = \frac{9q(1-\nu)}{2Eh} \quad , \quad c = \sqrt{12(1-\nu^2)}\sqrt{\frac{a}{h}} \tag{5-29}$$

which can be obtained by evaluating $\frac{d\Pi}{dw_0} = 0$ and $\frac{d\Pi}{dc} = 0$, neglecting terms in w_1. This merely means that w_0 is assumed to be the correct linear deflection. But if this is so then the terms with coefficients E_{11} and E_{01} must also cancel, as Friedrichs has pointed out, and could be omitted from the energy and equilibrium equations. That this was the correct procedure can be demonstrated using a simple potential energy formula which contains both a linear and nonlinear term.

Let $$\Pi_0 = P\delta - \tfrac{1}{2}k_1\delta^2 + k_2\delta^3 \tag{5-30}$$

δ^2 can be considered linear since its derivative is linear. This special definition applies since Π is actually the integral of the physical quantities which are linear or nonlinear. Also the deflection, δ , is broken into a linear term which is valid near $\delta = 0$, and a nonlinear term, δ_1 .

$$\delta = \delta_0 + \delta_1$$

Then

$$\Pi_0 = P\delta_0 + P\delta_1 - \tfrac{1}{2}k_1\delta_0^2 - k_1\delta_0\delta_1 - \tfrac{1}{2}k_1\delta_1^2$$
$$+ k_2\delta_0^3 + 3k_2\delta_0^2\delta_1 + 3k_2\delta_0\delta_1^2 + k_2\delta_1^3$$

or

$$-\Pi_0 = \tfrac{1}{2}k_1\delta_0^2 + k_1\delta_0\delta_1 - 3k_2\delta_0^2\delta_1 - 3k_2\delta_0\delta_1^2$$
$$+ \tfrac{1}{2}k_1\delta_1^2 - k_2\delta_1^3 - P\delta_0 - P\delta_1 - k_2\delta_0^3 \tag{5-31}$$

Notice that if $w_0 = \delta_0$, $w_1 = \delta_1$, $\Pi_0 = \bar{\Pi}$, then Eq.(5-31) is very similar to Eq. (5-28). The former is much simpler, however, and can be studied to determine the importance of the terms. The general solution can be found from

$$\frac{\partial \Pi_0}{\partial \delta} = P - k_1 \delta + 3k_2 \delta^2 = 0$$

In this case there is a maximum or buckling pressure which occurs at

$$\frac{\partial P}{\partial \delta} = k_1 - 6k_2 \delta = 0$$

or $\delta = \frac{k_1}{6k_2}$ and $P_{max} = \frac{k_1^2}{12k_2}$

Now the same result could be found using $\delta = \delta_0 + \delta_1$. When Eq. (5-31) is differentiated with respect to δ_1, the following is obtained:

$$-\frac{\partial \Pi_0}{\partial \delta_1} = k_1\delta_0 - 3k_2\delta_0^2 - 6k_2\delta_0\delta_1 + k_1\delta_1 - 3k_2\delta_1^2 - P \qquad (5\text{-}32)$$

and P_{max} occurs at $\frac{\partial P}{\partial \delta_1} = -6k_2\delta_0 - 6k_2\delta_1 + k_1 = 0 \qquad (5\text{-}33)$

$$\text{or } \delta_1 = \frac{k_1}{6k_2} - \delta_0 \qquad \text{and } \delta = \delta_0 + \delta_1 = \frac{k_1}{6k_2}$$

which is the result obtained before for the deflection at buckling. Notice that in Π_0 the terms which contribute to (5-33) are only $\frac{1}{2}k_1\delta_1^2$, $-3k_2\delta_0\delta_1^2$, and $-k_2\delta_1^3$. Since δ_0 is the linear solution, $\delta_0 = P/k_1$. Using this result and the deflection at maximum P in Eq. (5-32) gives

$$P_{max} = \frac{k_1^2}{12k_2}$$

In finding P_{max}, four terms in Π_0 are needed. Besides the three which serve to determine the critical deflection, $-3k_2\delta_0^2\delta_1$ is required. If the latter is omitted, the value of P_{max} is twice

the correct value. The interesting result is therefore that the linear solution, δ_0, must be included in two nonlinear terms, $\delta_0^2\delta_1$ and $\delta_0\delta_1^2$ in order to give the correct results. In passing it should be noted that the terms in π_0 containing δ_0^2, $\delta_0\delta_1$, $P\delta_0$, and $P\delta_1$ cancelled out since δ_0 is the linear solution.

When the results of the preceding study were applied to the terms in $\bar{\pi}$, Eq. (5-28), it was found that the terms with coefficients E_{20}, E_{11}, E_{10}, and E_{01} could be dropped but that all the others had to be kept. Finally the energy equation took the form

$$\bar{\pi} = E_{21}w_0^2w_1 + E_{12}w_0w_1^2 + E_{02}w_1^2 + E_{03}w_1^3 + E_{04}w_1^4 \quad (5\text{-}34)$$

and the equilibrium conditions are

$$\frac{\partial\bar{\pi}}{\partial w_1} = 0 \qquad \text{and} \qquad \frac{\partial\bar{\pi}}{\partial b} = 0 \quad (5\text{-}35)$$

or $$E_{21}w_0^2 + 2E_{12}w_0w_1 + 2E_{02}w_1 + 3E_{03}w_1^2 + 4E_{04}w_1^3 = 0 \quad (5\text{-}36)$$

and $$D_{21}w_0^2w_1 + D_{12}w_0w_1^2 + D_{02}w_1^2 + D_{03}w_1^3 + D_{04}w_1^4 = 0 \quad (5\text{-}37)$$

where the D's are derivatives with respect to b of the E's. The E's found in Eq. (5-34) are given in Appendix C.

D Solution

The procedure for solution of the problem is to satisfy the two equations (5-36) and (5-37) simultaneously for w_1 and b at various values of Q, the applied pressure parameter. Each set of values for Q, w_1, and b which satisfy the equations define an equilibrium position for the shell. If a series of quantities for Q and w_1 from such positions are plotted, a loading curve is obtained. In this report it was found convenient to plot $-w_0$ versus $-w_0 + w_1$ since $-w_0$ is proportional to pressure and $-w_0 + w_1$ is the central deflection.

The first attempt at a solution was made with a somewhat less complete formula for Π. Since $e^{-b\alpha}$ is rather small for large b, all terms with an exponential were excluded. This meant that all trigónometric functions were also omitted since they occur only in conjunction with the exponential. Hence the E's contained only powers of b, making the equations rather easy to solve. Terms containing $e^{-b\alpha}$ were also neglected in the expression for w, Eq. (5-27). And finally $E_{21}w_0^2w_1$ was neglected because it did not seem reasonable for the linear solution, w_0, to be of importance in nonlinear terms. The two equilibrium equations, $\frac{\partial \Pi}{\partial w_1} = 0$ and $\frac{\partial \Pi}{\partial b} = 0$, were solved for a number of values of Q. Eauilibrium positions were obtained first far into the post-buckling range, and the solution was then continued, working backwards towards buckling. The post-buckling part of the curve was about right. However, at a point near what should have been the maximum point of the curve, the pressure rose sharply

towards infinity and the value of b became imaginary. Although this solution attempt failed, it gave some useful information for assistance on the next try. It was found that b would have a value near that of c and that the value of b rose to a maximum near P_{cr}. Thus a curve of b versus deflection should be similar to a load-deflection curve.

The difficulties experienced in the first try could be traced mainly to the omission of all terms containing $e^{-b\alpha}$. True, $e^{-b\alpha}$ was much smaller than $1/b$, with which it was usually compared, especially if b were approximately equal to c. However, when the derivatives of both terms were taken, the situation was different. Then the comparison was between $be^{-b\alpha}$ and $1/b^2$ and the two terms are nearly equal for b = 36.

In the second attempt at a solution, the procedure outlined in most of this chapter was used. The nonlinear terms $E_{21}w_0^2w_1$ and $E_{12}w_0w_1^2$ were retained, all quantities containing $e^{-b\alpha}$, $e^{-2b\alpha}$, $e^{-3b\alpha}$ and $e^{-4b\alpha}$ were retained, and $E_{20}w_0^2$, $E_{11}w_0w_1$, $E_{10}w_0$ and $E_{01}Qw_1$ were cancelled out. The remaining E's were very complicated functions of b as can be seen from the formulas in Appendix C. The normal procedure for the solution of Eq. (5-36, 5-37) is to specify Q and solve for w_1 and b. However it is also possible to specify b and solve for Q and w_1 if that is more convenient.

In the present case computations were made by evaluating the E's and D's at certain values of b. b was successively assigned

values for each percent of c, that is, b(i) = 0.01(i)c where i was an index running from 30 to 120. This range of b was suggested by the results of the first attempt at solution and the interval was chosen to give reasonable results for the derivatives. The latter were computed by a four point central difference formula from reference (25). For example

$$D_{12}(i) = \frac{1}{12(.01)c}\left[-E_{12}(i-2) + 8E_{12}(i-1) - 8E_{12}(i+1) + E_{12}(i+2)\right]$$

and here the range of i was narrowed to 32 to 118.

The computations of the E's and D's were programmed in Fortran language for use on the IBM 7090 at M.I.T. The program was written in essentially the order given for the calculations in Appendix C.

When these evaluations had been made, the simultaneous equations of equilibrium, (5-36, 5-37) were ready for solution. Since each set of these equations were for a fixed value of b, w_0 and w_1 (or Q and w_1) were treated as unknowns. The remaining calculations were made by hand. The method used was to try to solve a few sets of equations for b near 0.9 c. When a solution of any set was obtained then a set for a nearby value of b was attempted. To aid in solution, the two equilibrium equations were rewritten as

$$-w_0 = \frac{\frac{E_{02}}{E_{12}} + 1.5\frac{E_{03}}{E_{12}}w_1 + 2\frac{E_{04}}{E_{12}}w_1^2}{1 + \frac{E_{21}w_0}{2E_{12}w_1}} \qquad (5\text{-}38)$$

$$w_1 = \frac{-\frac{D_{21}}{D_{02}} w_0^2}{1 + \frac{D_{12}}{D_{02}} w_0 + \frac{D_{03}}{D_{02}} w_1 + \frac{D_{04}}{D_{02}} w_1^2} \qquad (5\text{-}39)$$

Then the equations were solved by relaxation. That is, values for w_0 and w_1 were estimated and placed in (5-38) and a new value for w_0 was found. Then with the estimate for w_1 and the new value for w_0, w_1 was evaluated using the second equation. The process was repeated until a set of solutions was found or until it became apparent that the values of one or both of the unknowns would lie outside the range of interest. When successive values of w_0 and w_1 agreed to three figures, the equations were considered solved. The values of w_0 and w_1 obtained were plotted immediately to assist in estimating the next solutions.

For the graphs shown in Fig. 16, the plot was made of $-w_0$ versus $-w_0 + w_1$ and then the ordinate scale was changed to make a pressure versus center deflection curve. The pressure versus volume change curves were made by plotting $-w_0$ versus L as given by Eq. (5-26).

The preceding calculations were all for "free" deflections, that is w_1 and b were varied independently to minimize the total potential energy. However, when an experiment was run with volume control, this freedom was not present. To duplicate this case analytically, a restriction was applied to w_1 and b so that the volume L could be held constant while deflection and pressure changed. The method

used here was outlined in the discussion following Eq. (5-4). $M(u,v) = 0$, the restraint condition, was replaced by $L - L_0 = 0$, where L_0 is the value of L at some designated point. For instance, the value of L at P_{cr} was set equal to L_0. Then with the constraint condition, equilibrium positions shown in Fig. 15 duplicated the curve of an actual shell undergoing constant volume testing (see Fig. 10).

For both free and volume control testing it was possible to establish curves of energy versus deflection. These were simply made by using the values w_1, b, and Q which were already known at specific points and evaluating $\bar{\Pi}$ from Eq. (5-28).

During the solution of the equations, it was found that the terms with E_{12} and E_{21} were very important in the initial portion of the loading curve up to buckling. Also in this initial portion the terms with E_{03} and E_{04} were not required and E_{02} was contributing a very small amount even at buckling. The situation was reversed for equilibrium positions in the large deflection range. The terms with E_{03} and E_{04} were dominant, and E_{12} and E_{21} were essentially negligible. The linear term E_{02} was of importance throughout the range of parameters.

One effect of the unimportance of $E_{21}w_0^2w_1$ and $E_{12}w_0w_1^2$ for large deflections was the poor definition of w_0 and, therefore, pressure. Thus when w_1 was large, one equation was solved for w_1 almost independently of w_0. Thus the usual interaction of simultaneous equations was not present and the values of pressure were somewhat

doubtful. Also for large deflections the potential energy was not well defined since it was a small difference between large quantities. Since the term $E_{04}w_1^4$ was the largest energy term as w_1 became greater than, say, 0.01, it seemed apparent that terms in w_1^5, w_1^6, etc. would be of importance.

E Analytical Results

A detailed analysis as outlined in the Solution Section was completed only for a configuration like that of experimental shell number 23. Fig. 14 was plotted from the analysis of "free" deflection, that is, with both w_1 and b as independent parameters. The calculations were terminated in the post-buckling range when it seemed that the pressure was no longer adequately defined. Fig. 15 was for the same configuration, but for a case of volume control. Again the calculations were terminated at a point in the large deflection range.

A number of analyses were made for the "free" deflection case and the resulting load-deflection curves are plotted in Fig. 16. (The buckling pressures for these analyses were listed in Appendix D). From this figure it can be seen that the buckling loads were much too high, averaging about 1.3 times the linear buckling load. There is some variation between the values of the peak pressures and there is even a difference for the two cases with equal λ. The latter circumstance points up the fact that λ was not the only parameter needed to specify shape; α was also required in the analysis. This is of course due to the use of $c \sin \alpha$, $\sin c\alpha$ and $c/b \sin b\alpha$, which would all be designated as $c\alpha$ or $\lambda/\sqrt{2}$ in the shallow shell analysis. Hence it is quite possible that λ is not the only important parameter for deep shell buckling, but some depth measure such as α or H is needed.

Since the computed buckling loads were much above experimental results and even above the calculated buckling pressures of Budiansky, it was apparent that the deflected shape was too restricted. Not only was the only form of deflection a central dimple, but no variations were possible for the mode shapes.

The pressure-volume change curves of Fig. 14 and 15 show that the initial portion of the loading curve should be linear, at least for large λ. This was indeed the case in the experimental work (see Fig. 16).

There was some difficulty in finding the proper range of b for each shell. As may be seen in Appendix D, the values of b for the peak of the curve varied in no orderly fashion. Further it was found that b varied rapidly near buckling for some cases and very slowly for others. At least the values of b which were of interest were always near 90% of c. In all cases the value of b increased as the loading proceeded, reached a maximum value early in the post-buckling range and then decreased. Thus most of the sets of equations had two sets of solutions, one for small deflection and the other for large.

The difficulties encountered in finding equilibrium positions at large deflections have already been discussed in the Solution Section. Evidently more nonlinear terms are required in the equation for π. This would mean constructing a more appropriate order of magnitude criterion than used herein. Then strain-displacement relations could be simplified using the new criterion. Probably the equations of

Love used in this report should be reviewed to determine if they are valid for very large deflections.

Some of the added problems just described may be avoided or simplified if the loading problem is divided into two parts: the buckling problem and the large deflection problem. At least for the buckling problem, the present order of magnitude criterion and strain-displacement relations are quite adequate.

The deflected shape used in this analysis is not recommended for a future attempt. A reasonable formula for deflection should satisfy all boundary conditions, conform to the known and expected mode shapes, have as few terms as possible per parameter, and be reasonably integrable.

CHAPTER 6 SUMMARY AND CONCLUSIONS

In the experimental portion of this study, thirty nine plastic spherical shell segments were tested under external pressure. Most of the tests were made with displacement control so that buckling occurred without a change in average displacement. A few tests were also made with pressure control since the latter situation best approximates a practical case. In this group of shells, the shell shape parameter, λ , varied from 3.5 to 25. The test procedures used in the experiments were listed in some detail because of the important effect of creep and time on the buckling loads.

All the shells were buckled a number of times and the buckling loads were found to be repeatable under unchanged conditions.

With the tests under displacement control a measure of deflection was known at each stage of loading. Hence a load versus deflection curve was plotted in some cases. Important points on this curve, were the buckling pressure, pressure to which the shell jumped at buckling, pressure at unbuckling and the minimum pressure on the curve. The critical pressures were found to fall in a fairly narrow range in the midst of test results of other investigators, the results for constant pressure tests being slightly above those with volume control. The critical pressures exhibited a slight downward trend with increase in λ and the minimum pressure was evidently a function of shell depth instead of λ. The other two important pressures were definitely functions of λ.

A discussion of the occurrence of buckling is presented in Section 4D, describing the variations of buckle sizes and positions, the shape of the loading curves, and the changes in the buckling phenomenon with changes in λ.

The effect of imperfections in the shell were investigated, but no relationship between imperfection and critical load was found. The accuracy with which the shell was clamped in the test chambers had a noticeable effect on the critical load. Since the plastic of the shells exhibited some creep, this also changed the critical loads. A simple analysis of the creep effect was made and used to cancel out this effect.

The energy criterion of Tsien was reviewed and compared with experimental results. However, Tsien predicted buckling loads under constant pressure would be about half those under constant volume (displacement control) and this was not verified by the experiments.

The tests have served as an indication of the value of plastic as a testing material and of the importance of repeatable testing of the same specimen.

A variational or energy method was used in the analytical study. The equation for total potential energy for symmetric buckling in deep spherical shells was derived. A formula for deflected shape was chosen based on the shape seen in the experimental work. The equilibrium equations derived from the energy equation were found to be adequate in the range of deflection near buckling but not so

good for large deflections. For an analysis far into the post-buckling range a new order of magnitude analysis and new strain-displacement relations would probably be needed.

The equilibrium equations were solved to find equilibrium positions and thence load-deflection curves. In two cases a plot of energy versus deflection was also made. Analyses were made for five shells with from 14 to 25. Since these were considered deep shells, it was found necessary to specify both λ and α. The curves were quite similar to those plotted during the experimental study but ctitical loads were 3 or 4 times too high. That the analytical buckling pressures are even above those of other investigators is probably due to a restricted form for deflected shape which failed to account for small undulations which occur in the surface prior to buckling.

There is a large spread between theoretical and experimental buckling pressures and even quite a range between test results. This scatter is probably due to clamping conditions during testing (5% or 10% but possibly a much larger effect), imperfections in the shell (unknown effect), and nonaxisymmetry of buckling. The tests indicate that the latter effect may be rather minor.

CHAPTER 7 SUGGESTIONS FOR FURTHER STUDY

This investigation has developed many questions and problems which still need a solution Among these are the following topics for study:

1. Unsymmetric modes of deformation should be considered in determining buckling loads. Techniques with a reasonable chance of success in the project are those of Weinitscke, Thurston, Budiansky, and Caseman.

2. The correlation between edge restraint and buckling load should be studied. In practical situations, the edge support will not be clamped or pinned but merely restrained to some degree.

3. A general theory for the effect of imperfections on shell buckling is much needed. First the mode shapes for any λ must be known and then the interaction of imperfection size and position and modal deformations could be considered.

4. The equations of equilibrium should be derived and a study made of the importance of terms for any amount of deformation. Many such studies have been made but usually a priori and not based on any conrete results.

5. It would be useful to make some experiments with as little error caused by testing conditions as possible and true constant pressure tests should be performed as well as constant volume tests. To reduce the effects of minor imperfections, the shells should be thick and the shells should be clamped between rings with a spherical

surface so that no rim would be required.

6. The effect of rate of change of load over the surface should be considered. So far uniform loads have been most popular, but wind loads and point loads also produce buckling.

CHAPTER 8 BIBILIOGRAPHY

(1) Zoelly, R. (in German)
On a Buckling Problem of the Spherical Shell.
Dissertation, Zurich, 1915

(2) Timoshenko, S.
Theory of Elastic Stability.
McGraw-Hill Book Company, Inc., 1936.

(3) Van der Neut, A. (in German)
The Elastic Stability of a Thin Spherical Shell.
Dissertation, Delft, 1932

(4) Von Karman, T., and Tsien, H. S.
The Buckling of Spherical Shells by External Pressure.
Journal of the Aeronautical Sciences, Vol. 7, No. 2, 1939

(5) Friedrichs, K. O.
On the Minimum Buckling Load for Spherical Shells.
Theodore von Karman Anniversary Volume, California Institute of Technology, 1941

(6a) Mushtari, K. M. and Surkin, R. G. (in Russian)
On the Nonlinear Stability Theory of Elastic Equilibrium of a Thin Shell under the Influence of Uniformly Distributed Normal External Pressure.
Prikladnaia Matematika i Mekhanika, Vol. 14, p. 573, 1950

(6b) Mushtari, K. M. (in Russian)
On the Theory of Stability of a Spherical Shell under the Action of External Pressure.
Prikladnaia Matematika i Mekhanika, Vol. 19, p. 251, 1955

(7) Feodosev, V. I. (in Russian)
On the Stability of Spherical Shells under the Action of a Uniform External Pressure.
Prikladnaia Matematika i Mekhanika, Vol. 18, p. 35, 1954

(8) Tsien, H. S. (experimental work included)
A Theory for the Buckling of Spherical Shells by External Pressure.
Journal of Aeronautical Sciences, Vol. 9, No. 10, 1942

(9) Kaplan, A. and Fung, Y. C. (experimental work included)
A Nonlinear Theory of Bending and Buckling of Thin Elastic Shallow Spherical Shells.
U.S. N.A.C.A. Technical Note 3212, 1954

(10) Homewood, R.H., Brine, A. C., and Johnson, A. E.
(Experimental work included)
Instability of Monocoque Shells.
Experimental Mechanics, Jour. of Society for
Experimental Stress Analysis, March 1961, p. 88

(11) Archer, R. R.
Stability Limits for a Clamped Spherical Shell Segment under
Uniform Pressure
Quarterly of Applied Mathematics, Vol. 15, No. 4, p. 355, 1958

(12a) Weinitschke, H. J.
On the Nonlinear Theory of Shallow Spherical Shells.
Journal of the Society for Industrial and Applied Mathematics,
Vol. 6, No. 3, p. 209, 1958

(12b) Weinitschke, H. J.
On the Stability Problem for Shallow Spherical Shells.
Journal of Mathematics and Physics, Vol. 38, No. 4, p. 209,
1960

(13) Von Willich, G. P. R.
The Elastic Stability of Thin Spherical Shells.
Journal of the Engineering Mechanics Division, American
Society of Civil Engineers, Jan. 1959

(14) Chen, W. L.
Effect of Geometrical Imperfection on the Elastic Buckling of
Thin Shallow Spherical Shells
Sc.D. Thesis, Dept. of Civil Engineering, M.I.T., 1959

(15) Caseman, A. B.
Influence of the Assumed Deflected Shape in Applying the
Energy Method to Determine the Elastic Buckling Pressure
of Thin Shallow Spherical Shells.
Sc.D. Thesis, Department of Civil Engineering, M.I.T., 1961

(16a) Reiss, E. L., Greenberg, H. J., and Keller, H. B.
Nonlinear Deflections of Shallow Spherical Shells.
Journal of the Aeronautical Sciences, Vol. 24, No. 7, p. 533,
1957

(16b) Keller, H. B. and Reiss, E. L.
Spherical Cap Snapping.
Journal of the Aeronautical/Space Sciences, Vol. 26, p. 643,
1959

(17) Thurston, G. A.
A Numerical Solution of the Nonlinear Equations for Axisymmetrical Bending of Shallow Spherical Shells.
Paper presented at Xth International Congress of Applied Mechanics in Stresa, Italy, 1960

(18) Budiansky, B.
Buckling of Clamped Shallow Spherical Shells.
Proc. of IUTAM Symposium on the Theory of Thin Elastic Shells, Delft, 1959, p. 64

(19) Rabotnov, J. N.
Local Stability of Shells
Comp. Rend. (Doklady), Vol. 52, No. 2, p.111, 1946

(20) Kloppel, K. and Jungbluth, O. (experimental work, in German)
Contributions to the Problem of Buckling in Thin-walled Spherical Shells.
Der Stahlbau, Vol. 22, No. 6, p. 121, 1953

(21) Washizu, K.
On the Variational Principles of Elasticity and Plasticity.
Tech. Report 25-18 of Aeroelastic and Structures Research Laboratory of M.I.T., March 1955

(22) Love, A. E. H.
A Treatise on the Mathematical Theory of Elasticity.
Dover Publications, New York, 1944

(23a) Novozhilov, V. V.
Foundations of the Nonlinear Theory of Elasticity.
Graylock Press, New York, 1953

(23b) Novozhilov, V. V.
The Theory of Thin Shells.
Noordhoff Ltd., Groningen, The Netherlands, 1959

(24) Reissner, E.
Stresses and Small Displacements in Shallow Spherical Shells.
Journal of Mathematics and Physics, Vol. 25, p. 279, 1947

(25) Hildebrand, F. B.
Methods of Applied Mathematics
Prentice-Hall, Inc., Englewood Cliffs, N. J., 1960

(26) Norris, C. H.
Investigation of Strength and Buckling Characteristics of Transverse Bulkheads in Cylindrical Shells - Final Report. Dept. of Civil and Sanitary Engineering, M.I.T., 1955

(27) Ostlund, Lars
Stability of Concrete Structures Submitted to Long-Time Loads Nordisk Betong 1957, Vol. 1, #1, p. 77

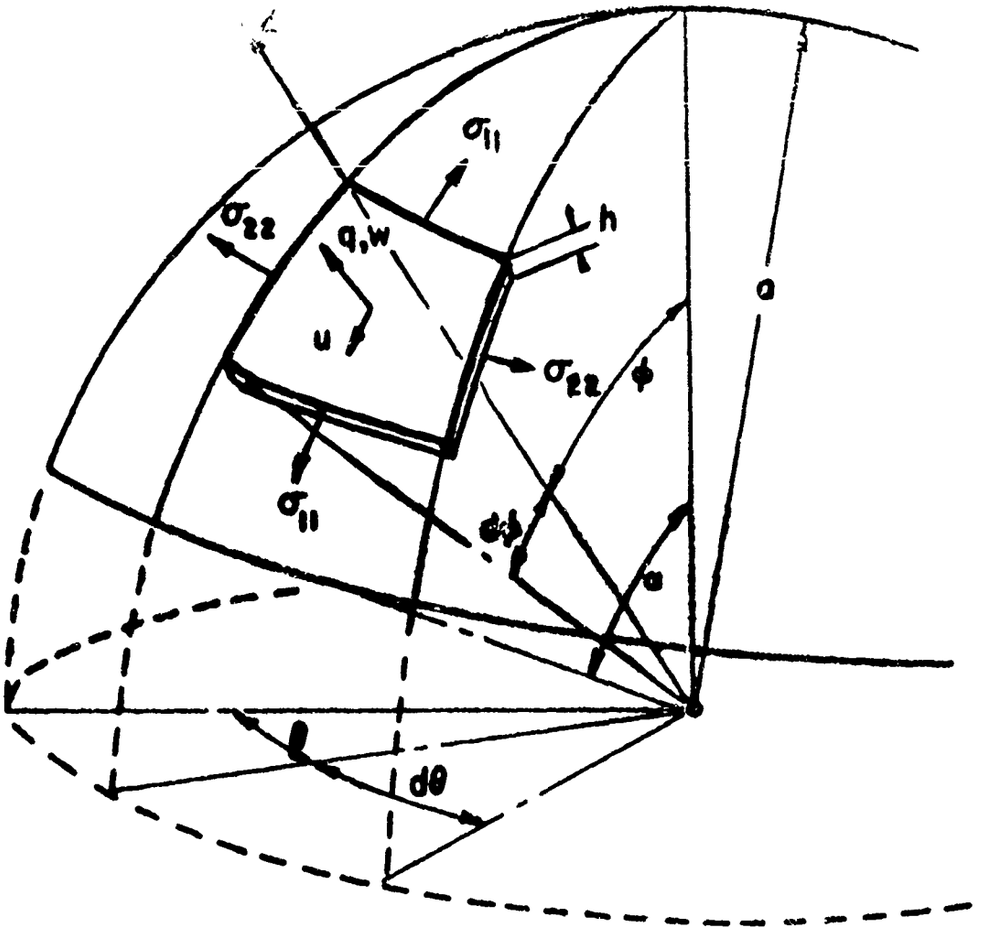

FIG. 1 NOTATION ON SHELL ELEMENT

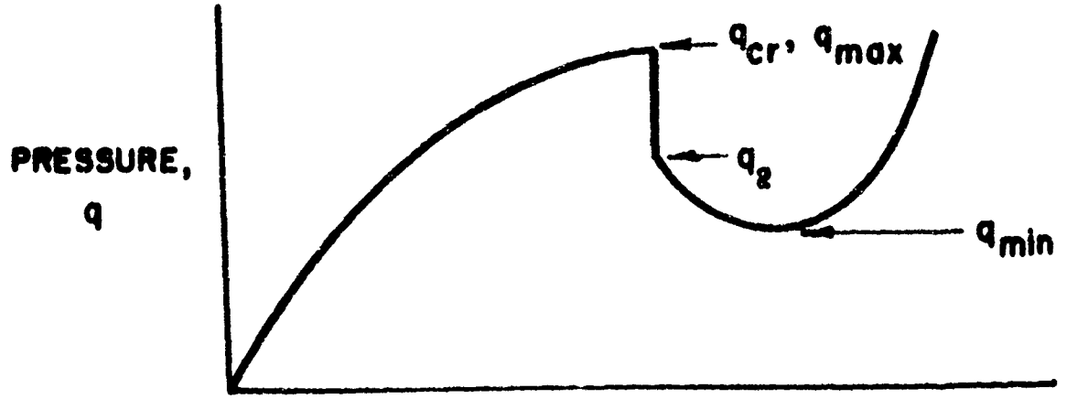

FIG. 2 LOAD-DEFLECTION CURVE

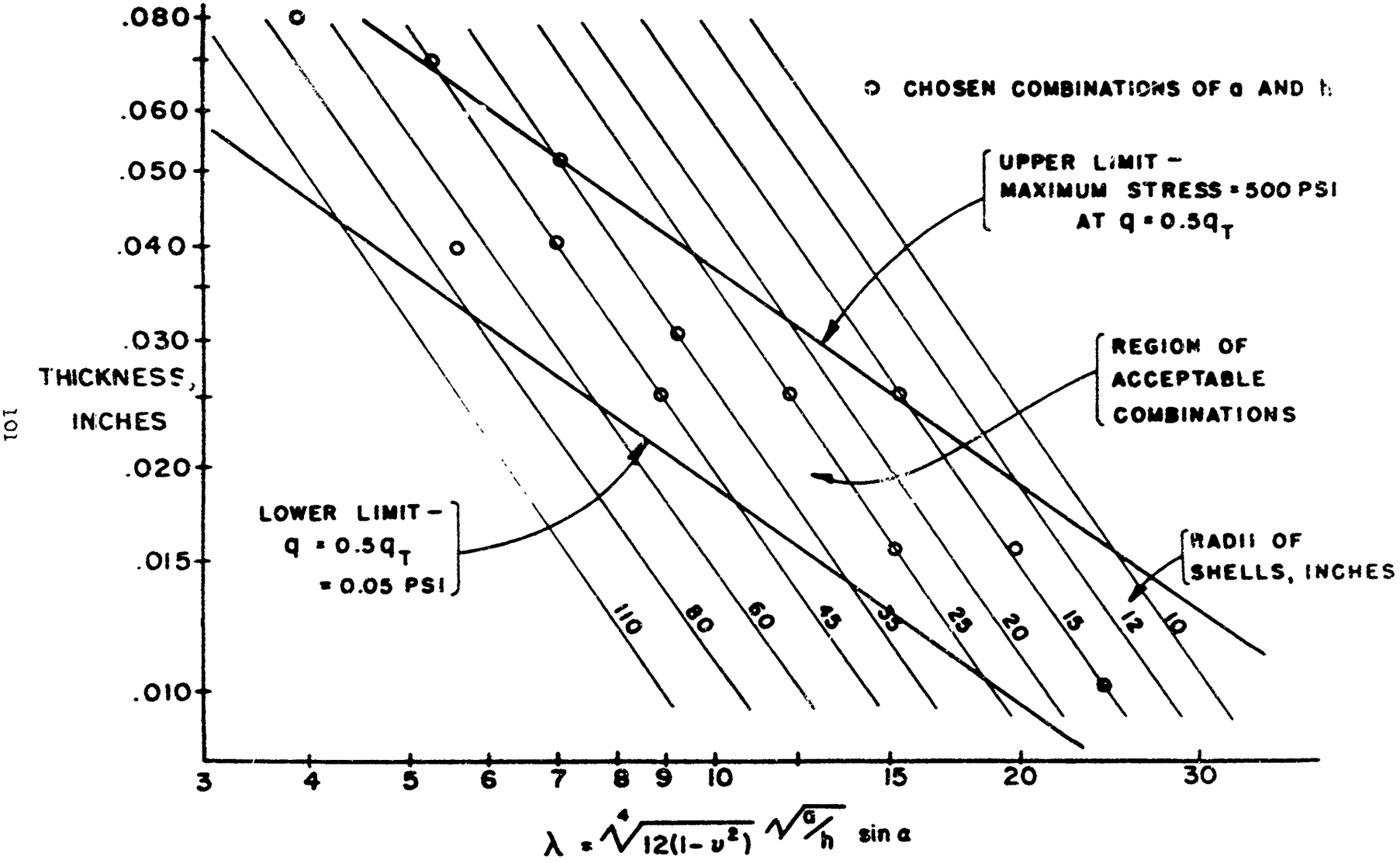

FIG. 3 RANGE OF POSSIBLE THICKNESS–RADIUS COMBINATIONS

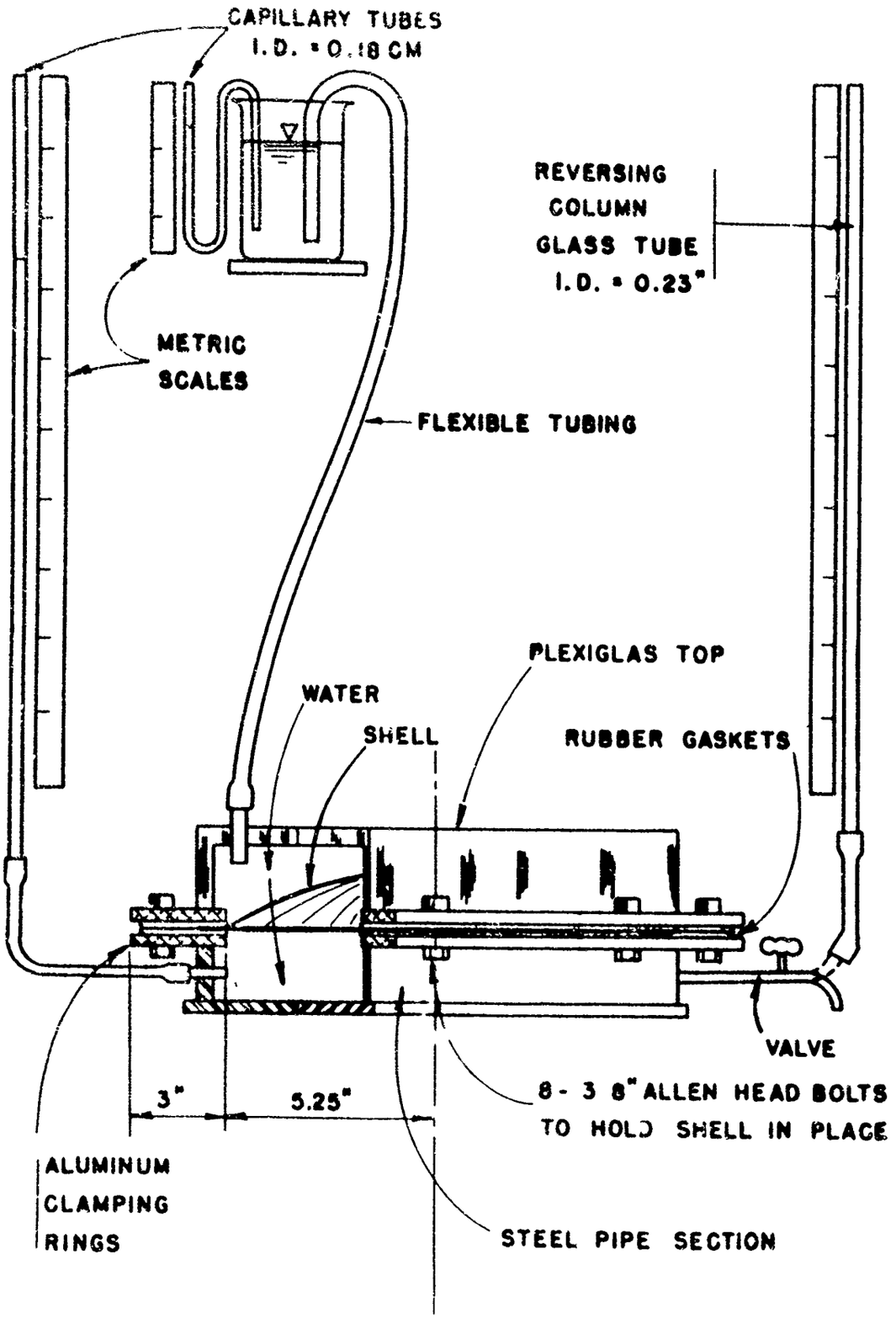

FIG. 4 SCHEMATIC OF TEST APPARATUS

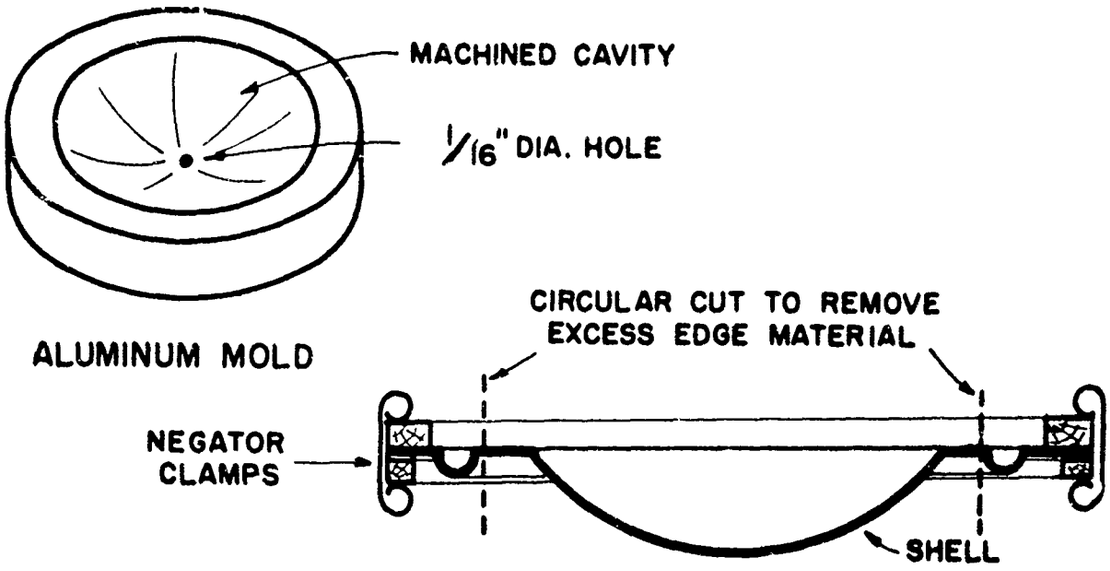

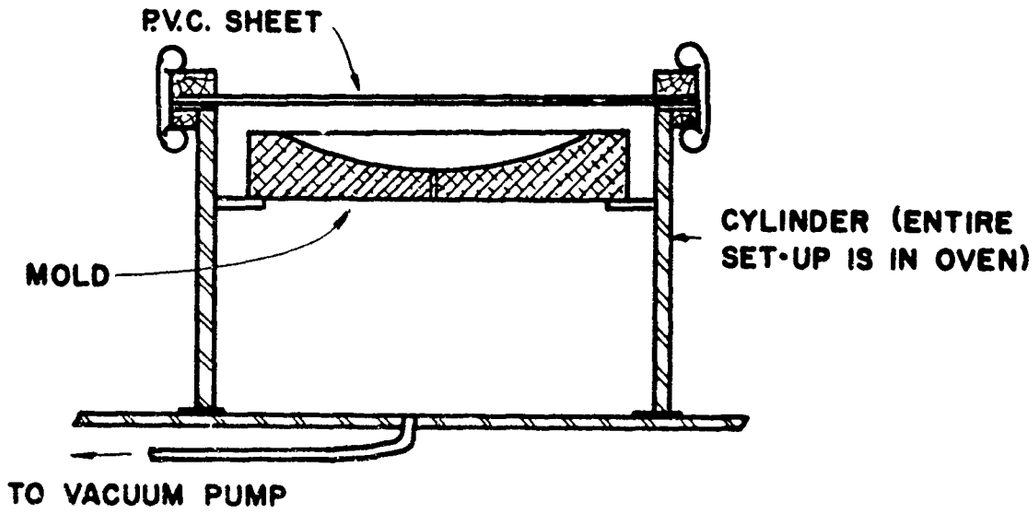

VACUUM DRAWING EQUIPMENT

FIG. 4A SHELL FORMING

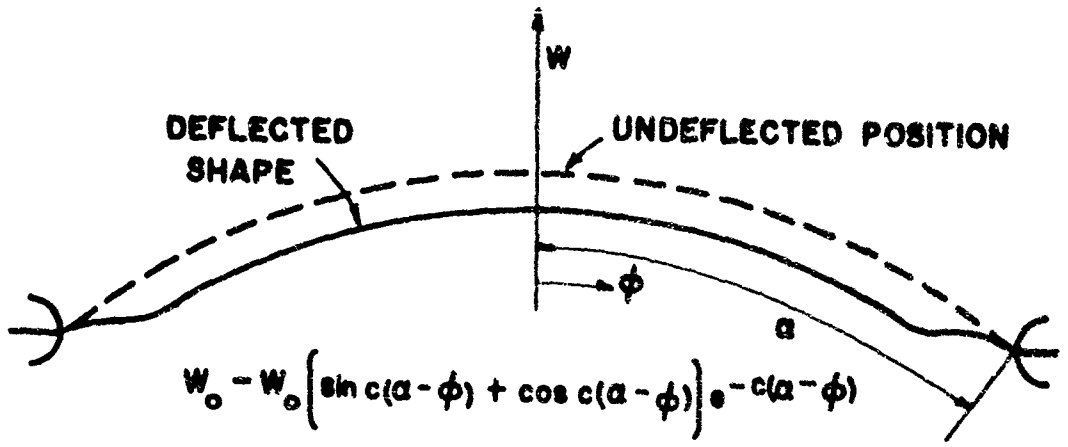

LINEAR DEFLECTION DUE TO CLAMPED EDGE

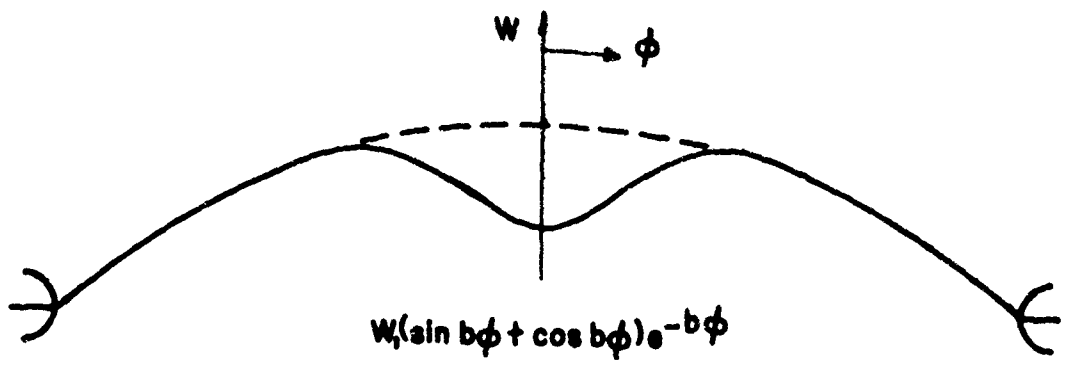

BUCKLE DEFLECTION

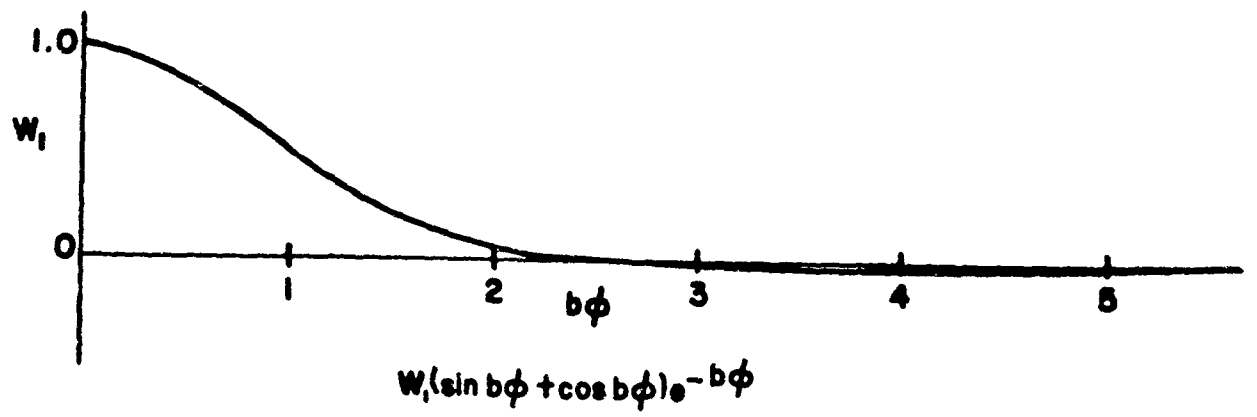

BUCKLE DEFLECTION

FIG. 4B DEFLECTED SHAPE

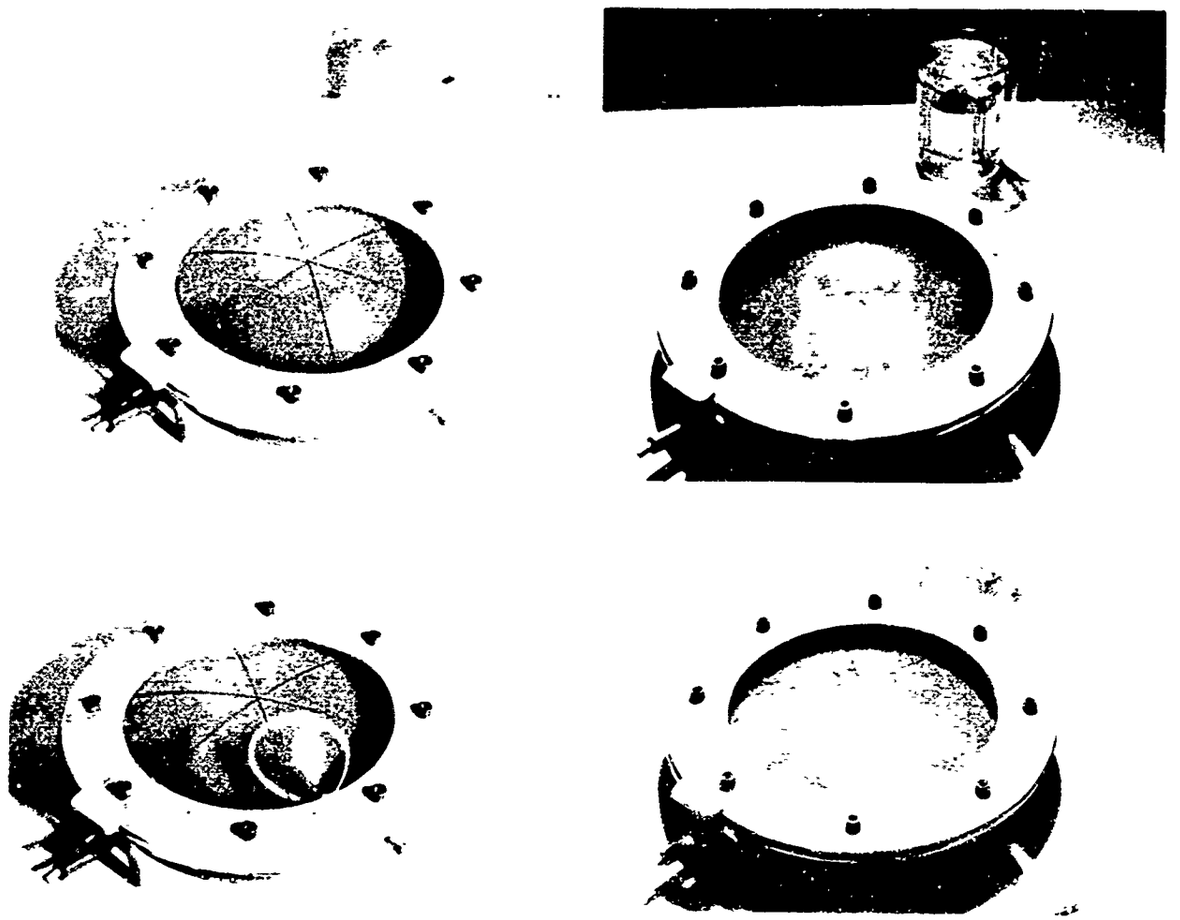

FIG. 5
SHELL AND CHAMBER

THE FOUR PHOTOS OF THE CHAMBER WITHOUT THE PLEXIGLAS TOP SHOW THE UNBUCKLED SHELL, CENTER BUCKLE, EDGE BUCKLE, AND NEAR CENTER BUCKLE. AT LEFT IS THE TEST APPARATUS READY FOR AN EXPERIMENT

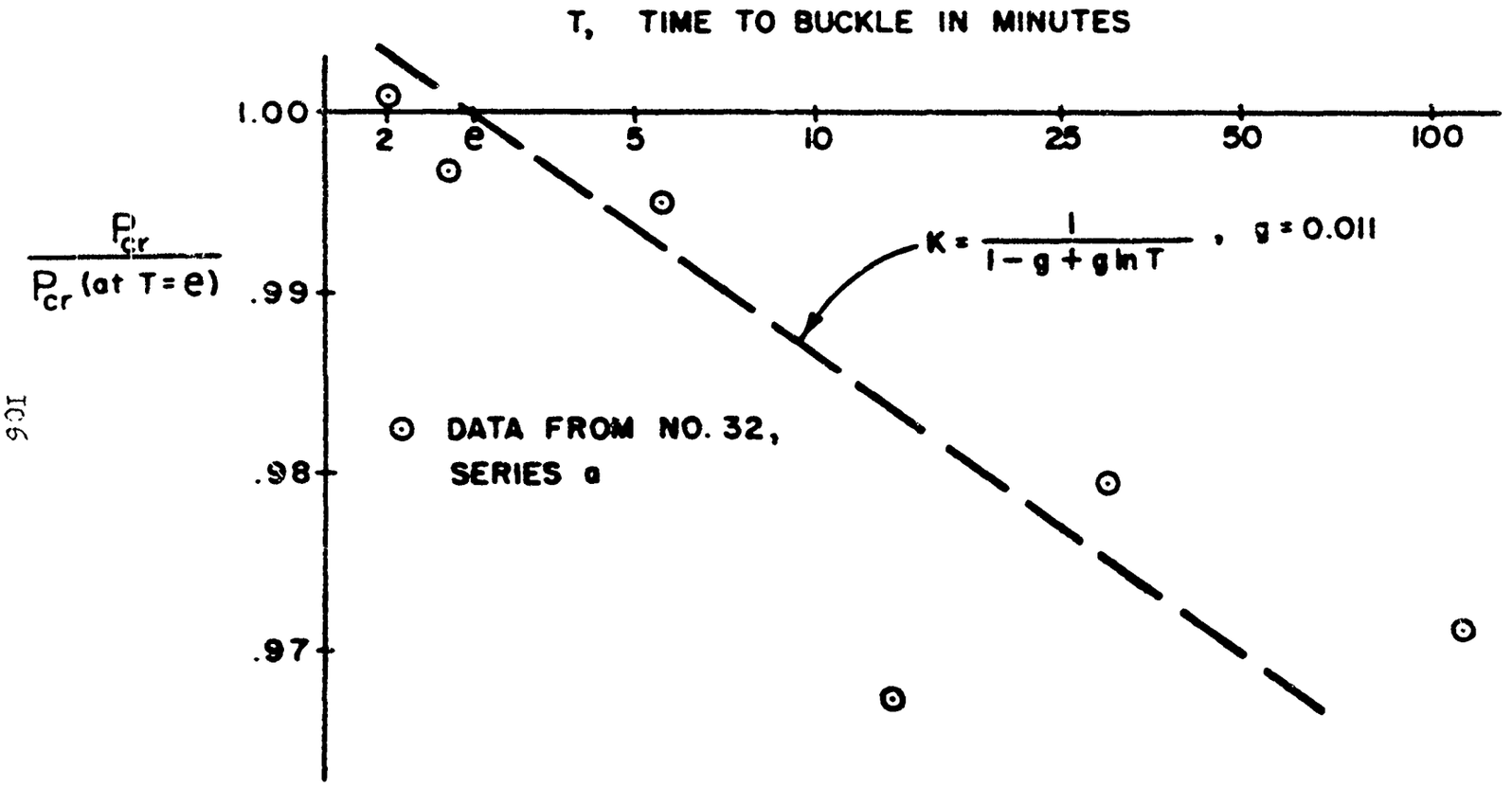

FIG. 6 EFFECT OF CREEP ON BUCKLING LOADS

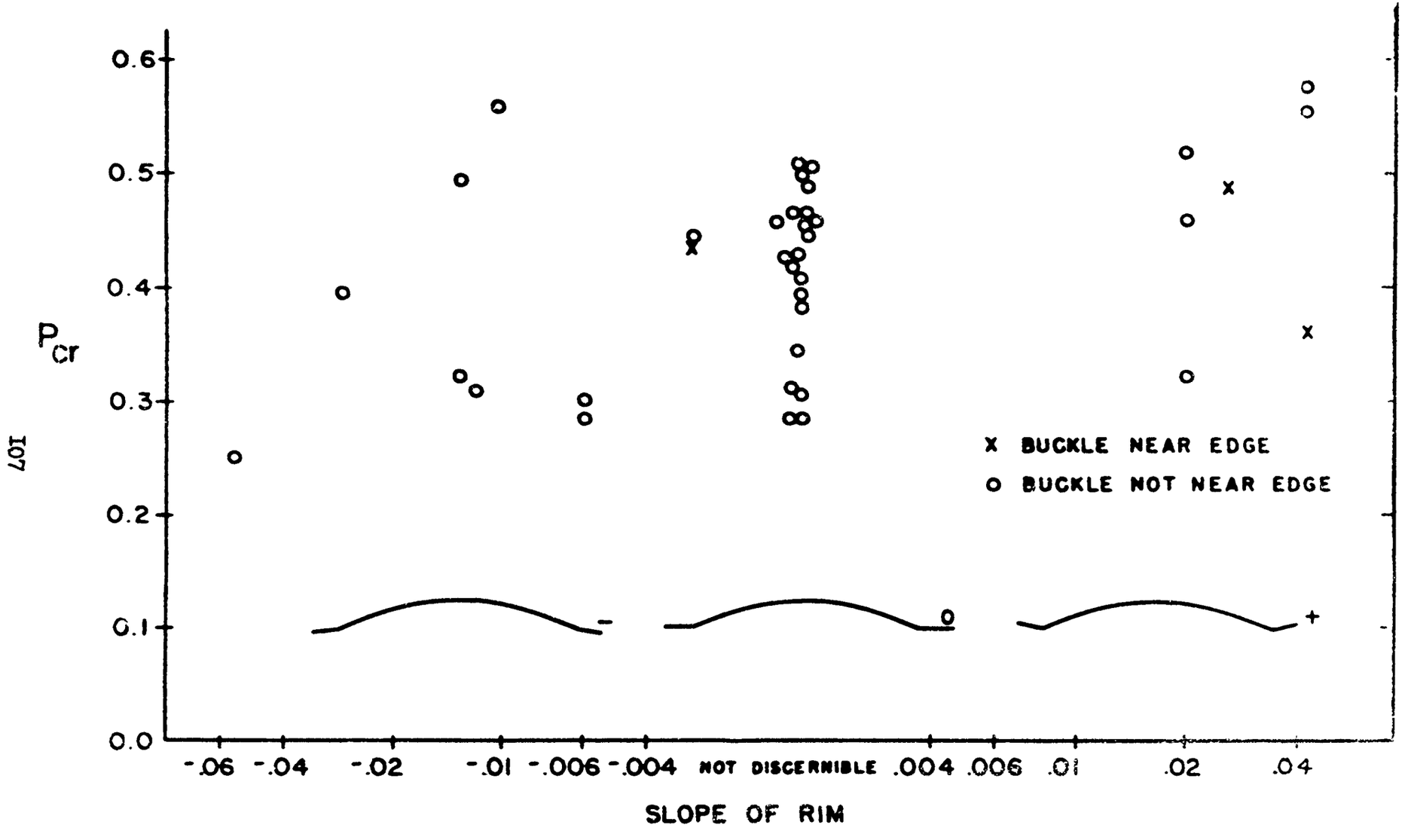

FIG. 7 EFFECT OF SLOPE ON BUCKLING LOADS

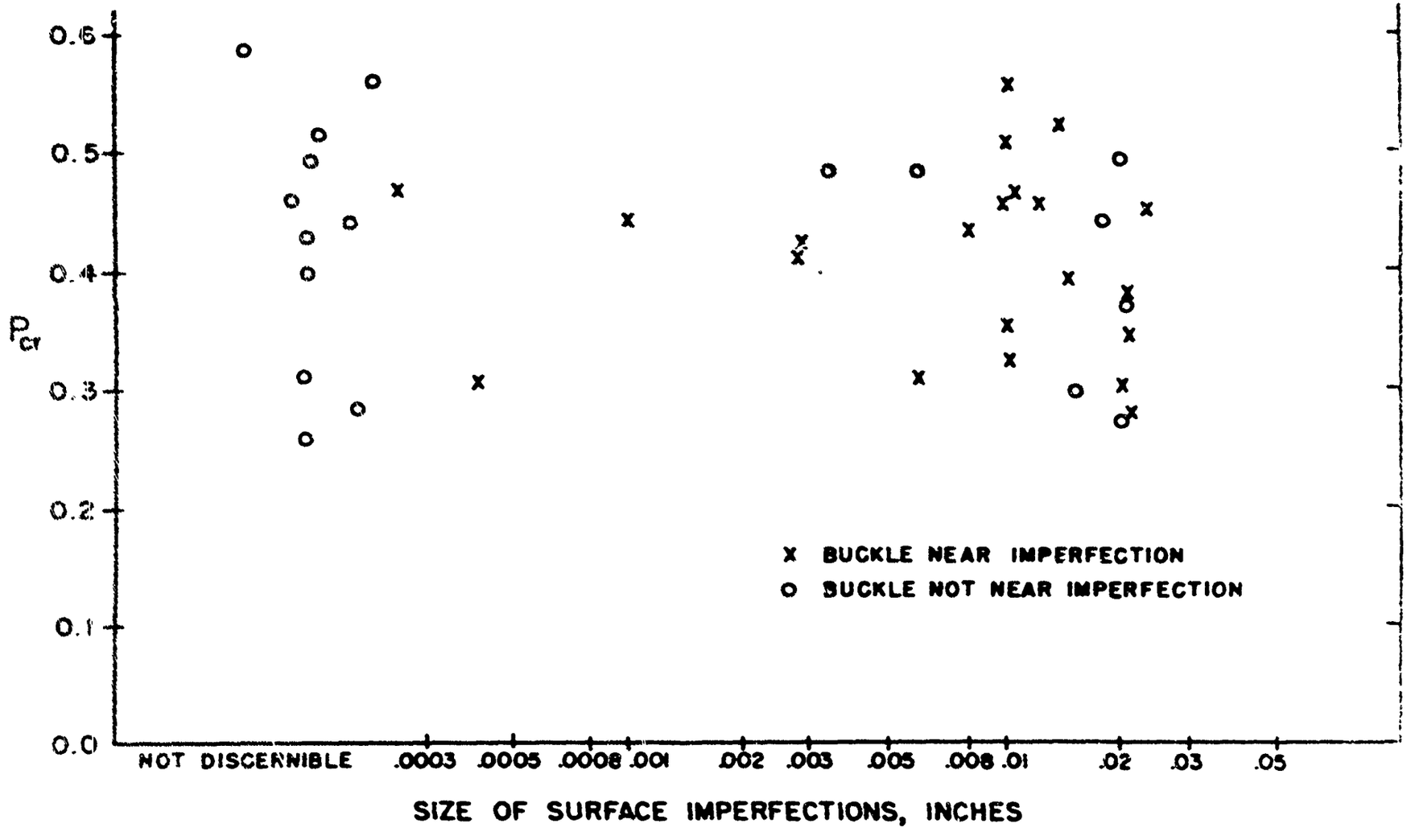

FIG. 8 EFFECT OF SURFACE IMPERFECTIONS ON BUCKLING LOADS

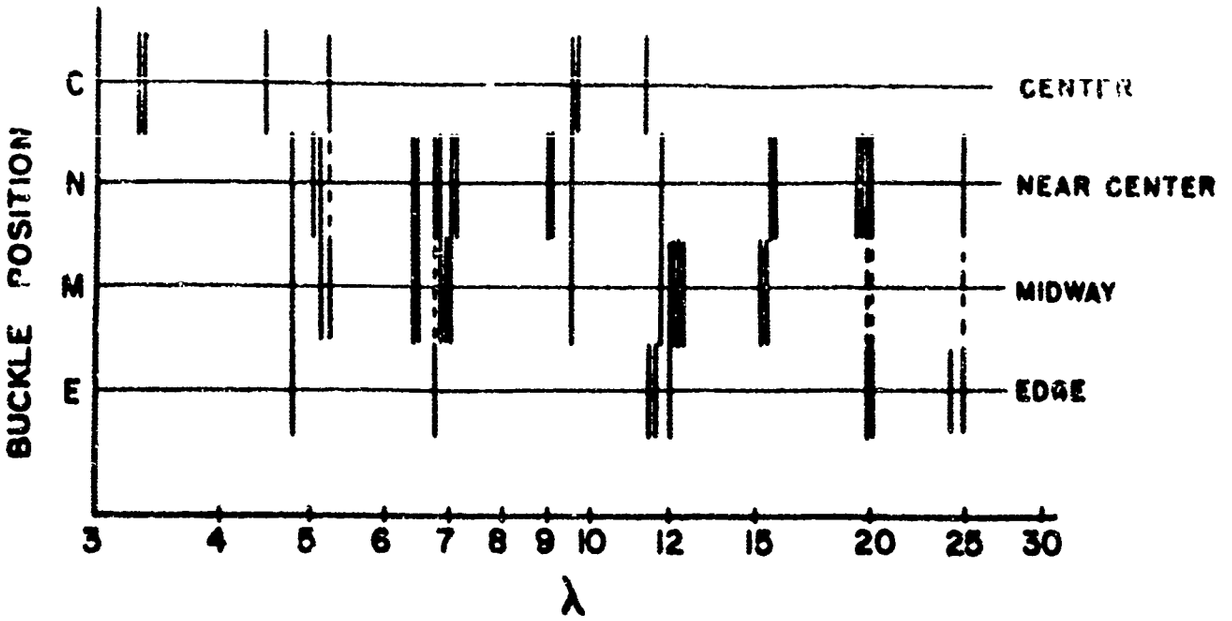

FIG. 9a VARIATION OF BUCKLE POSITION WITH λ

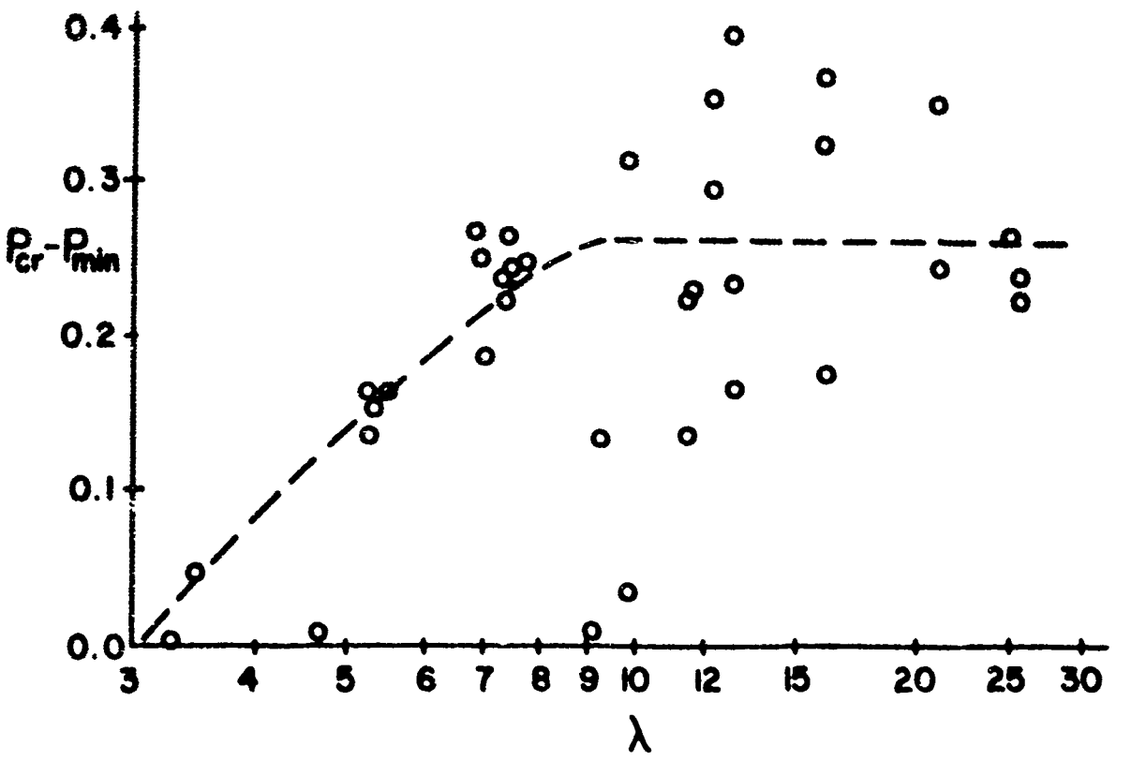

FIG. 9b DEPENDENCE OF A LOAD PARAMETER ON λ

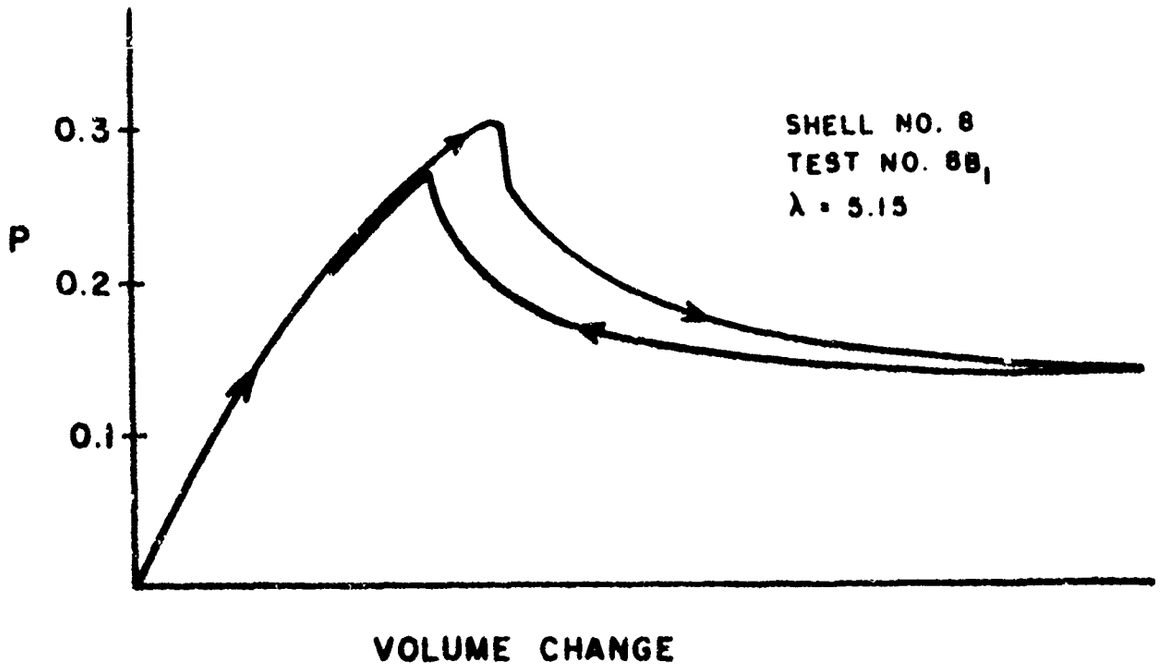

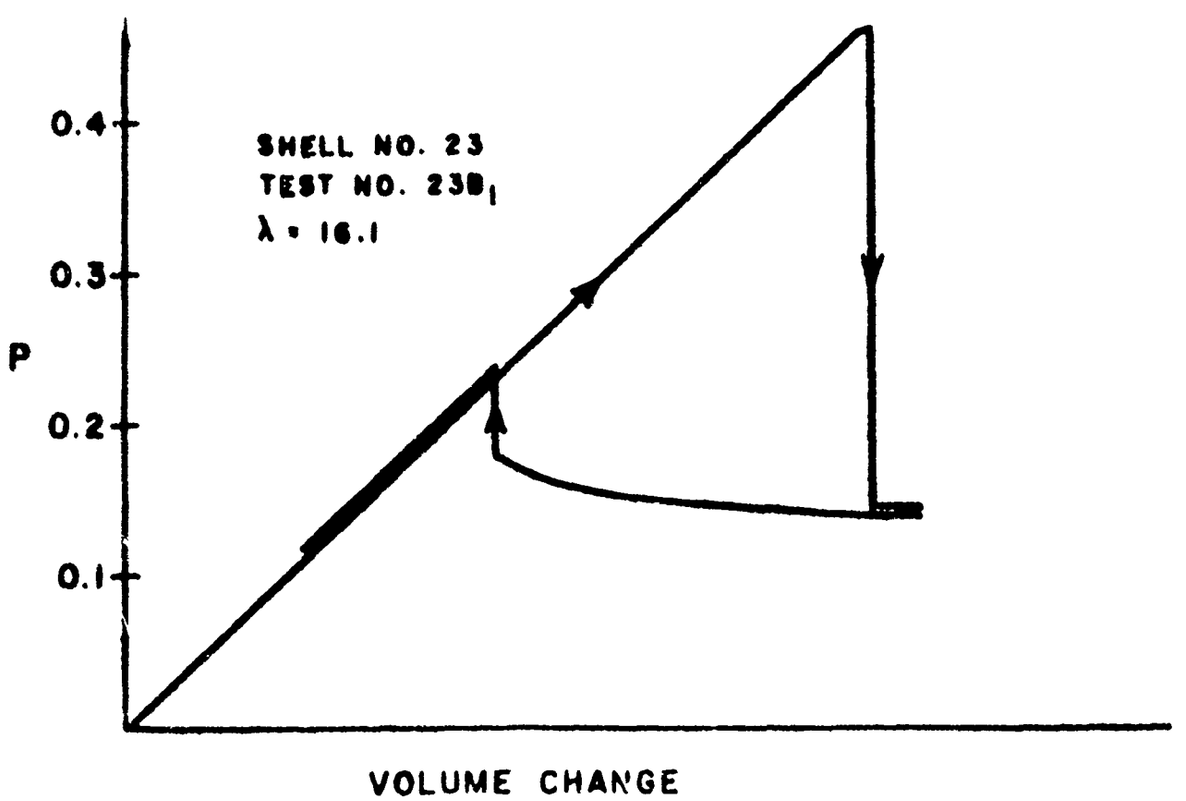

FIG. 10 LOAD-VOLUME CHANGE CURVES

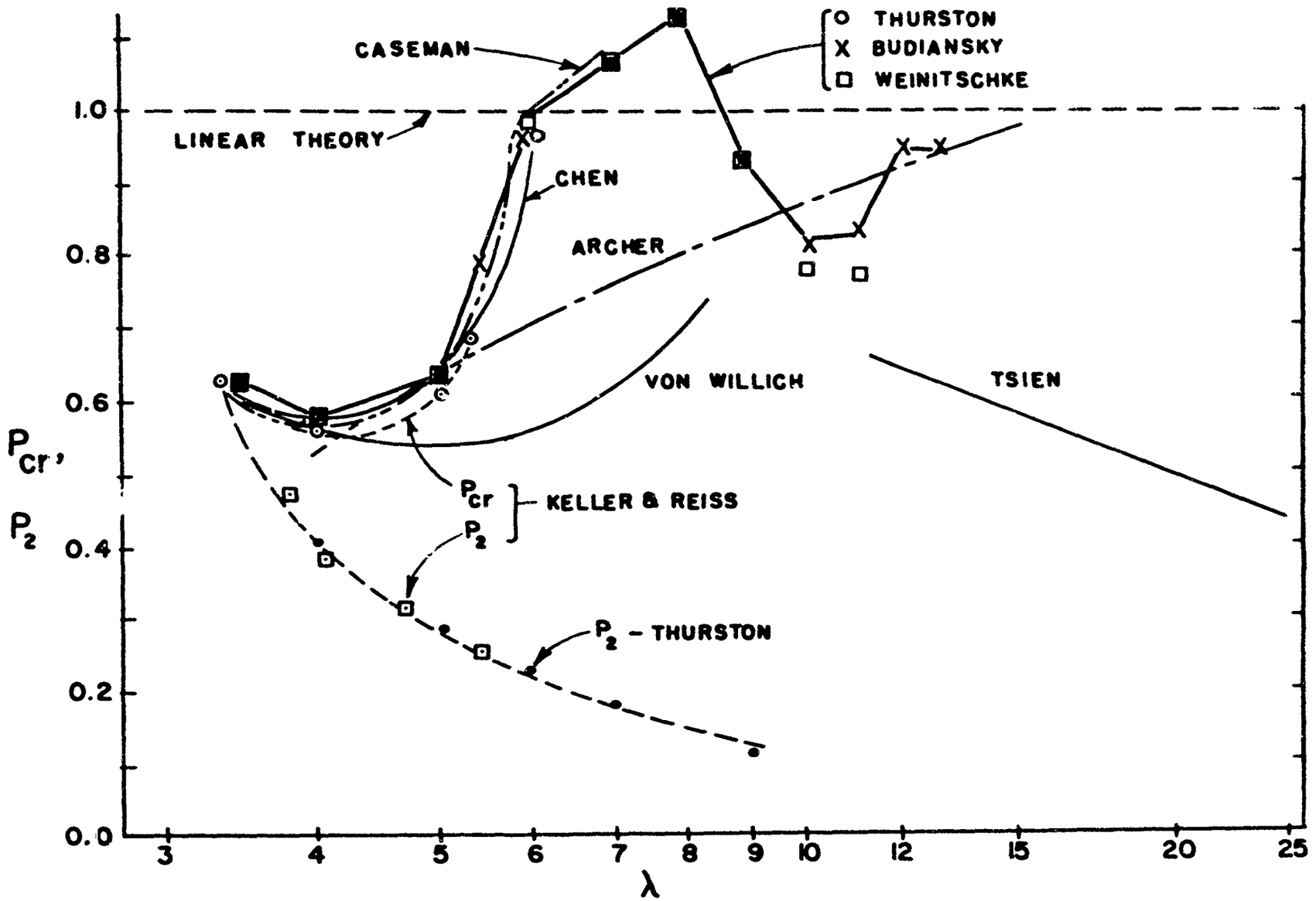

FIG. 11 THEORETICAL BUCKLING LOADS FOR PERFECT CLAMPED SPHERICAL SHELLS

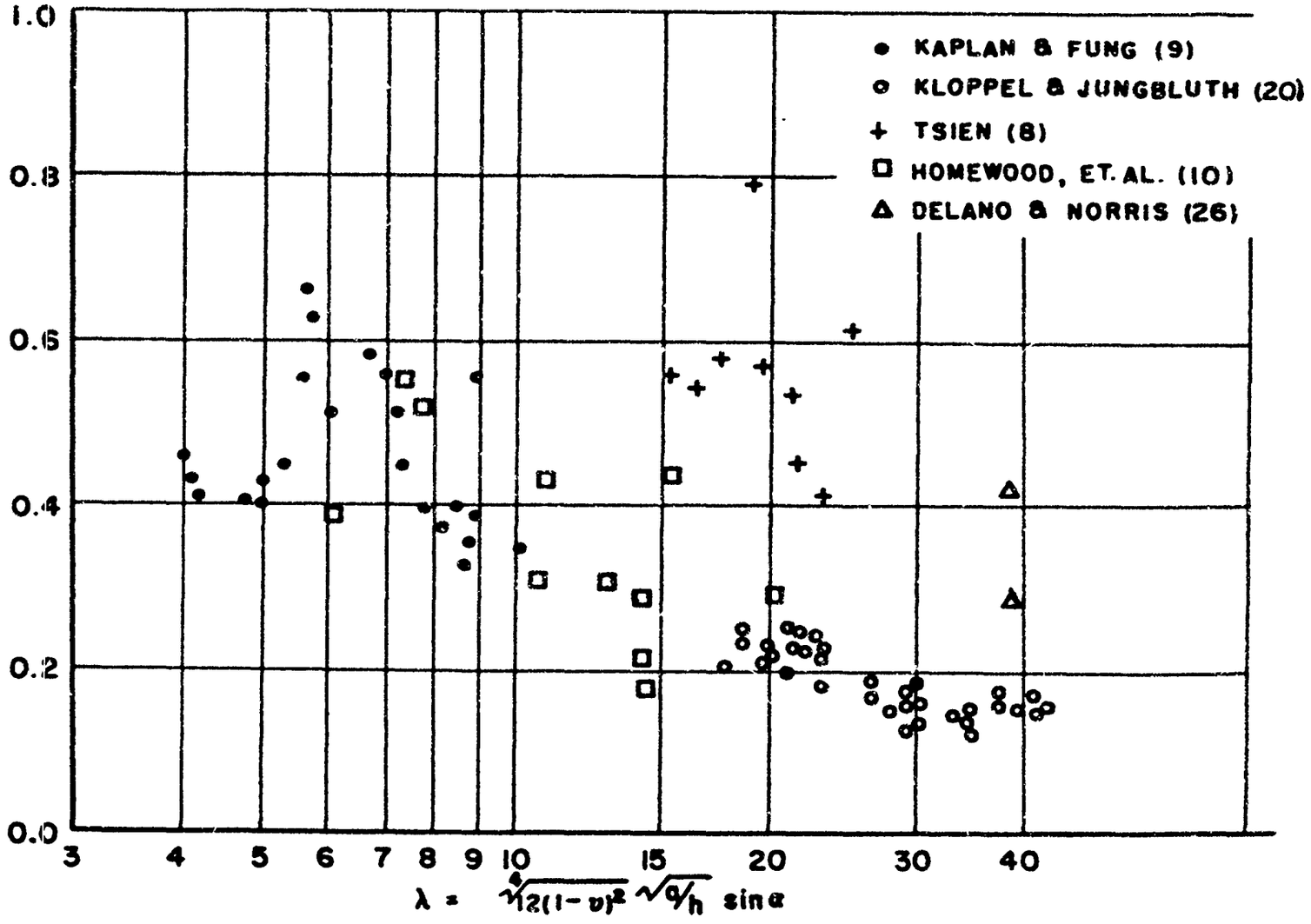

FIG. 12 EXPERIMENTAL BUCKLING LOADS OF OTHER INVESTIGATORS

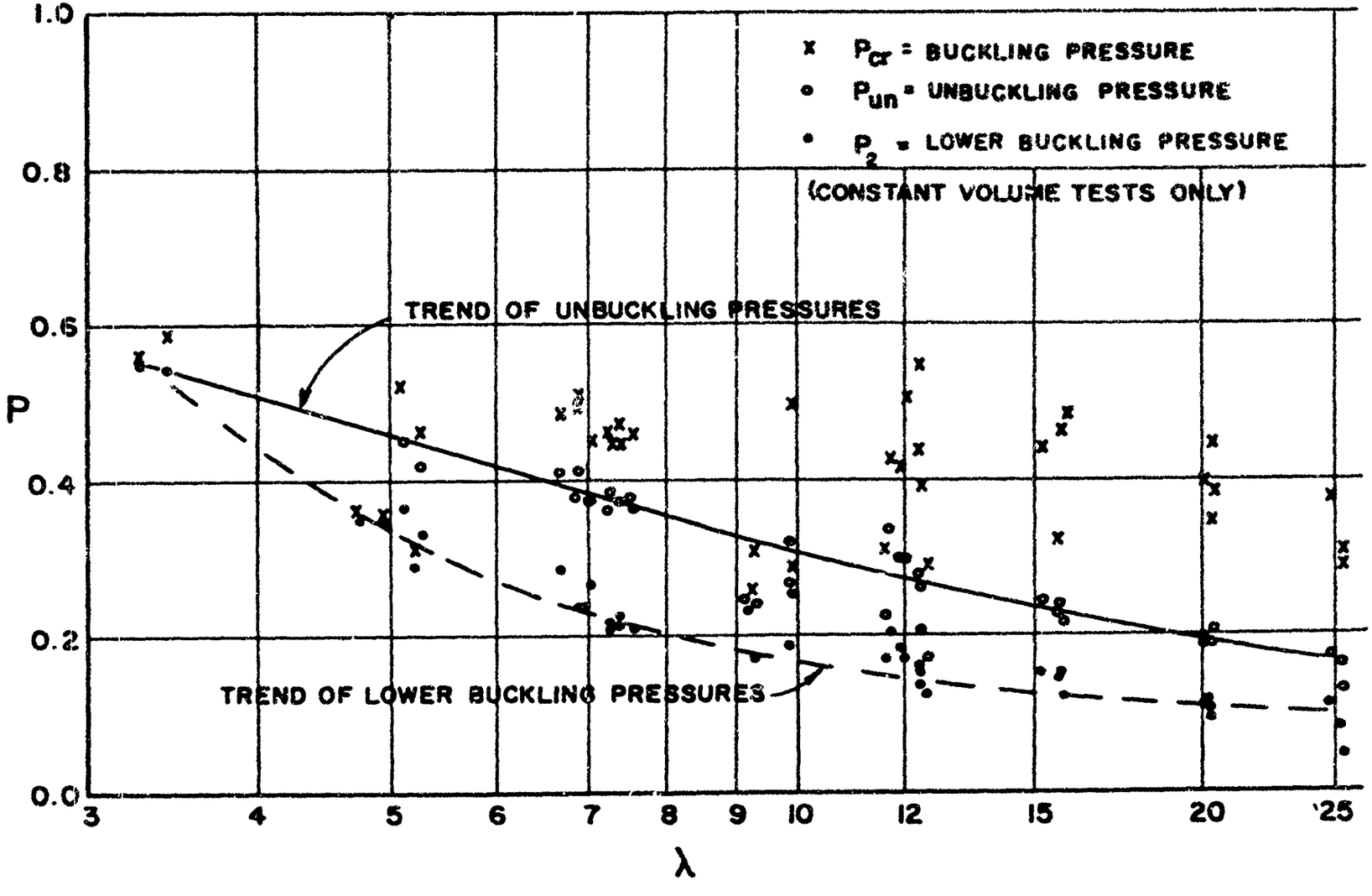

FIG. 13 P_{cr}, P_{un}, P_2 FOR TESTS IN THIS REPORT

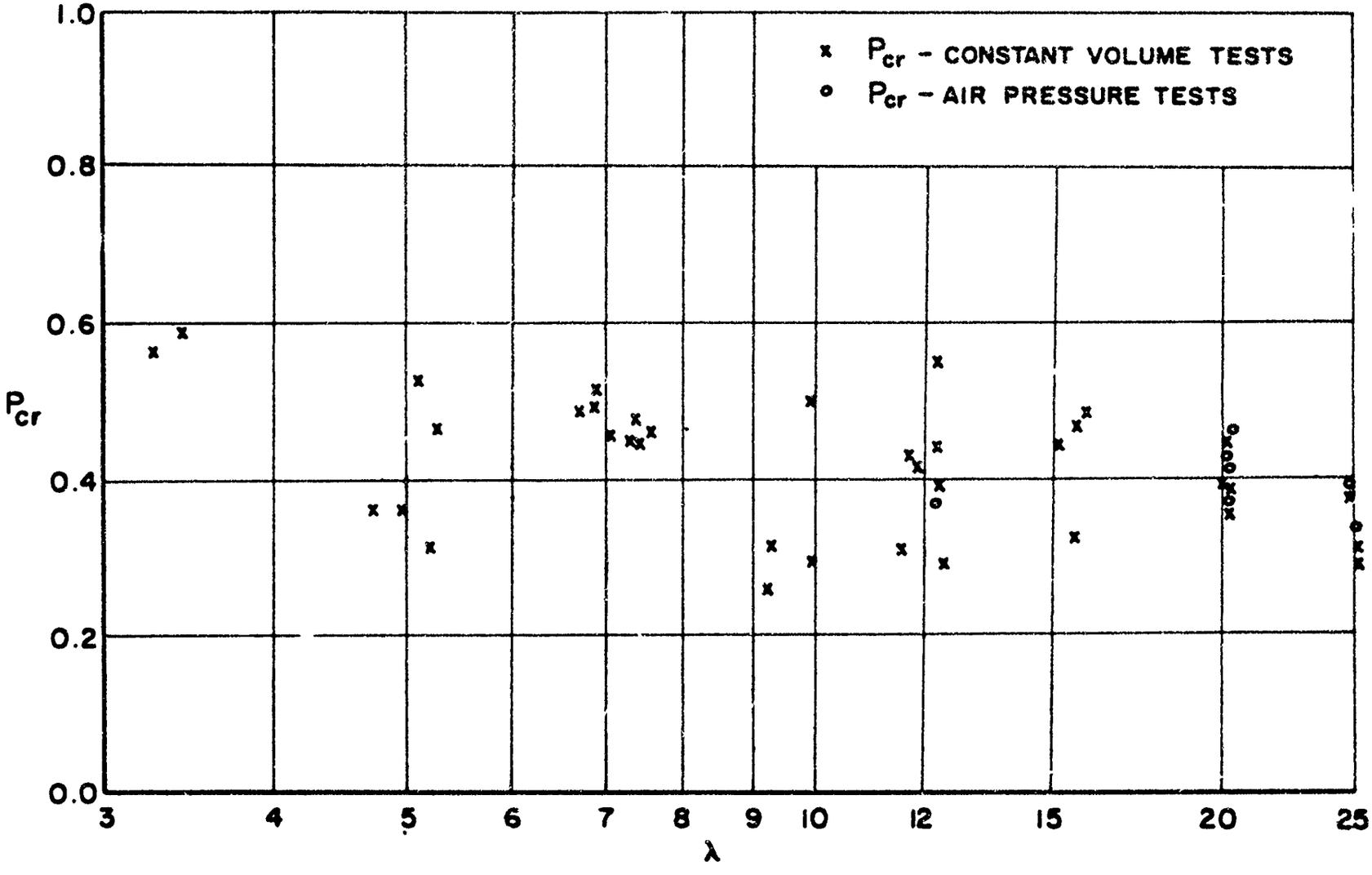

FIG. 13A P_{cr} FOR TESTS OF THIS REPORT

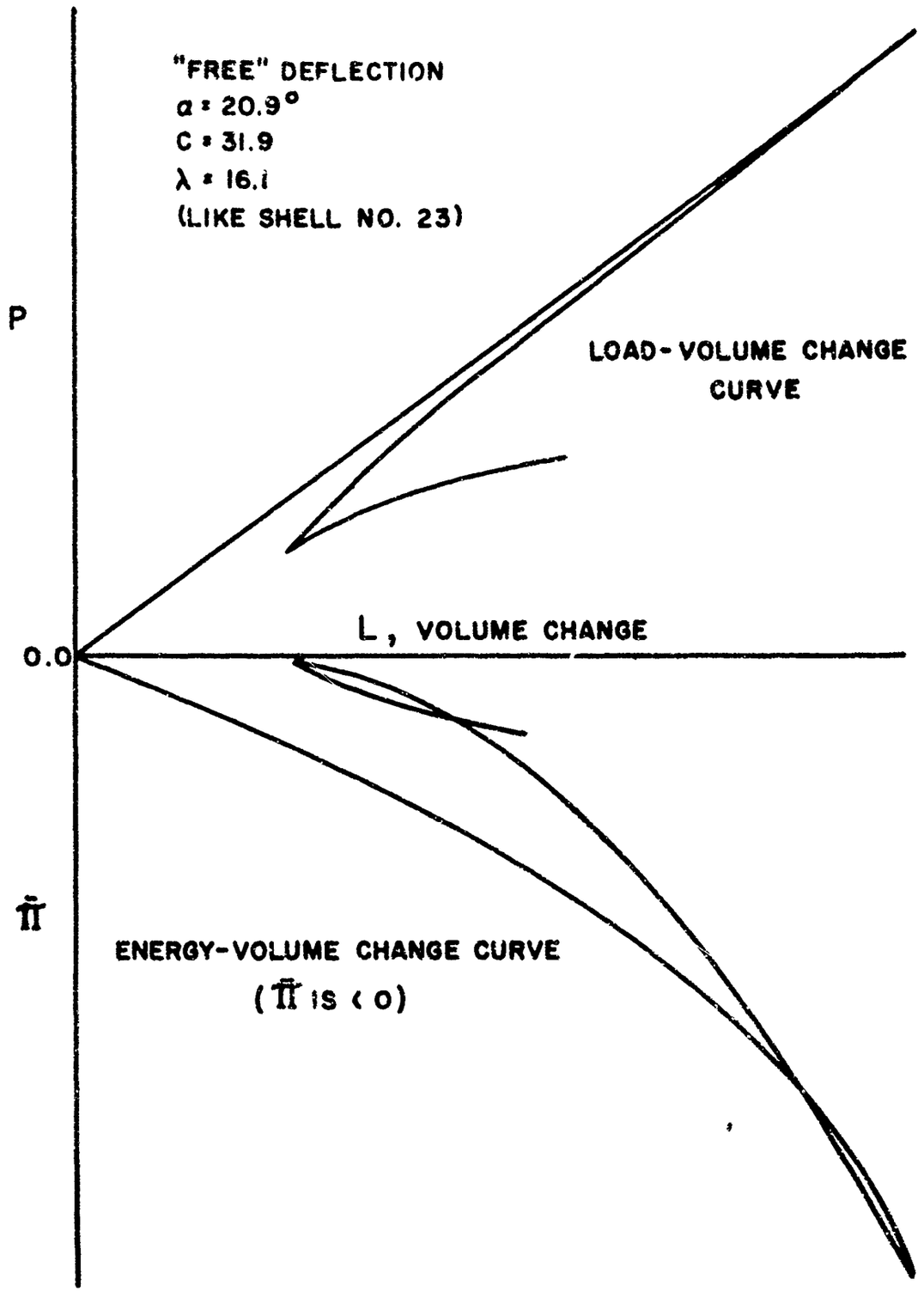

FIG. 14 LOADING CURVES FROM ANALYSIS

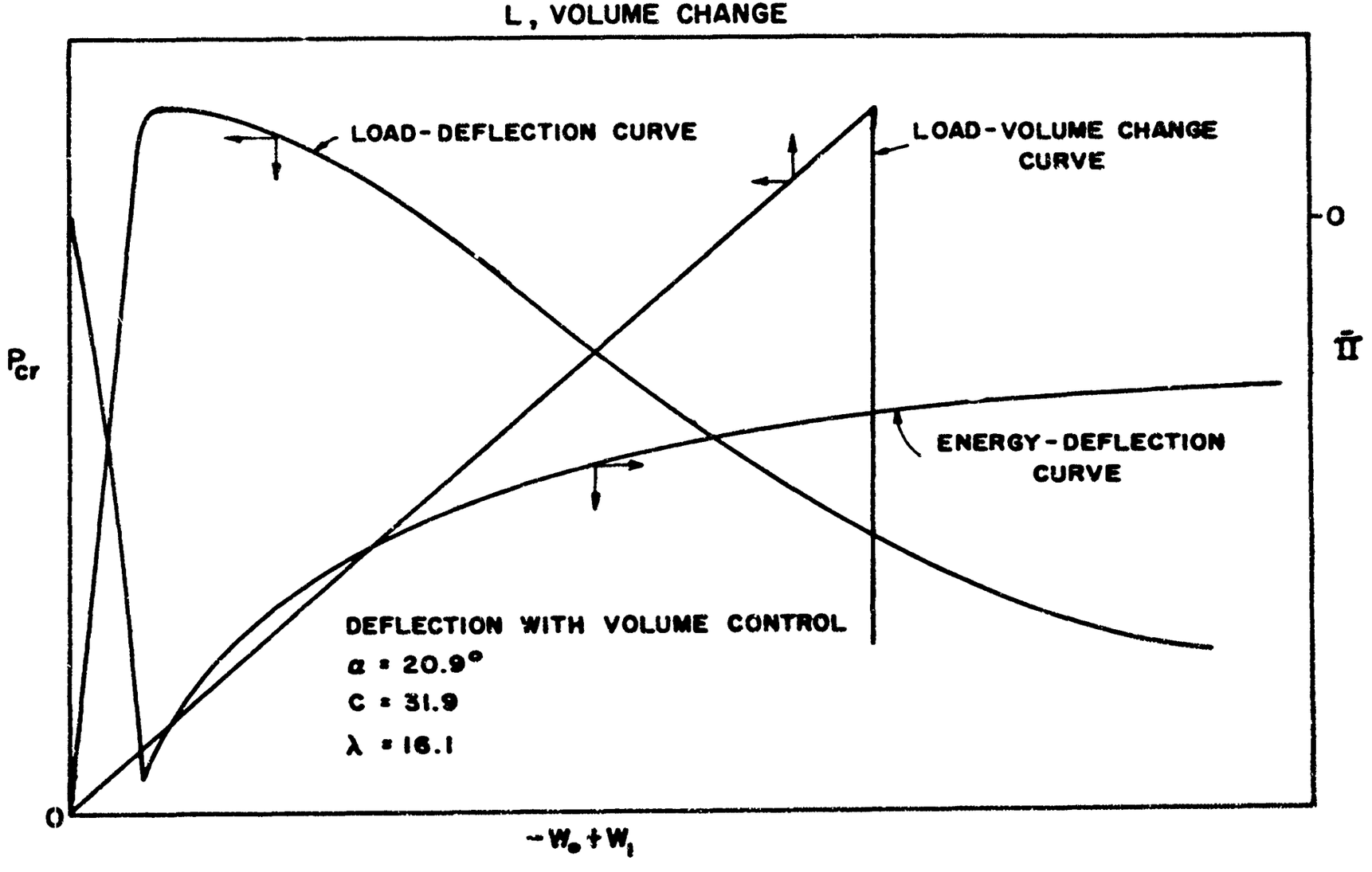

FIG. 15 CONSTANT VOLUME LOADING CURVES

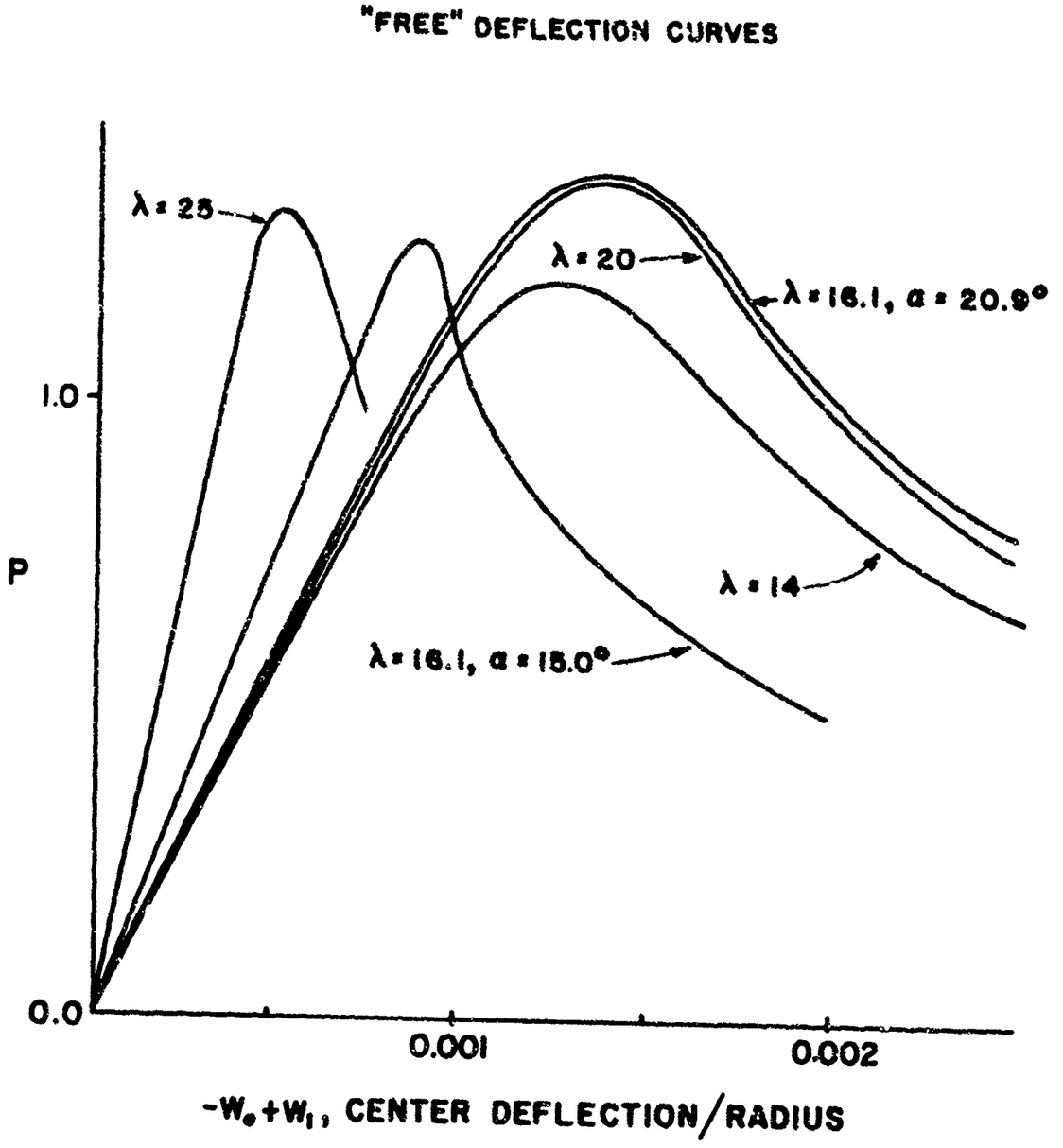

FIG. 16 LOADING CURVES FROM ANALYSIS

APPENDIX A EXPERIMENTAL RESULTS

The data for Table 1 were taken from tests of spherical plastic shells performed in accordance with the procedures described in the Experimental Chapter of this report. Shells to be tested were clamped into the testing chamber and buckled a series of times. Then the chamber was opened and the shell was reclamped. With the slightly altered boundary conditions, a new series of tests was run. The main tests were made under water pressure to maintain control of the displacement. The few tests made under air pressure were so designated. When the same series letter was applied to both water and air pressure tests, it meant that both sets of tests were run without changing the clamping conditions.

The buckling loads were normalized using Eq. (4-4) to make the values of P_{cr} correspond to E_1. Since the results for each series were nearly identical and corresponded to one set of conditions, average values of $(P_{cr})_N$, P_2, and P_{un} were recorded for each series.

The buckle and imperfection positions are given as:

- c center of shell
- n near center
- m midway between center and edge
- e next to edge of shell

Following the values of q_T, λ, a/h, and α for each shell there is a brief description of observed surface imperfections. If the edge strip or rim curled up (with the shell convex up) after forming, a positive slope was indicated. An estimate of the height of bumps and their location on the shell was made: This information follows the slope.

In the table E_i = 498,000 psi and g, the creep coefficient, is 0.011.

Table 1 - Buckling Loads

Series	$(P_{cr})_N$	P_2	P_{un}	Buckle Position
Shell #1	(q_T = .237 psi, λ = 9.25, a/h = 1635, α = 7.40°, slope = -.006, imp. = .015", at c)			
a	.319	.175	.251	n
b	.296	.160	.240	n
c	.295	.164	.237	n
ave	.303	.167	.243	
Shell #2	(q_T = .272 psi, λ = 9.20, a/h = 1525, α = 7.62° slope = -.06, imp. = none)			
a	.265	.256	.256	n
b	.253	.243	.246	n
c	.240	.226	.229	n
ave	.253	.242	.244	
Shell #3	(q_T = .670 psi, λ = 12.3, a/h = 972, α = 12.75° slope = -.03, imp. = none)			
a	.400	.167	.261	m
b	.390	.156	.264	m
ave	.395	.161	.261	
d(air)	.368	--	--	
Shell #4	(q_T = .782 psi, λ = 4.67, a/h = 898, α = 4.11° slope = ∱.02, imp. = none)			
a	.373	.363	--	c
b	.359	--	--	c
c	.348	.342	--	c
ave	.360	.352	--	
Shell #6	(q_T = .494 psi, λ = 3.43, a/h = 1135, α = 3.29° slope = ∱.04, imp. = none)			
a	.610	--	--	c
b	.698	--	--	c
c	.556	.545	.545	c
ave	.588	.545	.545	

Shell #7 (q_T = 2.275 psi, λ = 4.92. a/h = 527, α = 6.92°
slope = /.04, imp. = .01" at m)

a	.352	--	--	m
b	.376	.367	--	n
c	.353	.345	--	e
ave	.360	.356	--	

Shell #8 (q_T = 2.375 psi, λ = 5.15, a/h = 516, α = 7.32°
slope = -.015, imp. = .0004" at m)

a	.313	.307	--	n
b	.315	--	--	n
c	.294	.290	--	n
ave	.307	.298	--	

Shell #9 (q_T = 1.320 psi, λ = 7.32, a/h = 692, α = 9.05°
slope = none, imp. at m)

a	.447	.216	.375	n
b	.475	.215	.380	n
c	.491	.199	.371	n
ave	.471	.210	.375	

Shell #10 (q_T = 1.400, λ = 7.32, a/h = 672, α = 9.19°
slope = -.003, imp. none)

a	.449	.229	.381	n
b	.442	.217	.372	m
ave	.445	.223	.376	

Shell #11 (q_T = 1.435, λ = 7.25, a/h = 662, α = 9.10°
slope = -.003, imp. = .001" in symmetric rings)

a	.447	.205	.366	m
b	.436	.201	.358	m
ave	.442	.203	.362	

Shell #12 (q_T = 1.350, λ = 7.47, a/h = 684, α = 9.24°
no slope, imp. none)

a	.452	.211	.355	--
b	.466	.211	.371	--
ave	.459	.211	.363	

Shell #13 (q_T = 1.352, λ = 7.34, a/h = 693, α = 9.08°
no slope, central hollow)

a	.456	.213	.388	--
b	.459	.210	.381	--
ave	.458	.212	.385	

Shell #14 (q_T = .189 psi, λ = 5.2, a/h = 1735, α = 4.03°
slope = ∱.02, imp. = .01" at m, 1" dia. bump)

a	.428	.333	.404	c
c	.485	.315	--	m
c	.472	.338	.432	m
ave	.462	.329	.418	

Shell #15 (q_T = .209 psi, λ = 5.1, a/h = 1740, α = 3.94°
slope = ∱.02, point imp.)

a	.544	.377	.467	n
b	.515	.396	.462	m
c	.494	.323	.428	m
ave	.518	.365	.452	

Shell #16 (q_T = .663 psi, λ = 7.03, a/h = 977, α = 7.27°
no slope, imp. = .023" at m in symmetric ring)

a	.425	.269	.362	e
b	.468	.263	.381	n
c	.460	.260	.381	n
ave	.451	.264	.375	

Shell #17 (q_T = .629 psi, λ = 6.87, a/h = 1000, α = 7.02°
no slope, point imperfection at c)

a	.493	.238	.388	n
b	.496	.240	.372	m
c	.480	.240	.387	m
ave	.490	.239	.382	

Shell #18 (q_T = .638 psi, λ = 6.86, a/h = 995, α = 7.02°
no slope, imp. = .01" at e, various bumps)

a	.535	.253	.417	n
b	.500	.238	.402	n
c	.493	.229	.389	n
ave	.509	.240	.403	

Shell #19 (q_T = .518 psi, λ = 5.76, a/h = 1105, α = 6.57°
slope = ∱.03, hollow at c)

a	.447	.272	.394	m
b	.515	.269	.405	m
c	.490	.292	.417	m
ave	.484	.278	.405	

Shell #20 (q_T = .522 psi, λ = 3.31, a/h = 1100, α = 3.32°
slope = ∱0.4, imp. = .01" at n)

a	.549	.549	--	c
b	.571	.571	--	c
ave	.560	.560		

Shell #21 (q_T = .582 psi, λ = 12.0, a/h = 1040, α = 12.08°
no slope, imp. = .013" at m)

a	.514	.155	.302	n
b	.512	.154	.296	m
c	.533	.187	.296	-
ave	.520	.165	.298	

Shell #22 (q_T = 1.620 psi, λ = 16.1, a/h = 625, α = 21.3°
slope = -.015, imp. .01" at c)

a	.325	.148	.230	n
b	.317	.147	.226	n
c	.330	.153	.225	n
ave	.324	.149	.227	

Shell #23 (q_T = 1.535 psi, λ = 16.1, a/h = 642, α = 20.9°
no slope, imp. = .01" at c)

a	.459	.135	.236	n
b	.463	.143	.235	n
c	.460	.142	.243	n
ave	.461	.140	.238	

Shell #24 (q_T = .495 psi, λ = 9.85, a/h = 1130, α = 9.48°
slope=-.015, imp.=.02" at e)

a	.525	.184	.270	c
b	.472	.187	.338	m
c	.492	.187	.350	n
ave	.496	.186	.319	

Shell #25 (q_T = .481 psi, λ = 9.90, a/h = 1145, α = 9.48°
no slope, hollow at c of unknown magnitude)

a	.259	.234	.238	c
b	.313	.271	.296	c
ave	.286	.252	.267	

Shell #26 (q_T = .221 psi, λ = 11.6, a/h = 1695, α = 9.10°
no slope, imp. = .006" at m)

a	.328	.187	.271	c
b	.291	.157	.174	c
ave	.309	.172	.222	

Shell #27 (q_T = .228 psi, λ = 11.7, a/h = 1670, α = 9.24°
no slope, imp. = .003" at e)

a	.421	.228	.340	e
b	.446	.205	.350	e
c	.404	.169	.314	e
ave	.424	.201	.335	

Shell #28 (q_T = .233 psi, λ = 11.8, a/h = 1645, α = 9.42°
no slope, imp. = .003" at e)

a	.412	.162	.262	e
b	.352	.160	.268	e
c	.474	.219	.369	e
ave	.413	.180	.300	

Shell #29 (q_T = .232 psi, λ = 15.2, a/h = 1650, α = 12.2°
no slope, imp. = .008" at e)

a	.448	.150	.247	m
b	.433	.148	.239	m
c	.418	.146	.238	m
ave	.433	.148	.241	

Shell #30 (q_T = .223 psi, λ = 15.7, a/h = 1680, α = 12.4°
no slope, imp. at c, bump)

a	.483	.141	.246	m
b	.518	.104	.195	m
c	.454	.099	.207	m
ave	.485	.115	.216	

Shell #31 (q_T = .606 psi, λ = 20.5, a/h = 1020, α = 21.1°
no slope, imp. = .02" at c, rise)

a'	.366	.085	--	n
a	.246	.131	.174	e
c	.390	.096	.200	e
d	.347	.092	.182	n
g	.382	.104	.196	n
ave	.346	.102	.188	
a'(air)	.377	--	--	n
b(air)	.384	--	--	n
c(air)	.352	--	--	e
c'(air)	.392	--	--	e

Shell #32 (q_T = .606 psi, λ = 20.6, a/h = 1020, α = 21.2°
no slope, imp. = .015" at c, rise)

a	.423	.092	.211	e
b	.427	.084	.208	e
c	.452	.084	.194	e
a'	.470	.097	.216	n
ave	.443	.089	.207	
a(air)	.452	--	--	e
b(air)	.448	--	--	e
c(air)	.470	--	--	e

Shell #33 (q_T = .616 psi, λ = 20.2, a/h = 1015, α = 20.9°
no slope, imp. = .015" at c, rise)

a	.339	.115	.192	--
b	.450	.104	.203	n
ave	.395	.109	.197	
b(air)	.432	--	--	e

Shell #34 (q_T = .606 psi, λ = 20.3, a/h = 1020, α = 20.9°
no slope, imp. = .02" at c, rise)

a	.319	.109	.184	--
b	.421	.099	.207	n
c	.409	.100	.182	n
ave	.383	.103	.191	
b(air)	.415	--	--	n
c(air)	.411	--	--	n

Shell #35 (q_T = .243 psi, λ = 25.6, a/h = 1615, α = 20.9°
no slope, imp. = .02" at c, rise)

a	.277	.033	.116	n
b	.283	--	--	e
b	.329	.107	.181	n
c	.331	.105	.182	n
ave	.305	.082	.160	

Shell #36 (q_T = .243 psi, λ = 25.6, a/h = 1615, α = 20.9°
no slope, imp. = .02" at c, rise)

a	.259	.054	.135	e
b	.310	.042	.141	e
c	.293	.037	.124	n
ave	.287	.045	.133	
a(air)	.315	--	--	e
b(air)	.349	--	--	e

Shell #37 (q_T = .272 psi, λ = 24.7, a/h = 1525, α = 20.8°
no slope, imp. = .02" at c, rise)

a	.406	.119	.206	e
b	.335	.121	.171	e
c	.352	.082	.139	e
ave	.373	.107	.172	
a(air)	.390	--	--	e

Shell #38 (q_T = .600 psi. λ = 12.4, a/h = 1025, α = 12.6°
slope = -011, imp. at e)

a	.510	.148	.262	m
b	.589	.150	.274	m
c	.557	.165	.300	--
ave	.552	.154	.279	

Shell #39 (q_T = .700 psi, λ = 12.6, a/h = 950, α = 13.3°
slope = -.006, no imp.)

a	.309	.116	.168	m
b	.267	.128	.170	-
ave	.288	.122	.169	

Shell #40 (q_T = .616 psi, λ = 12.4, a/h = 1010, α = 12.6°
no slope, no imp.)

a	.425	.144	.209	e
b	.436	.137	.205	m
c	.440	.130	.197	-
ave	.434	.137	.204	

APPENDIX B

Modulus and Creep Coefficient Determination

Beam Tests

Samples of the shell material, cut to 6" by 1½", were tested as simple beams to determine the modulus of elasticity. The sample numbers correspond to the shell numbers since they came from the same sheet.

Table 2 - Modulus from Beam Tests

No.	Thickness	Width	E_1, psi	No.	Thickness	Width	E_1, psi
4	.0828"	1.445"	495,000	12	.0504"	1.490"	503,000
5	.0830	1.448	500,000	13	.0500	1.456	500,000
6	.0777	1.456	489,000	14	.0419	1.515	509,000
7	.0829	1.429	477,000	15	.0427	1.480	494,000
8	.0783	1.446	532,000	16	.0429	1.519	490,000
9	.0512	1.412	491,000	17	.0419	1.515	498,000
10	.0508	1.510	492,000	18	.0424	1.437	502,000
11	.0508	1.477	479,000	19	.0419	1.420	524,000

The average value of E_1 is 498,000 psi and the standard deviation of this value is 1.4%

Tensile Tests

The tensile tests were run using SR-4 strain gages and a dead weight. The gages and the glue attaching them to the specimens take a certain amount of load. To take account of the added stiffness, the apparent modulus can be modified according to equation

$$E_1 = E_{apparent}\left(1 - \frac{B}{area}\right)$$

in which B describes the gage stiffness. If B and E_1 are assumed to be constants for the tensile specimens, a least squares formulation can be used to give

$$E_1 = 514{,}000 \text{ psi}$$

$$B = .00687$$

The standard deviation of the value for E_1 is 1.8%.

Table 3 - Modulus from Tensile Tests

No.	Thickness	Width	$E_{apparent}$	$E_1 = E_{app}\left(1 - \frac{.00687}{wt}\right)$
5	.0829	1.447	556,000	524,000 psi
6	.0789	1.457	545,000	512,000
8	.0770	1.449	539,000	506,000
9	.0512	1.414	578,000	523,000
16	.0429	1.528	556,000	498,000
17	.0428	1.462	583,000	518,000

The adjustment for gage effect is from 6 to 11% and suggests that this tensile modulus is rather questionable.

Gages placed crosswise on some of the specimens gave a value for Poisson's ratio of 0.41.

Creep Coefficient

The curve of strain versus time for the tensile specimens follows the equation

$$\varepsilon = \frac{\sigma}{E_1}\left[1 + g \ln (t + t_{.1})\right]$$

fairly well in the range of interest. Denoting the strain at one minute by ε_1, and that at 10 minutes by ε_{10}, the value of g can be found from

$$g = \frac{\frac{\varepsilon_{10}}{\varepsilon_1} - 1}{\ln 10}$$

The tensile tests then give the values found in Table 4

Table 4 - Creep Coefficient

No.	$\varepsilon_{10}/\varepsilon_1$	g	No.	$\varepsilon_{10}/\varepsilon_1$	g
5	1.022	.00955	9	1.021	.00911
6	1.020	.00867	16	1.039	.01690
8	1.029	.01255	17	1.026	.01128

The average value of g is .0113.

Beam End Rotation

Since the simply supported beam used in the modulus determination undergoes considerable deflection, the end rotation may be a nonlinear function of load. To determine this relationship, let

P = load on the beam

ℓ = length of beam *between supports, fixed*

M = moment in beam

γ, γ_E, γ_L = rotation, rotation at ends, rotation in the linear theory

x = variable horizontal distance measured from center

s = variable distance along beam from center

s_ℓ = value of s at $x = \ell/2$

$$dx = \cos\gamma\, ds$$

$$x \cong \int_0^s \left(1 - \frac{\gamma^2}{2}\right) ds$$

$$M = \frac{P}{2}\left(\frac{\ell}{2} - x\right) = \frac{P}{2}\left[\frac{\ell}{2} - s + \int \frac{\gamma^2}{2}\, ds\right]$$

$$\gamma = \int \frac{M}{EI}\, ds = \frac{P}{2EI}\iint\left[\frac{\ell}{2} - s + \int \frac{\gamma^2}{2}\, ds\right] ds$$

$$\gamma_E = \frac{P}{4EI}\left[\ell s - s^2\right]_0^{s_\ell} + \frac{P}{4EI}\iint \gamma^2\, ds\, ds$$

In the nonlinear term let $\gamma = \frac{P}{4EI}(\ell s - s^2)$ for the integration and $s_\ell = \frac{\ell}{2}$ for evaluation. Using these approximations in the equation for x gives

$$\frac{\ell}{2} = s_\ell - \frac{1}{240}\left(\frac{P\ell^2}{EI}\right)^2 \ell$$

Therefore

$$\gamma_E = \frac{1}{16}\frac{P\ell^2}{EI} + \left(\frac{P\ell^2}{EI}\right)^3 \frac{1}{6 \cdot 2^{12}}$$

but

$$\gamma_L = \frac{P\ell^2}{16EI}$$

Then the first nonlinear approximation is

$$\gamma_E = \gamma_L + \frac{\gamma_L^3}{6}$$

APPENDIX C ENERGY EQUATION

The energy equation is

$$\bar{\Pi} = E_{21}\omega_0^2\omega_1 + E_{12}\omega_0\omega_1^2 + E_{02}\omega_1^2 + E_{03}\omega_1^3 + E_{04}\omega_1^4 \qquad (5\text{-}34)$$

This equation is obtained by performing the integrations of Eq. (5-25), rearranging, and eliminating terms which cancel with the aid of Eq. (5-29).

If the integrals of Eq. (5-26) were evaluated exactly, many terms would be obtained which are as small as those neglected already. Retaining such small terms is unreasonable and so a criterion was set up to eliminate them. The evaluated energy function contains the following types of terms:

$$\frac{1}{b^n} \quad \text{and} \quad \frac{1}{b^{n-1}} e^{-mb\alpha}$$

These two types are basically different since the exponential is not readily compared with 1/b and also because the exponential term increases on differentiation while the other decreases. Therefore the highest order terms of each type were retained. This criterion allowed for liberal use of approximations in evaluating $\bar{U}_3$ since this whole term is essentially of second order.

The E's of the equation will be defined below in the same manner as they were for the Fortran statement used in their evaluation.

$$E_{11} = 1.857\,G_1 - 2.857 \sin\alpha \tan\alpha\,(P_{11}P_2 + P_1 P_{12})$$

$$E_{12} = 1.857\,G_2 - 2.857 \sin\alpha \tan\alpha\,(P_1 P_{22} + P_2 P_{12}) + P_2$$

$$E_{02} = 1.857\,G_3 - 1.429 \sin\alpha \tan\alpha\, P_3^2 + \frac{.2275}{c^4} P_4$$

$$E_{03} = 1.857\,G_4 - 2.857 \sin\alpha \tan\alpha\, P_2 P_{22}$$

$$E_{04} = 1.857\,G_5 - 1.429 \sin\alpha \tan\alpha\, P_{22}^2$$

The G's and P's are given by the following:

$$G_1 = 2R_1(R_{21} + R_{31}) - 1.4H_1(R_{22} + R_{32}) + R_{22}\left(4 - \frac{2.6H_2}{c}\right)(1 - \cos\alpha)$$

$$+ 2.6 R_{12} R_{21}(1 - \cos\alpha) + S_1$$

$$G_2 = 2R_1(R_{22} + R_{32}) + R_{23}\left(4 - \frac{2.6H_2}{c}\right)(1 - \cos\alpha) - 1.4H_1(R_{23} + R_{33})$$

$$+ 2.6 R_{12} R_{22}(1 - \cos\alpha) - 2R_{32}(.7H_2\cos\alpha + 2H_{32})(1 - \cos\alpha) + S_2$$

$$G_3 = 2.6 R_1 R_{12} + 1.69 R_{12}^2(1 - \cos\alpha) + S_3$$

$$G_4 = 2R_1(R_{23} + R_{33}) + 2.6 R_{12} R_{23}(1 - \cos\alpha) - 4H_{32} R_{33}(1 - \cos\alpha)$$

$$+ S_4$$

$$G_5 = (R_{23}^2 - R_{33}^2)(1 - \cos\alpha) + S_5$$

$$P_1 = 1.3\left(1 - \frac{2}{c\sin\alpha} + \frac{1}{2c^2\sin^2\alpha}\right)$$

$$P_2 = 1.3\left[\left(\cos b\alpha + \sin b\alpha + \frac{1}{b}\cos b\alpha \cot\alpha\right)e^{-b\alpha} - \frac{\cos\alpha}{2b^2\sin^2\alpha} - \frac{H_2\cos\alpha}{2} + \frac{R_{12}}{1+\cos\alpha}\right]$$

$$P_3 = -\frac{.2835}{c} - \frac{.637 H_2}{cb^2} - \frac{1.82 b^2 e^{-2b\alpha}}{c}\frac{\sin^2\alpha}{\cos\alpha}\left\{\frac{6(c-b)\sin b\alpha - 2(a+7b)\cos b\alpha}{15(2c^2-2cb+5b^2)}\right.$$

$$\left.+\frac{2(c-3b)\sin b\alpha + 2(3c-4b)\cos b\alpha}{15(2c^2-6cb+5b^2)} + \frac{c\sin 2b\alpha - 2b\cos 2b\alpha}{24(c^2+4b^2)} + \frac{H_{11}}{6}\cos 2b\alpha\right\}$$

$$+.02275\left(\frac{H_2}{c}\right)^2\left(\frac{\sin^4\alpha}{\cos\alpha} + \frac{4.5\sin 2\alpha}{(1+\cos\alpha)^2}\right) - \frac{1.3}{c^2}(R_{23}+R_{33})\cot\alpha\frac{1+\nu\cos\alpha}{1+\cos\alpha}$$

$$+(.4175 + \frac{.91 H_2}{b^2})\ln\cos\alpha\left(1 - \frac{H_2}{c}\frac{1+\nu\cos\alpha}{1+\cos\alpha}\right)$$

$$-\frac{2.167}{c}H_2^2 H_3\left(-4.925 + \frac{3}{\cos\alpha} + \frac{4.86}{1+\cos\alpha} - .6\cos\alpha - .105\cos^2\alpha + 6.9\ln\cos\alpha\right.$$

$$\left.-7.56\ln\frac{1+\cos\alpha}{2}\right) - 2.167 H_2^2\left(3\frac{\sin^2\alpha}{\cos\alpha} - .8 + .9\cos\alpha - .1\cos^3\alpha\right.$$

$$\left.+5.4\ln\cos\alpha\right)$$

$$P_4 = 1.2b^2 + b^2 e^{-2b\alpha}\left(-2b\sin\alpha + b\cos 2b\alpha\sin\alpha + b\sin 2b\alpha\sin\alpha\right.$$

$$-\cos\alpha + \tfrac{1}{2}\cos b\alpha\cos\alpha + 4\sin^2 b\alpha\cos\alpha - \frac{16}{15}\sin b\alpha - \frac{8}{15}\cos b\alpha$$

$$\left.-\frac{\sin 2b\alpha}{6} - \frac{\cos 2b\alpha}{6}\right) - 8H_2 - 4bH_2 e^{-b\alpha}\sin b\alpha\sin 2\alpha$$

$$+8H_2 e^{-b\alpha}(\sin b\alpha + \cos b\alpha)\cos^2\alpha + \frac{4}{3}H_2^2(1-\cos^3\alpha)$$

$$P_{11} = .095\, c\cot\alpha + \frac{R_{21}+R_{31}}{1+\cos\alpha}$$

$$P_{12} = .7cb\cot\alpha e^{-b\alpha}\left[\frac{(c-b)\cos b\alpha + (c+b)\sin b\alpha}{c^2+b^2} + 4H_{11}(\sin b\alpha - \cos b\alpha)\right]$$

$$-.7 H_2\cos\alpha\left(1 - \frac{\cot\alpha}{2c}\right) + \frac{R_{22}+R_{32}}{1+\cos\alpha}$$

$$P_{22} = .1606\frac{\cos\alpha}{\sin^2\alpha} + b^2 e^{-2b\alpha}\left(-1 - \frac{\cot\alpha}{2b} + \cos 2b\alpha - \frac{1}{4b}\sin 2b\alpha\cot\alpha +\right.$$

$$+\frac{1}{4b}\cos 2b\alpha\cot\alpha + \frac{2.8}{15}\cos b\alpha + \frac{5.6}{15}\sin b\alpha + \frac{.7}{12}\cos 2b\alpha + \frac{.1}{12}\sin 2b\alpha)$$

$$+H_2 e^{-b\alpha}[2b\sin b\alpha\sin\alpha - .7(\cos b\alpha + \sin b\alpha)\cos\alpha] + \frac{.7H_2\cos\alpha}{b^2\sin^2\alpha}$$

$$+\frac{H_2^2}{12}\left(0.7 - 5.4\sin^2\alpha + \frac{.6+2\cos\alpha}{1+\cos\alpha}\right) + \frac{R_{23}+R_{33}}{1+\cos\alpha}$$

The H's and R's and S's are in turn defined as follows:

$$H_1 = \frac{\sin\alpha}{c} - \frac{\cos\alpha}{2c^2}$$

$$H_2 = \frac{2b\sin b\alpha\, e^{-b\alpha}}{\sin\alpha}$$

$$H_3 = \left(1 - \frac{1}{2c\sin\alpha}\right)\frac{\sin\alpha}{1-\cos\alpha}$$

$$H_{11} = \frac{(c-b)^3}{4(c-b)^4+1}$$

$$H_{12} = \frac{(c-2b)^3}{4(c-2b)^4+1}$$

$$H_{21} = \frac{(2c-b)^3}{4(2c-b)^4+1}$$

$$H_{22} = (\sin b\alpha + \cos b\alpha)e^{-b\alpha} - H_2\cos\alpha$$

$$R_1 = -\frac{.35}{b^2}\left[1 - e^{-b\alpha}\sin\alpha(2b\cos b\alpha - \sin b\alpha\cot\alpha + \cos b\alpha\cot\alpha)\right]$$

$$+.35H_2\sin^2\alpha + 2H_{22}(1-\cos\alpha)$$

$$R_{12} = \frac{.65}{b^2(1-\cos\alpha)}\left[-1 + e^{-b\alpha}\sin\alpha(2b\cos b\alpha - \sin b\alpha\cot\alpha + \cos b\alpha\cot\alpha)\right]$$

$$+.65H_3(1+\cos\alpha)$$

$$R_{21} = \frac{c\sin\alpha - \cos\alpha}{4(1-\cos\alpha)}$$

$$R_{22} = \frac{cb\sin\alpha}{1-\cos\alpha} e^{-b\alpha}\left[\frac{-(c-b)\cos b\alpha - (c+b)\sin b\alpha}{c^2+b^2}\right.$$

$$\left. + 4H_{11}(\cos b\alpha - \sin b\alpha)\right] + H_2\left[1+\cos\alpha - \frac{\sin 2\alpha}{c(1-\cos\alpha)}\right]$$

$$R_{23} = -\frac{\sin\alpha}{1-\cos\alpha}\left(\frac{b}{2} - \frac{b}{4}\cos 2b\alpha + \frac{b}{4}\sin 2b\alpha + \frac{\cot\alpha}{4} + \frac{\sin 2b\alpha\cot\alpha}{8}\right)e^{-2b\alpha}$$

$$+ \frac{1}{4(1-\cos\alpha)} + H_2(1+\cos\alpha)(\sin b\alpha + \cos b\alpha)e^{-b\alpha}$$

$$+ \frac{H_2^2}{2(1-\cos\alpha)}\left(\frac{2}{3} - \cos\alpha + \frac{\cos^3\alpha}{3}\right)$$

$$R_{31} = \frac{.175\cos\alpha}{1-\cos\alpha}\left(1 - \frac{5\cot\alpha}{8c}\right)$$

$$R_{32} = \frac{.7cb\cos\alpha e^{-b\alpha}}{1-\cos\alpha}\left[\frac{-2cb\cos b\alpha + (c^2-b^2)\sin b\alpha}{(c^2+b^2)^2} + 16H_1^2\sin b\alpha\right]$$

$$+ .7\frac{H_2H_1\cos\alpha}{1-\cos\alpha}$$

$$R_{33} = \frac{.7\sin\alpha e^{-b\alpha}}{1-\cos\alpha}\left(\frac{b}{24}\cos 2b\alpha + \frac{166}{75}\cos b\alpha + \frac{16}{35}\sin b\alpha\right.$$

$$\left. + \frac{2}{375}\sin b\alpha\cot\alpha + \frac{44}{375}\cos b\alpha\cot\alpha - \frac{1}{96}\sin 2b\alpha\cot\alpha + \frac{1}{96}\cos 2b\alpha\cot\alpha\right)$$

$$\frac{-.089425}{1-\cos\alpha} + \frac{.35H_2}{b^2(1-\cos\alpha)} - \frac{.35H_2e^{-b\alpha}}{b^2(1-\cos\alpha)}\left(b\cos b\alpha\sin 2\alpha\right.$$

$$\left. - \sin b\alpha\cos 2\alpha + \cos b\alpha\cos 2\alpha\right) - \frac{.13125H_2^2}{1-\cos\alpha}\left(\cos\alpha - \frac{\cos 3\alpha}{9} - \frac{8}{9}\right)$$

$$S_1 = .49c\cos\alpha e^{-b\alpha}\left[-8H_{11}\left(\frac{cb\sin b\alpha - b^2\cos b\alpha}{c^2+b^2}\right) + \right.$$

$$+9H_{11}H_{31}(c-5b)(\sin b\alpha-\cos b\alpha)+\frac{(c-5b)\cos b\alpha+c\sin b\alpha}{2c^2-2cb+b^2}$$

$$\frac{+(2c-7b)\cos b\alpha-(2c+7b)\sin b\alpha}{4(4c^2+b^2)}+3b^2\frac{(c+b)\cos b\alpha-(c-b)\sin b\alpha}{(c^2+b^2)(4c^2+b^2)}\Big]$$

$$+1.05H_1H_2\cos\alpha-.1225H_2\cot\alpha\left(\sin 2\alpha-\frac{5\cos 2\alpha}{4c}\right)$$

$$-1.9H_{32}\cos\alpha\left(1-\frac{5\cot\alpha}{8c}\right)$$

$$S_2=-1.96b^2e^{-2b\alpha}\sin\alpha\Big[\frac{(2c-7b)\cos b\alpha+(4c+b)\sin b\alpha}{15(2c^2-2cb+5b^2)}$$

$$+\frac{(2c-b)\cos b\alpha+(4c-7b)\sin b\alpha}{15(2c^2-6cb+5b^2)}+\frac{(c-2b)\cos 2b\alpha+(c+2b)\sin 2b\alpha}{48(c^2+4b^2)}$$

$$+\frac{H_{12}}{12}(\cos 2b\alpha+\sin 2b\alpha)\Big]+.49H_2e^{-b\alpha}\sin 2\alpha\Big[\frac{(c-b)\cos b\alpha+(c+b)\sin b\alpha}{2(c^2+b^2)}$$

$$+2H_{11}(\cos b\alpha+\sin b\alpha)\Big]+.06125H_2^2\left(3H_1-\frac{\sin 3\alpha}{c}+\frac{3\cos 3\alpha}{2c^2}\right)$$

$$+.49cb\cos\alpha e^{-2b\alpha}\Big[\frac{(c^2+3cb-2b^2)\cos 2b\alpha-(c^2-3cb-2b^2)\sin 2b\alpha}{(c^2+b^2)(c^2+4b^2)}$$

$$+16H_{11}H_{12}(\cos 2b\alpha-\sin 2b\alpha)-\frac{8cH_{11}}{c^2+b^2}$$

$$+\frac{1.96H_2H_{11}\sin 2\alpha}{c^2+b^2}e^{-b\alpha}\Big[(c^2-cb+b^2)\cos b\alpha+c^2\sin b\alpha\Big]$$

$$S_3=\frac{.18375}{b^2}-.1225\frac{e^{-2b\alpha}}{b}\sin\alpha\left(2+\cos 2b\alpha+\sin 2b\alpha+\frac{\cot\alpha}{b}\right.$$

$$+\frac{1}{2b}\cos 2b\alpha\cot\alpha-\frac{.49H_2}{b^2}\Big[1-e^{-b\alpha}(b\sin 2\alpha\cos b\alpha-$$

$$+9H_{11}H_{31}(c-5b)(\sin b\alpha-\cos b\alpha)+\frac{(c-b)\cos b\alpha+c\sin b\alpha}{2c^2-2cb+b^2}$$

$$\left.\frac{+(2c-7b)\cos b\alpha-(2c+7b)\sin b\alpha}{4(4c^2+b^2)}+3b^2\frac{(c+b)\cos b\alpha-(c-b)\sin b\alpha}{(c^2+b^2)(4c^2+b^2)}\right]$$

$$+1.05H_1H_2\cos\alpha-.1225H_2\cot\alpha\left(\sin 2\alpha-\frac{5\cos 2\alpha}{4c}\right)$$

$$-1.9H_{32}\cos\alpha\left(1-\frac{5\cot\alpha}{8c}\right)$$

$$S_2=-1.96b^2e^{-2b\alpha}\sin\alpha\left[\frac{(2c-7b)\cos b\alpha+(4c+b)\sin b\alpha}{15(2c^2-2cb+5b^2)}\right.$$

$$+\frac{(2c-b)\cos b\alpha+(4c-7b)\sin b\alpha}{15(2c^2-6cb+5b^2)}+\frac{(c-2b)\cos 2b\alpha+(c+2b)\sin 2b\alpha}{48(c^2+4b^2)}$$

$$\left.+\frac{H_{12}}{12}(\cos 2b\alpha+\sin 2b\alpha)\right]+.49H_2e^{-b\alpha}\sin 2\alpha\left[\frac{(c-b)\cos b\alpha+(c+b)\sin b\alpha}{2(c^2+b^2)}\right.$$

$$\left.+2H_{11}(\cos b\alpha+\sin b\alpha)\right]+.06125H_2^2\left(3H_1-\frac{5\sin 3\alpha}{c}+\frac{3\cos 3\alpha}{2c^2}\right)$$

$$+.49cb\cos\alpha e^{-2b\alpha}\left[\frac{(c^2+3cb-2b^2)\cos 2b\alpha-(c^2-3cb-2b^2)\sin 2b\alpha}{(c^2+b^2)(c^2+4b^2)}\right.$$

$$+16H_{11}H_{12}(\cos 2b\alpha-\sin 2b\alpha)-\frac{8cH_{11}}{c^2+b^2}$$

$$\left.+\frac{1.96H_2H_{11}\sin 2\alpha}{c^2+b^2}e^{-b\alpha}\left[(c^2-cb+b^2)\cos b\alpha+c^2\sin b\alpha\right]\right]$$

$$S_3=\frac{.18375}{b^2}-.1225\frac{e^{-2b\alpha}}{b}\sin\alpha\left(2+\cos 2b\alpha+\sin 2b\alpha+\frac{\cot\alpha}{b}\right.$$

$$\left.+\frac{1}{2b}\cos 2b\alpha\cot\alpha-\frac{.49H_2}{b^2}\left[1-e^{-b\alpha}(b\sin 2\alpha\cos b\alpha-\right.\right.$$

$$+1.96\,H_2\left[-.025898+\frac{e^{-3b\alpha}}{90}(3b\sin 2\alpha+2\cos 2\alpha)\right]$$

$$+.49\,H_2^2\left\{\frac{2}{75}\left[(46\cos b\alpha+3b\sin b\alpha)\sin^3\alpha+(.3\sin b\alpha+1.65\cos b\alpha)(\cos\alpha-\right.\right.$$

$$\left.\left.\cos 3\alpha)\right]+\frac{1}{192}\left[46\cos 2b\alpha\sin^3\alpha+\frac{3}{4}(\cos 2b\alpha-\sin 2b\alpha)(\cos\alpha-\cos 3\alpha)\right]\right\}e^{-2b\alpha}$$

$$+.49\,H_2^2\left[\frac{3}{8b^2}-\frac{e^{-2b\alpha}}{46}(2+\cos 2b\alpha+\sin 2b\alpha)\cos^2\alpha\sin\alpha\right]$$

$$+.030625\frac{H_2^3}{b}\cos b\alpha\,e^{-b\alpha}(\sin 4\alpha-2\sin 2\alpha)+\frac{.49}{128}H_2^4\left(-5\cos\alpha\right.$$

$$\left.+\frac{5}{6}\cos 3\alpha-.1\cos 5\alpha+\frac{128}{3}\right)+1.96\,H_2\,e^{-3b\alpha}\left[(-96\cos 2b\alpha\sin 2\alpha\right.$$

$$+\frac{54}{13}\sin 2b\alpha\cos 2\alpha+116\sin 2b\alpha\sin 2\alpha-\frac{40}{13}\cos 2b\alpha\cos 2\alpha)\frac{1}{390}$$

$$+(3b\cos b\alpha\sin 2\alpha-\frac{6}{5}\sin b\alpha\cos 2\alpha-b\sin b\alpha\sin 2\alpha+\frac{8}{5}\cos b\alpha\cos 2\alpha)\frac{1}{480}$$

$$\left.-(3b\cos 3b\alpha\sin 2\alpha+3\sin 3b\alpha\sin 2\alpha+2\cos 3b\alpha\cos 2\alpha)\frac{1}{864}\right]$$

In all of the above, Poisson's ratio has been taken as 0.3.

APPENDIX D ANALYTICAL RESULTS

The analyses outlined in the Solution Section was performed on five shell configurations. The results of Table 5 are for buckling loads which were obtained. The deflection and the value of b at buckling were also listed.

Table 5

		P_{cr}	w_1	$-w_0+w_1$	b/c
16.1	20.9°	1.368	.000 37	.001 31	.83
16.1	15.0°	1.27	.000 273	.000 73	.87
20.0	26.0°	1.372	.000 413	.001 35	.97
25.0	20.9°	1.31	.000 085	.000 46	.92
14.0	18.0°	1.20	.000 45	.001 27	.93